Investigating the therapeutic effect of combined hyperthermia and radiotherapy on the growth and viability of 3D FaDu spheroids

A step closer to in vivo conditions

J. Berkhout

Master of Science Thesis

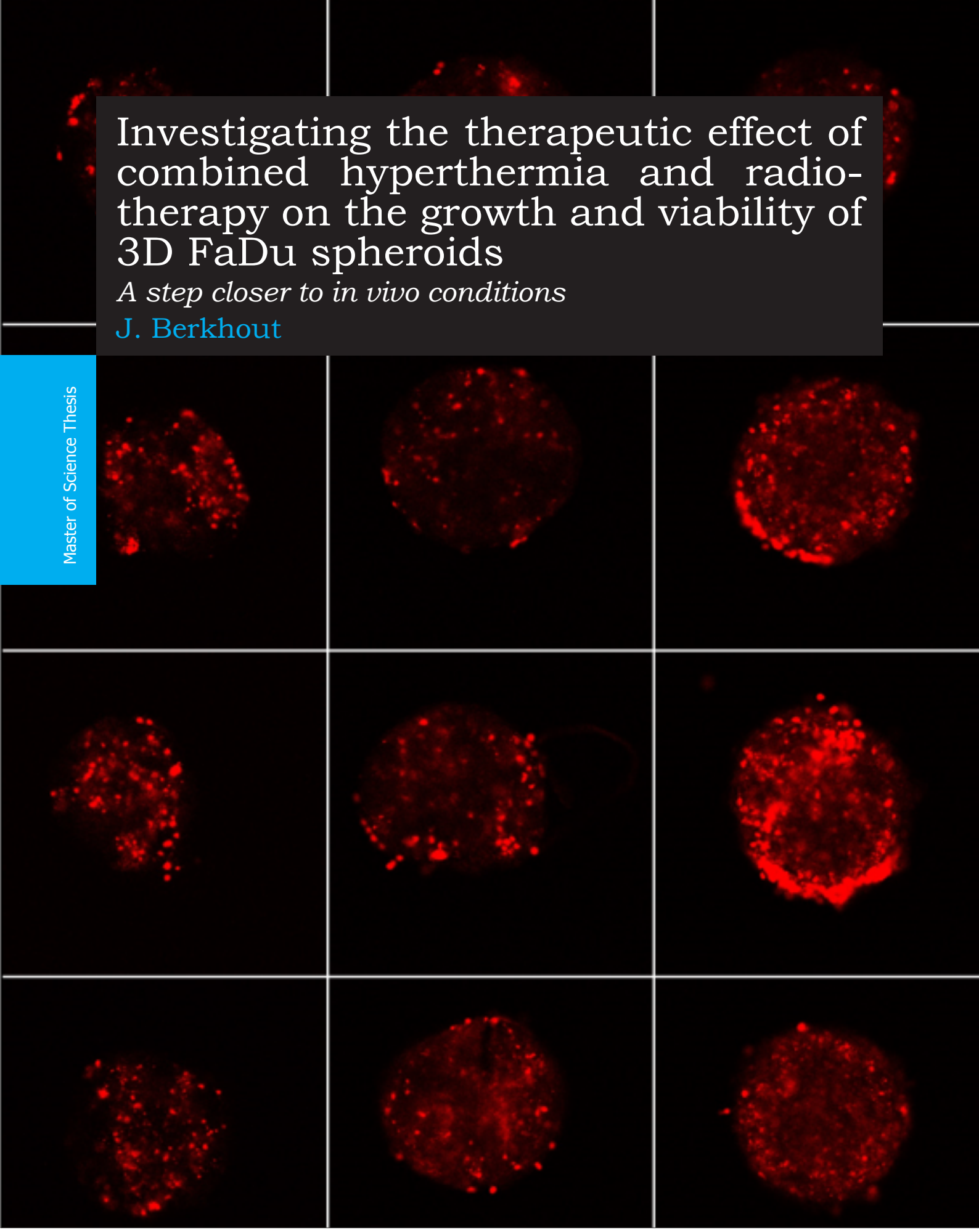

TU Delft Delft University of Technology

Challenge the future

Investigating the therapeutic effect of combined hyperthermia and radiotherapy on the growth and viability of 3D FaDu spheroids

A step closer to in vivo conditions

by

J. Berkhout

in partial fulfillment of the requirements for the degree of

Master of Science
in Chemical Engineering

at the Delft University of Technology,
to be defended publicly on Tuesday July 12, 2022 at 10:00 AM.

Supervisor:	Dr. ir. A. G. Denkova	
Thesis committee:	Dr. ir. R. M. De Kruijff,	TU Delft
	Dr. ir. K. Djanashvili,	TU Delft

TU Delft Delft University of Technology

REACTOR INSTITUTE DELFT

Abstract

Combining different treatment modalities has proven to improve patient outcome compared to applying single treatments. Consequently, mild hyperthermia (HT) and radiotherapy (RT) are combined to radiosensitize tumour cells by inhibiting DNA damage repair mechanisms. In this study, it was investigated if combining both treatment modalities shows an improved therapeutic effect on 3D tumour models made of FaDu cells. To this end, the spheroid size and cell viability were measured over time after treatment. It was also attempted to obtain further qualitative information of the effect on the spheroids using confocal microscopy.

During experiments spheroids were formed of FaDu tumour cells, cells of a head-and-neck squamous cell carcinoma, using Matrigel®. These spheroids grew fast within the first 10 days of seeding up to a size of 550-600 μm reliably. These spheroids were then exposed to both single HT and RT as well as combined HT and RT. Both single treatment modalities showed a decrease in cell growth and cell viability with increasing treatment dose. The thermal doses of 30 and 120 CEM_{43} and radiation doses of 2 and 6 Gy were chosen to be used in the combined treatment experiments.

Combined treatment showed an improved effect on the cell growth and cell viability for most treatment groups, both for HT followed by RT and the other way around, with the determining factor seemingly being the thermal dose. The thermal dose of 120 CEM_{43} combined with 6 Gy of radiation dose showed the highest cell killing potential, with 9±2% of the cell viability remaining when using radiotherapy before hyperthermia and 18±3% when starting with HT before using RT. The most significant difference in effect due to the order in which RT and HT were administered was seen in the group treated with 2 Gy of radiation dose and 120 CEM_{43} of thermal dose. In this group RT preceding HT resulted in a cell viability of 13±2% on day 7 after treatment, whilst HT preceding RT resulted in a cell viability of 48±8%. Visual inspection of the spheroids showed an increased effect in the form of less growth, as well as flaking around the edges of the spheroids.

Obtaining qualitative information on the effect that combined treatment had on spheroids using confocal microscopy was unsuccessful. Both using a live and dead cell staining kit, as well as PI staining proved ineffective in accurately visualizing the dead cells in spheroids.

Abbreviations

Abbreviation	Definition
CEM_{43}	Cumulative effective minutes at 43°C, unit used to indicate the thermal dose
CT	Combined treatment
DNA	Deoxyribonucleic acid
DSB	Double-strand break
ECM	Extracellular matrix
Gy	Gray, unit used to indicate the radiation dose
HR	Homologous recombination
HT	Hyperthermia treatment
HTRT	Hyperthemia treatment preceeding radiation treatment
MCTS	Multicellular tumour spheroids
NHEJ	Non-homologous end joining
PI	Propidium iodide
RT	Radiation treatment or radiotherapy
RTHT	Radiation treament preceeding hyperthermia treatment
SCC	Squamous cell carcinoma
TER	Thermal enhancement ratio

Preface

First and foremost I would like to thank Robin Nadar for guiding me through all my daily work. By providing information on the general topic, methods for different experiments, possible topics to look at and answers to all my questions my project was able to progress smoothly. Furthermore, you also helped me through the difficulties I often had with interpreting the results found during the research. In general, I would not have been able to finish this thesis without you and therefore your help was invaluable to me over the past year.

I would also like to thank Prof. Antonia Denkova. For both being a member of my defense committee, as well as for meeting with me every two weeks. These meetings helped me with keeping some order in my results and the overall progress of the project. Furthermore, the meetings were a great place to discuss unexpected results and possible future steps, providing me with both useful information and a clear path for the next steps of the project.

Next, I would like to thank Dr. Kristina Djanashvili and Dr. Robin de Kruijff for being members of my defense committee. As well as Astrid van der Meer for showing me around the lab and teaching me how to work with cells in a sterile environment. Without her I wouldn't have been able to perform any experiments successfully. Additionally, I would also like to thank Kristen David for helping me get acquainted with the confocal microscope set up at the PPE group, without whom I wouldn't have been able to add the final part of my research. Lastly of course, I can't forget all my fellow students, researchers and staff, who have kept me sane during this process by providing both help and some well-deserved distraction over the course of the last year.

To finish off, I would like to thank the Applied Radiation & Isotopes group for providing me with the opportunity, place and topic to base my research around. It was an honour, as well as a great learning experience to work here alongside you.

J. Berkhout
Delft, July 2022

Contents

1

Introduction

Modern medicine has come a long way compared to the early days of trying to heal diseases with different types of berries, leaves and other substances. Nevertheless, still many challenges are present nowadays in detecting, diagnosing and treating illness. A particularly difficult disease in this category is cancer, which is a general term for diseases where a portion of someone's cells grow uncontrollably and are able to spread and invade different body parts [1]. Cancer is undeniably one of the most widespread diseases in the modern developed world, as it is estimated that 39.5% of the population will be diagnosed with a type of cancer at some point in their life [2]. In the European Union alone this will amount to 2.7 million new cancer cases diagnosed in 2025, as well as 1.4 million cancer related deaths [3].

Problems arise quickly when diagnosing and treating cancer due to the ambiguous nature of the disease. There are currently more than 100 different types of cancer known [1] and the symptoms of these cancers can be rather non-specific by nature [4], which makes diagnosis difficult. Furthermore, in some cases patients tend to remain asymptomatic or are just asymptomatic in the beginning of the disease, therefore giving the disease time to develop and spread, further hindering possible (already difficult) treatment.

After diagnosis, the next step in a patients cancer trials is the actual treatment of cancer. Here, expectedly, more problems arise, specifically in the selectivity (or the lack thereof) of the types of treatment used. The chemotherapy and radiation therapy methods currently used lack the ability to differentiate between cancerous tissue and healthy tissue, therefore leading to side-effects in patients and in some cases even death [4]. Furthermore, metastasis (the spread of cancer cells from their place of origin to other parts in the body [5]) also increases the difficulty of treatment even more [4]. Finding methods to increase this selectivity is thus vital in the battle against cancer.

This all brings us to the current state of things. New and improved diagnosing and treatment methods are necessary to effectively tackle cancer. Specifically, some interest has been going out to using hyperthermia (HT) as a stand-alone method of treating cancers. This has been investigated since the early 1970's and is based on the direct cell-killing potential of temperatures above 41°C [6]. With different types of HT treatments possible [7] and also different ways of applying HT treatments [8], there is still much to be gained when investigating this technique, both as an individual treatment method, as well as, in combination with other treatment modalities [9]. Lately, it was suggested that to use HT in combined treatment alongside conventional treatment methods would improve the overall efficiency of cancer treatment [10][11][12][13]. These combined methods are already showing promise in terms of local tumour control, objective response rates and relapse free survival [14].

In this specific project the attention was directed towards cancer cells of the FaDu cell line, which is a type of head-and-neck cancer cells [15]. Specifically, the cells come from a hypopharyngael (bottom part of the throat) squamous cell carcinoma (SCC) [15]. Whilst skin SCC is the second most common form of skin cancer and mostly curable when diagnosed early [16], there are still an estimated

500000 cases of SCC of the head and neck diagnosed each year, which implies that the disease is still a significant public health problem worldwide [17]. Furthermore, the FaDu cell line is also somewhat radioresistant, meaning that consecutive irradiation of a tumour of this cancer type would result in non-optimal results [18]. In detail, FaDu cells demonstrate a more active DNA repair ability after radiation treatment (RT), by overexpressing the PARP1 enzyme, an important enzyme for initiating various forms of DNA repair [19]. Luckily, research already showed that HT has influence on the inhibition of DNA repair mechanisms associated with the PARP1 enzyme [20][21]. Warranting more research into this type of anti-cancer therapy.

To this end, this research report will try to find new information on this type of anti-cancer therapy. Specifically, this report will take a look into the topic of combined treatment. Hence, an attempt will be made to answer the questions whether there is an improved effect when combining both RT and HT by using 3D tumour models, spheroids, made of FaDu cells and if this effect can be qualitatively observed using different imaging modalities. However, preparing 3D spheroids from these cells to imitate *in vivo* tumours has proven to be difficult. In this thesis, a method utilizing a Matrigel® matrix for creating spheroids was used. The goals of this thesis are therefore to prepare 3D FaDu tumour models and to use them to determine the effect of single and combined RT and HT by investigating the growth and viability of *in vitro* spheroid culture. Furthermore, it was attempted to study the effect that these treatments have on the spheroids qualitatively using confocal microscopy by trying to visualize both live and dead cells in the spheroids.

2

Theory

The following chapter will give an overview of the theoretical background required to understand this report. Firstly, a section details information on the used cell line and different cell models, which are used to grow 3D aggregates of cancer cells. Following this, the different treatments used in this research and their effect on the working of cells are described. Next, information is provided on the means by which the different treatments can be delivered to the cancer cells, as well as models for the different treatment types to define the dose delivered by that treatment. Lastly, some information is given about the different methods used to visualize the viability of the used spheroids after treatment, both by using bioluminescence, as well as fluorescence imaging.

2.1. FaDu cell line

The basis of this research lies in the cell line that is used for all the different experiments. There are many different cancer cell lines used as *in vitro* tumour models, each with unique characteristics and responses to certain treatment types [22][23]. For this project the FaDu cell line was investigated. The origins of this cell line lie in 1968 when the cell line was established from cells of a hypopharyngael tumour, a tumour in the bottom part of the throat, from a patient with squamous cell carcinoma (SCC) [15]. SCC is characterized by abnormal, accelerated growth of squamous cells [16]. These squamous cells are found in the epidermis, the outer layer of the skin. When these squamous cells are exposed to ultraviolet light, DNA damage can occur in the cells, which can ultimately lead to the formation of a SCC [24].

The FaDu cell line is of particular interest as it is somewhat radioresistant. Consecutive irradiation of a tumour of this cell line would result in non-optimal results, with the effectiveness of treatment slowly decreasing over time [18]. Research showed that a culture of previously irradiated cells, FaDu-R cells, demonstrated a significantly higher cell survival rate when irradiated compared to normal FaDu cells, especially for treatment doses of 8 or 10 Gy [25]. One of the mechanisms behind this radioresistance is the overexpression of the PARP1 enzyme, which is important for initiating various forms of DNA repair. FaDu cells treated with radiation demonstrate a more active DNA repair ability by overexpressing this enzyme [19]. Furthermore, hypoxia and the presence of certain adaptor proteins also show to contribute to radioresistance in hypopharyngael tumours [26][27]. Overall, the radiosensitization of FaDu cells could prove vital in treatment of this type of cancer.

2.2. Cell aggregates

As it can be imagined, it is difficult to accurately determine *in vitro* the effect of different types of cancer treatments. This is due to the difficulty in reproducing the conditions tumours experience *in vivo* and as mentioned in the introduction the difficulty in creating tumour like aggregates *in vitro*. Furthermore, the use of animal and human test subjects poses more problems in the form of ethical concerns, availability of test subjects and for animal tests the ability to adequately predict clinical efficacy [28]. To this end multiple different models are used *in vitro* to study tumour cells. These are mainly classified in 2D and

3D models, both having their own advantages and disadvantages. The following section will discuss these different models and the relevance for this research.

2.2.1. From 2D models to 3D models

As of the present, *in vitro* 2D cell cultures are conventionally used to research different treatments in cancer biology. These cell cultures mainly consist of cells attached to a glass or plastic container submerged in growth medium. Under these conditions the cells will grow as a monolayer. This method of growth has certain advantages associated to it, those mainly being the simplicity of working with such cultures and the low-cost needed to maintain these cultures. Additionally, these cell cultures also show a favourable proliferation of cells and are easily reproducible [29]. Nevertheless, 2D cell cultures also show disadvantages compared to its 3D counterparts. The main problem arises when trying to replicate *in vivo* tumour structures and characteristics. These *in vivo* 3D cultures differ in cell-cell and cell-extracellular environment interactions, which in turn are responsible for most of the cellular functions of the tumours, influencing for example the proliferation of cells, the expression of certain genes and proteins and cell differentiation [30][31]. Whereas a 2D cell culture has more surface area that comes in contact with culture medium and plastic, therefore not replicating realistic physiological conditions [32]. Therefore, it can be concluded overall that 2D cultures differ in morphology compared to 3D cultures and thus lack the ability to mimic cell functions exhibited by *in vivo* tumours [33]. This means that moving from 2D to 3D models, although it might be difficult for certain models [34], is valuable in obtaining essential information when evaluating different types of cancer treatment [35].

2.2.2. Multicellular tumour spheroids

The most used 3D aggregates are multicellular tumour spheroids (MCTS), which were first described in the early 1970s [36]. This model is an intermediate form between complex *in vivo* tumours and 2D cultures [37]. This model immediately showed potential at providing information about the effects of nutrition and oxygenation on growth [38] and due to these similarities in proliferative and metabolic gradients, these spheroids are able to better reflect the complex environment of *in vivo* tumours [39][40]. Additionally, using the MCTS model later showed to be a more convenient method to evaluate post treatment tumour growth and cell survival as well [41].

The biological similarity between MCTS and actual tumours can also be shown schematically (see figure 2.1). Dependent on the size of the spheroids, these spheroids can display different layers within the spheroid each with their own characteristics. Spheroids typically show a diffusion limit of about 150-200 µm for molecules like oxygen, due to inter-cellular tight junctions and necrotic cells [42]. This results in smaller spheroids remaining well oxygenated, while larger spheroids of a size between 400-500 µm start showing gradients in oxygen and nutrients [43]. These larger spheroids will hence generally display 3 layers, which are more or less present in *in vivo* tumours as well. The outer layer is the proliferative zone. Here cells are rapidly multiplying as nutrients and oxygen are readily available. The second layer is the quiescent zone. In this zone the cells are still viable, however, due to a gradient decrease in both oxygen and nutrients, cells are less active compared to the outer cells. The final layer is the necrotic core of the spheroid. Here the cells have died due to necrosis and apoptosis resulting from a lack of nutrients and oxygen [43]. Now looking at figure 2.1, similar zones are also visible in actual tumours, except tumours are not spherical like the MCTS. This shows how MCTS can mimic real tumours more accurately compared to 2D cell cultures.

Additionally, as briefly mentioned above, 3D cultures also display cell-cell interactions and cell-extracellular interactions. The extracellular environment is often also known as the extracellular matrix (ECM) and impacts cell proliferation, differentiation, cell survival and sometimes functions of whole organs. [39][44]. Therefore, increasing the similarities in ECM by using spheroids also poses an additional advantage over 2D cultures.

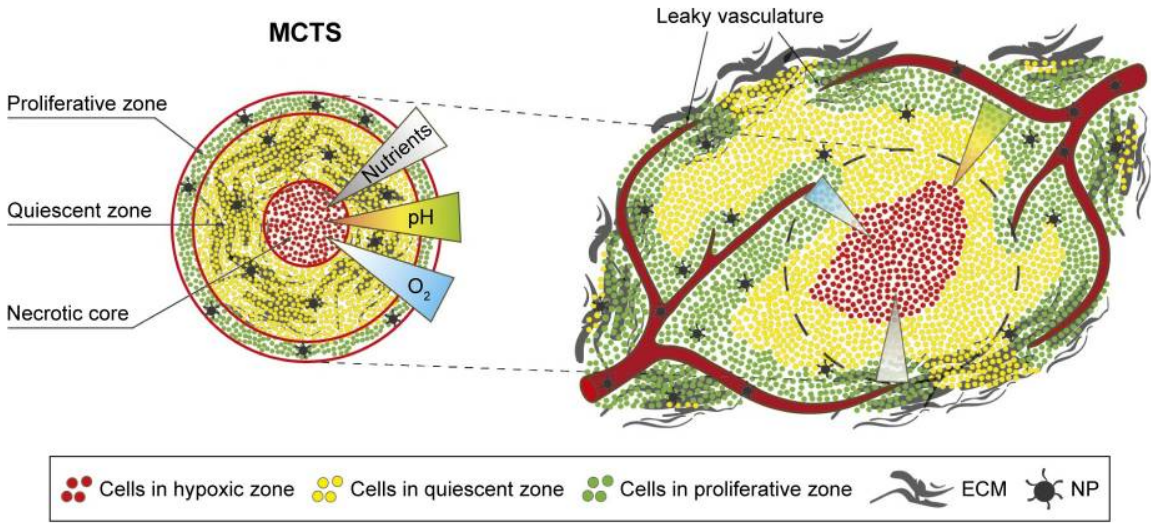

Figure 2.1: A schematical view of a tumour formed using the MCTS model (left) and an actual tumour (right). The MCTS tumour is composed of proliferative cells in the outer layer, quiescent cells in the middle layer and a necrotic core. Three concentration gradients (nutrients, pH and oxygen) are also shown to be comparable to the situation in an actual tumour. Extracellular matrix (ECM) and nanoparticles (NP) are also indicated. Taken from *Millard et al.* [41].

2.2.3. Spheroid growth

Now that the importance of taking the step from 2D cultures to 3D cultures has been established, it is time to look at methods to create 3D cell aggregates and specifically MCTS. MCTS are generally easily produced depending on the cell line used. Therefore, different methods have been established to produce these 3D cell aggregates, some of these methods will be described shortly in the following paragraph.

The first method is the hanging drop method. In this method a drop of cell suspension is placed hanging from a lid of a petri dish. After a while the cells will then accumulate at the tip of the drop and form spheroids. The second method is spontaneous spheroid formation. Ultra-low attachment plates are used in this method. These plates repel cells effectively and therefore forces the cancer cells to form aggregates, including spheroids. The third method makes use of suspension cultures. By keeping the cells suspended, adherence to surfaces is prevented and therefore in time the suspended cells will aggregate. Keeping the cells suspended can be done by either stirring or rotating the suspension or by increasing the viscosity of the medium. The fourth method is based on scaffold-based models. To this end, both natural or synthetic hydrogels are used to mimic the role of ECM *in vivo*, thus promoting cell-ECM interactions. To this end, both hydrogel coated plates are used to seed spheroids, as well as using a mixture of cells and hydrogel to seed spheroids [29][44][39].

2.3. Therapeutic background

Before the therapeutic response of treatments can be discussed, first an introduction must be given into the background of the two treatments relevant for this work, i.e. hyperthermia and radiotherapy. Therefore, in the following section, a short introduction is given into the origin of DNA damage, the mechanisms cells use to repair this damage and the means by which hyperthermia can influence these repair mechanisms.

2.3.1. DNA damage and repair

Deoxyribonucleic acid (DNA) is found in every living organism. It contains all genetic information in the two strands that DNA is composed of and therefore it is paramount for organisms to protect their DNA. Nevertheless, DNA will still always get exposed to mutations during the life cycle of an organism. These mutations can have different origins, some examples of origins being radiation, viruses, exposure to chemicals and problems during DNA replication [45][46]. For this research, damage done due to

radiation and the problems arising during DNA replication are mainly of interest. Damage done due to radiation can be classified in 2 main categories, those being direct damage and indirect damage. Both types of damage can be seen in figure 2.2. During the direct photon-DNA interaction the energy of incoming radiation is directly absorbed by the DNA, leading to damage of the DNA strands. The indirect interaction uses water radiolysis, where water is split into highly reactive free radicals. These free radicals are then capable of damaging DNA strands as well. When irradiated with x-rays both mechanisms affect DNA, with the direct interaction accounting for approximately 30% of total DNA damage and the indirect interaction for the remaining 70% [47]. Most of the time this damage can be repaired efficiently and reliably by DNA's own repair system, however under certain conditions repair can be unsuccessful and even impossible. The most noteworthy of the latter being DNA double-strand breaks (DSBs), this type of lesion is seen as the leading cause for cell death. Therefore, this specific type of DNA damage, specifically hindering the repair of this damage, is of interest when trying to improve the efficacy of anti-cancer treatment [48] [49].

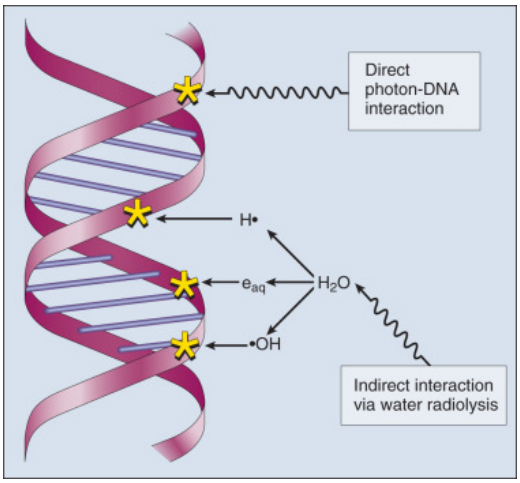

Figure 2.2: The two basic methods of DNA damage as a result of ionizing radiation. The direct effect happens when the incident photon directly reacts with the DNA. The indirect effect happens when the incident photon loses its energy by radiolyzing water, which creates reactive radicals that damage the DNA. Taken from *Zeman et al.* [47].

Once a DSB occurs in a cell, it will immediately start repairing the DNA damage. In the case of DSBs this is done using two different mechanisms, nonhomologous end joining (NHEJ) and homologous recombination (HR), where the relative contribution of each mechanism likely depends on the cell cycle stage in which the cell resides [46]. NHEJ is the faster method of the two, however it is also error-prone. The method directly connects broken strands back together without checking if there is homology between the two broken DNA ends. The mechanism therefore works quickly, but at the possible gain or loss of several nucleotides in a DNA strand [50]. On the contrary, HR repairs DNA without loss of genetic information. To this end, the broken strands are unwound and these unwound strands are introduced in a homologous DNA duplex molecule. This duplex acts as a template to resynthesize the missing nucleotides from the broken strands, resulting in two complete DNA molecules being left after the repairs are done [51][52].

2.3.2. Hyperthermia as a radiosensitizer

As briefly mentioned above, disturbing the repair of DSBs is an interesting way to increase the efficacy of anti-cancer treatment. Nevertheless, this is not the only way in which treatment efficacy can be improved. Like mentioned in the introduction, hyperthermia is of particular interest in this topic. Hyperthermia or heat treatment (HT) is a medical treatment type, which is based on heating up tumours to treat the cancer or sensitize it to different treatment modalities. HT has shown to induce multiple different biological effects in tumours, including inhibition of certain DNA repair mechanisms, but also inducing more direct tumour cell killing [53][54]. These effects have been seen from temperatures as low as 39°C [55][56].

The effects HT has on the effectiveness of radiotherapy and chemotherapy can be arranged in two groups. Additive effects, where using HT will linearly increase the effect of treatment, and synergistic effects, where there will be a nonlinear increase in efficacy of treatment when combined with other treatment modalities. Both types of effects can be seen in figure 2.3. As can be seen these effects range from increasing vasodilation (the widening of blood vessels) at low temperatures, to inhibiting DNA repair at higher temperatures. Some of these important effects will be shortly discussed, starting with inhibiting DNA repair. During DNA repair, like in all processes inside a living body, multiple different proteins will be active [56], which are vital for executing DNA repair correctly. Both NHEJ and HR are affected by HT, with HT decreasing the activity of DNA-PKcs [57], a protein which plays an important role in NHEJ, and degrading the BRCA2 and reducing BRCA1 proteins, which are vital for completing HR [58]. The synergistic effect here is easily seen, as less DNA breaks being repaired leads to more residual DNA breaks being left and this in turn leads to cell cycle arrest and apoptosis [53]. Moving on to some of the other aforementioned effects. Most of these effects have to do with reoxygenation of areas inside tumours. Hypoxia, the deprivation of oxygen, is generally seen as an adverse prognostic factor[59]. Using HT to counteract hypoxia has therefore shown correlation with improved clinical results [60]. HT can increase oxygenation by increasing the blood flow to tumour cells by vasodilation. This increase in oxygenation in turn increases the efficiency of radiotherapy [61]. Additionally, on a physiological scale, HT at higher temperatures will also directly induce more tumour cell killing by inducing the clotting of blood vessels [53][62].

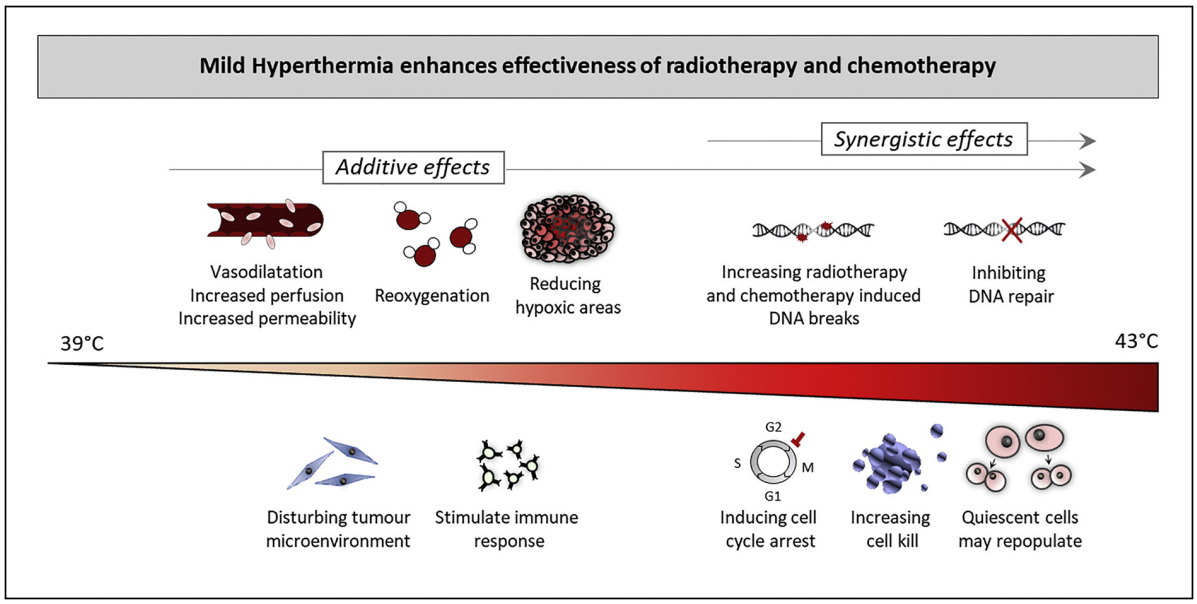

Figure 2.3: The effect which enhance the effectiveness of radiotherapy and chemotherapy when using mild HT. Increasing the temperature at which HT is performed increases the amount of additive and synergistic effects that will influence the efficacy of other treatment modalities. Taken from *Oei et al.* [53].

2.4. Therapeutic response

To examine the therapeutic response on the used spheroids three different treatment types are used. Radiotherapy, hyperthermia and combined treatment. In the following sections, all three types are discussed including information about the methods in which the treatments can be administered, the dose a treatment is associated with and problems with the treatment types.

2.4.1. Radiotherapy

Radiotherapy or radiation treatment (RT), is the most straightforward treatment method, in which tumour cells are bombarded with ionizing radiation as a means to damage the DNA in the cells, thus resulting in the cells no longer being able to proliferate. Problems with radiation are that it is non-specific, meaning that upon irradiation of tissue, healthy cells are also affected. Furthermore, to target entire tumour structures evenly is also a problem. The dose transferred by radiation is quantified using

the Gray (Gy) unit, which is equivalent to the transferred energy per unit mass (J/kg).

In this research specifically x-rays are used as a source of ionizing radiation. X-rays are produced in an x-ray tube. In an x-ray tube there are both a positively charged anode and a negatively charged cathode with a tungsten filament, which are under the influence of a very high voltage. Due to this voltage, the filament heats up and expels its surface electrons. The freed electrons are then accelerated by the electric field between the cathode and the anode towards the anode. When the freed electrons collide with the anode they lose their energy, both in the form of heat and x-rays [63]. These x-rays can then be used to irradiate targets, like tumour cells. The radiation doses used in this research are shown in table 3.1.

2.4.2. Hyperthermia

Hyperthermia or heat treatment (HT), is the second used treatment type in this research. HT is defined as "an artificial way of increasing the body tissue temperature by delivering heat obtained from external sources to destroy cancerous cells or prevent their further growth" [64]. So like mentioned above and in the definition heating tumour cells can directly destroy tissue, however it is used more commonly as a sensitizer for other treatment modalities, as heating can make the cancer cells more susceptible to other treatment methods by means of increased vascular permeability, increased blood flow, increased oxygenation of the tumour cells and inhibition of DNA repair [65]. HT is mainly used in three clinical applications: local, regional and whole-body HT, which are used for localized, advanced or deep seated and metastatic tumours, respectively [64]. Additionally, HT can be applied using multiple different methods to apply heat, including using microwaves, ultrasound, radiofrequency, or by directly heating up blood using perfusion and even using magnetic nanoparticles [8][64]. For this research, as experiments are only performed *in vitro*, HT is applied using a simple water bath.

After finding a way to apply HT, it is important to find a suitable relationship between temperature and exposure time, to be able to measure the dose delivered to tumour cells. Luckily the majority of biological systems exhibit a similar exponential relationship for this, as seen in equation 2.1 [66].

$$t_1 = t_2 R^{(T_1 - T_2)} \tag{2.1}$$

This equation shows the relationship between the time (t) and the temperature (T) as a function of R, which can be calculated using ΔH (the activation energy) and the absolute temperature from an Arrhenius plot. In general it is assumed that the value of R is constant depending on the temperature used. With R = 0.5 for temperatures greater than 43°C and R = 0.25 for temperatures below 43°C [66]. 43°C is therefore a useful temperature to use as an anchor point, to make sure different treatments are equivalent for comparison. Thus using this information, a general method to compare different treatments is obtained. The resulting thermal dose delivered in HT is provided in the general unit of cumulative effective minutes at 43°C (CEM_{43}), which is a normalizing method aimed to convert various different HT treatments into a comparable exposure time at the arbitrary reference temperature of 43°C [67]. The general equation for this can be seen in equation 2.2.

$$CEM_{43} = \int_0^t R^{(43-T)} dt \tag{2.2}$$

In this equation T is the actual applied temperature during treatment to the target tissue, t is the time in minutes during which the treatment is applied and R is a factor to compensate for a 1°C temperature change. This R value has the same values as above, so for T>43 R = 0.5 and for T<43 R = 0.25. Meaning that for a 1°C change above 43°C the equivalent time at 43°C doubles, whilst a similar temperature change below 43°C results in a fourfold decrease in the equivalent time [66]. Even though this model is often used in studies to find thermal dose-effect relationships, it still has its limitations compared to other models. Specifically, the model lacks in representation of thermally induced damage or cell-death [68]. Nevertheless, this model will still be used in this research to determine thermal doses, due to its simplicity and comparability. The eventual thermal doses used in this research can be found in table 3.2.

2.4.3. Combined treatment

Like mentioned before, combining treatment modalities has certain benefits, both in direct cell killing potential, as well as in sensitizing cells for different types of treatments. Similar to HT, it is therefore of importance to figure out a relationship to show the increased effect when combining treatment types. The model, however, does not need to make the dose of the treatments equivalent in terms of one overarching value, like the CEM_{43} model for HT. As treatments can be compared by simply looking at the doses of single treatments. Additionally, it is also important for this model to keep in mind that both the order in which HT and RT are administered and the time period between both treatments also influences that combined effect. Research showed that performing both treatments simultaneously maximizes the cell killing potential [69], whilst increasing the time period between both treatments (regardless of order) rapidly decreases the radiosensitisation achieved by the HT [61].

A model that considers most of these factors is the Thermal Enhancement Ratio model (TER), the definition of which is best shown in a formula, as shown in equation 2.3 [70].

$$TER = \frac{dose\ of\ radiation\ alone\ to\ achieve\ end\ point}{dose\ of\ radiation\ combined\ with\ heat\ to\ achieve\ end\ point} \tag{2.3}$$

Although this equation is an oversimplification of the actual mathematical equations that follow from this model, it does neatly show the end goal of the model. The model itself simply shows the effectiveness of the radiosensitisation, the higher the TER, the more effective the combined treatment is and the other way around.

2.5. Analytical techniques

The following section will discuss the different techniques used in this research and the theoretical background behind those techniques. To this end, an insight is provided to an indirect means of assessing the viability of samples using bioluminescence, as well as a method using immunofluorescence to analyse the viability of samples and composition of spheroids. The spheroids used in this research are also evaluated visually using a microscope and a camera, which does not necessitate further explanation, apart from the methods used, which will be discussed in chapter 3.

2.5.1. Bioluminescence

The first analytic method used to assess spheroids is based on bioluminescence, which is defined as a class of enzyme-catalyzed reactions. Specifically, in these reactions enzymes (luciferases) react with molecular oxygen, co-factors (most notably cytoplasmic ATP) and substrates (luciferins). The breakdown of the latter together with the co-factors provides energy to autonomously excite photons, which can then be observed [71].

In this research an ATP-based 3D CellTiter-Glo® assay (Promega, Madison, USA) was used. The working principle of this assay is based on the Ultra-Glo™ rLuciferase enzyme, which converts luciferin during the assay using cytoplasmic ATP in the cells as a co-factor [72]. During this conversion light is created that can be observed and quantified using a spectrophotometer. The process can also been seen in figure 2.4. The CellTiter-Glo® assay is often praised for its sensitivity, robustness and simplicity, which in turn allows for a high throughput screening [72][73]. Furthermore, when working with larger spheroids (350-850 um), the method showed to be the best and most reproducible way of determining the viability of these spheroids compared to the Trypan blue exclusion test and the Perfecta3D-Cell Viability assay [74] (two different cell viability assays). An additional advantage of the CellTiter-Glo® assay is the inhibition of endogenous ATPases, which are enzymes that degrade ATP during cell death, resulting in decreasing ATP levels once the metabolism of a cell stops [75].

Nevertheless, this method also has some drawbacks. Starting with the fact, that the inhibitors that keep the ATP stable in live cells, will also work in dead cells. Although the concentration of ATP will rapidly decrease upon cell death, there is always still a chance of some ATP being left behind, which in turn would influence the results. Furthermore, the method gives an indication of ATP presence in a spheroid, yet it gives no information about the origin of this ATP. Subsequently, no quantitative conclusion can be made about the number of living cells in a spheroid. Only a control group can be compared to treated groups. A direct method of differentiating between live and dead cells could therefore still be of use. In the next section a direct method will be discussed.

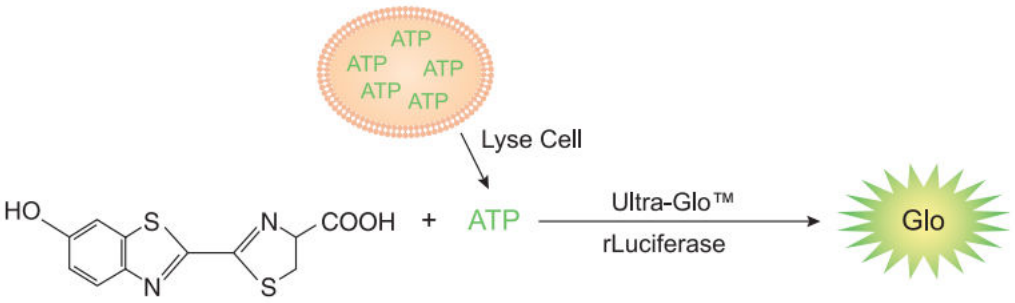

Figure 2.4: Basic working principle of luciferin (on the left) in the CellTiter-Glo® assay taken from *Fan et al.* [76].

2.5.2. Immunofluorescence

Immunofluorescence is an overarching term that describes techniques that utilize fluorescent-labeled antibodies to detect specific target antigens [77]. Like the name suggests, the technique is based around fluorescence, which is the phenomenon that certain molecules, known as fluorophores, have the ability to emit light after absorbing light of a typically shorter wavelength. In most cases the time between both excitation and emission is in the range of only nanoseconds. If the exciting light is then filtered out during data acquisition, it is possible to only see the objects that are fluorescent [78]. Moving back to the 'immuno' part of immunofluorescence. These fluorescent-labeled antibodies will only bind to their antigen counterpart. When these antibodies are then excited by light of the right wavelength, they will start emitting light at a certain wavelength [79]. If this light is then detected the location of that antigen can be located. Nowadays fluorescent-labeled antibodies exist for most antibodies, meaning it is only necessary to look into the antigens that are of interest for an experiment. Furthermore, there are multiple different immunofluorescence techniques, like direct and indirect immunofluorescence and complement binding indirect fluorescence [80] each with their own advantages and disadvantages. For this research direct immunofluorescence is the most important, as it is the only type used. This type of immunofluorescence uses a single antibody, which directly targets the antigen of interest. Subsequently, this antibody is also fluorescently-labeled, meaning it can immediately be detected using immunofluorescence [81].

Fluorescence microscopy

An easy way to detect fluorescence in samples is by using a fluorescence microscope. The principle of which is easy to understand. Excite a sample using light of a certain wavelength and block that same light upon returning to see the remaining fluorescence. The easiest way of blocking the returning light is by using filters [78][82]. One type of microscope was of particular interest for this research, that microscope being the confocal microscope. In confocal microscopy a laser is used to illuminate a certain spot of a sample at a certain depth with light of a predetermined wavelength. This results in fluorescence in this exact spot, which can then be detected. However, before this light is detected, it travels through a pinhole inside the optical pathway, thus cutting off any light signal that is out of focus, resulting in a sharper image of only the illuminated spot [83][84]. A schematical layout of a basic confocal microscope can be seen in figure 2.5. The dichroic mirror in the middle only allows for a certain small range of wavelengths to pass through. By changing the depth of the optical plane observed, 3D structures can be analyzed, albeit still limited by the sample penetration depth.

Fluorophores

A plethora of different fluorescent-labeled antibodies are used to investigate different types of cancer. However, other fluorescent compounds are used to stain cells, these are known as fluophores. Three compounds, which are important for this research, are discussed here. The first fluorophore pair is the pair of calcein-AM and ethidium homodimer-1. This pair is used in immunofluorescence as a fluorescent LIVE/DEAD viability assay [85]. Calcein-AM is responsible for the live part of this assay. It is nonfluorescent in this state, it is however cell-permeant, meaning it is able to enter cells freely. After this compound has permeated into living cells, it is cleaved by nonspecific esterase in those

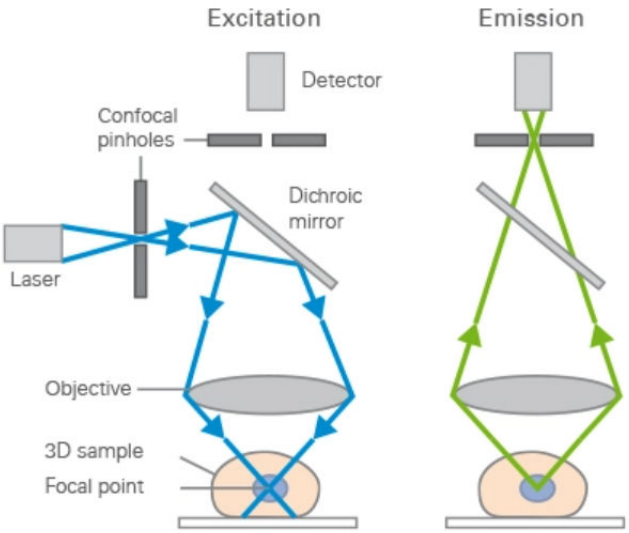

Figure 2.5: Excitation and emission light pathways in a basic confocal microscope configuration taken from *Ibidi®Confocal Microscopy* [83].

cells, producing calcein. This process can be seen in figure 2.6. Calcein is well retained in cells and is additionally fluorescent. Furthermore, when illuminating calcein stained cells with light of a wavelength of 495 nm, green fluorescence will occur at an emission wavelength of around 515 nm. Ethidium homodimer-1, on the other hand, is responsible for detecting dead cells. This compound readily enters cells with damaged cell membranes. Once it has entered the cell, it binds to the DNA in the cell with high affinity. In turn this results in a 40-fold enhancement of fluorescence of the compound. Upon illuminating these cells with light of a wavelength of 495 nm, the ethidium homodimer-1 will emit a bright red fluorescence at a wavelength of around 635 nm [86][87]. Resulting in a spectrum that shows live cells in green and dead cells in red, allowing for excellent differentiation between live and dead cells.

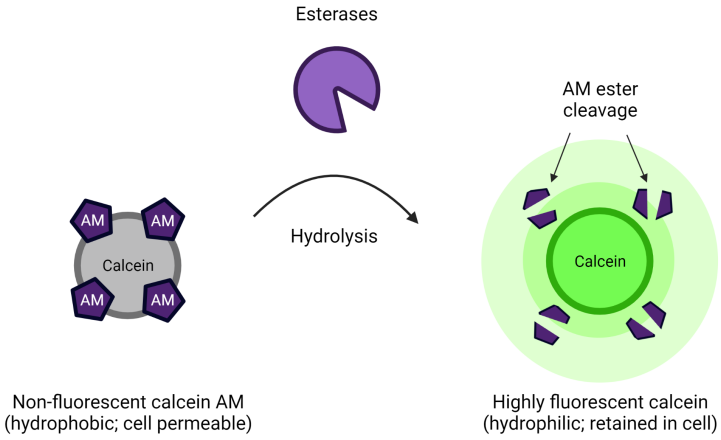

Figure 2.6: Non-specific intracellular esterase cleavage of AM ester groups converts calcein-AM into highly fluorescent calcein taken from *AAT Bioquest Calcein* [88].

The second fluorophore of interest for this research is propidium iodide (PI), which is a compound used to evaluate apoptosis in cells cultures [89]. PI behaves similarly to ethidium homodimer-1, as it is only permeable in dead cells in which it binds to DNA. Once bound, the fluorescence of the compound is enhanced 20- to 30-fold. The fluorophore can also be excited by light with a wavelength of 535 nm and in turn it emits light at a wavelength of 617 nm. This results in dead cells being shown as bright red when using PI during fluorescence imaging [90].

3

Materials & Methods

In this chapter an overview is presented of the used materials and methods during this research. First, a look will be taken at the methods used to culture the cells and how to create the spheroids used in this research. Then the methods and doses for the RT and HT and the combined treatments will be discussed, as well as the method to measure cell viability. This is followed by an overview of the fluorescence methods used in this research. Lastly, a short description of the data analysis performed during this research is given. All work with cells was conducted in a sterile *in vitro* environment using an Interflow laminar flow cabinet.

3.1. Cell culturing and Spheroid formation

3.1.1. Cell culturing

The FaDu cell line which was used in this research was obtained from the Erasmus MC department of genetics. Cells were cultivated in cell adherent culture flasks, which were kept in a humidified Hera Cell incubator at 37°C and 5% CO_2, when not being used. The cells were constantly kept in a culture medium, which contained equal parts Ham's F10 with L-Glutamine (F10, L0140-500, Biowest) and Dulbecco's Modified Eagle Medium (DMEM, L0103-500, 4.5 g/L glucose, Biowest). This mixture was supplemented with 10% Fetal Bovine Serum (FBS, S1810-500, Biowest) and 1% Penicillin/Streptomycin solution (Pen/Strep, 100x diluted, L0022-100, Biowest). Culture flasks were examined every other day using an inverted microscope. Cells were sub-cultured upon reaching approximately 80% confluency, which occurred about 5-7 days after initial culturing. During sub-culturing first the old culture medium was removed, before washing the still adherent cells with Dulbecco's Phosphate Buffered Saline (PBS, L0615-1000, Biowest). Cells were then resuspended using 1 mL Trypsin-EDTA 1x solution (L0930-100, Biowest). After all cells were resuspended and detached from each other a small portion (around 100 µL) was placed in a new culture flask with 5 mL of fresh culture medium.

3.1.2. Spheroid formation

After sub-culturing the leftover Trypsin-EDTA solution with cells was placed in a 10 mL tube and to that about 4 mL of culture medium was added, to reach 5 mL of cell solution. This solution was then centrifuged at 2000 rpm for 5 minutes using a VWR CompactStar CS 4 centrifuge. After this, the culture medium in the tube contained mostly dead cells and the live cells formed a pellet at the bottom of the tube. The culture medium was subsequently removed and to the live cell pellet 1 mL of fresh culture medium was added. The cells were then resuspended by lightly tapping the tube for a while and the resulting concentration of cells was counted using a Luna-II™ Automated Cell counter (Logos Biosystems). This information was then used to seed spheroids at a concentration of 2000 cells per 200 µL (determined in earlier research in the same group) of culture medium in cell-repellent, U-shaped 96-well plates (Greiner Bio-One GmbH, CELLSTAR®), which was supplemented with 1% Matrigel® Basement Membrane Matrix (Corning®). The outer ring of wells on the plate was filled with PBS to limit evaporation of culture medium during the experiments. After seeding the plate was centrifuged for 10 minutes at 14-15°C at 1000-1500 rpm to ensure all cells were in the bottom of the well. The plates were then left alone for at least 3 days to not unnecessarily disturb the forming spheroids.

3.2. Treatment methods and analytical techniques

Moving on to the treatments used in this research. Both individual as well as combined HT and RT were used, nevertheless all experiments followed the same standard schedule. This schedule can be seen in figure 3.1.

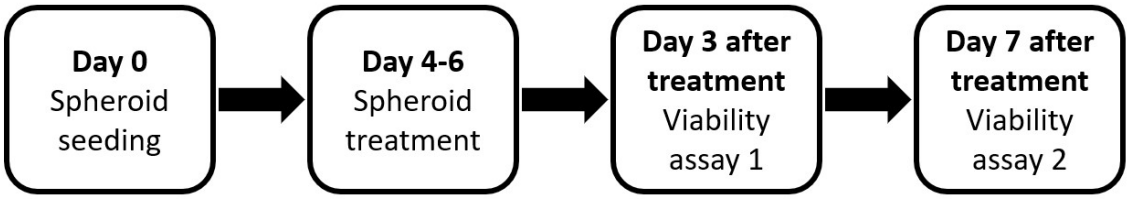

Figure 3.1: Standard treatment schedule

On day 0 the spheroids were seeded according to the method described above. After 4-6 days (depending on the spheroid size) the spheroids were inspected, photographed and measured. Once the spheroids were found to be at the desirable starting size of around 300 µm treatment could be applied to the spheroids. After all the treatments were done, 100 µL of culture medium in the wells was replaced, followed by a period of 3 days during which the spheroids were not disturbed. After these 3 days the first viability assay was performed. During this assay half of the seeded spheroids were used and discarded (usually 3-6 spheroids) and 100 µL of culture medium was refreshed for the remaining spheroids. On day 7 after treatment the second viability assay was performed using the remaining spheroids. Before every viability assay all spheroids were also inspected, photographed and measured. After seeding and between every step in the experiment schedule the spheroids were also incubated at 37°C and 5% CO_2.

Each time the spheroids were used for any kind of treatment, they were first inspected using an inverted bright-field light microscope. Followed by the spheroids being photographed. This was done using a 12MP camera, which was mounted on a binocular microscope with a 4x objective. This microscope was fitted with a moving platform that was able to accurately capture each well of the 96-well plates using in-house designed automated imaging software called SampleScan. These images were then analyzed using the free open-source image processing software ImageJ, which is elaborated on in chapter 3.3.

3.2.1. Radiotherapy

First, single RT was carried out. This treatment was done using an x-ray tube, specifically the x-ray beam was produced by an YXLON x-ray tube with a tungsten anode (YXLON International GmbH, Y.TU 320-D03, 3mm Beryllium filter with a wolfram anode). The x-ray tube was setup to produce a dose rate of approximately 30 Gy/h. To this end, the samples were placed around 30 cm from the radiation source within the x-ray tube and the tube itself was setup to produce x-rays at 300 kV, 5 mA, a 5.5 FOC using a 83 keV copper-filter (4 mm of copper) to harden the x-ray beam. The precise dose rate was determined before starting each treatment, this was done using a M23361 ionization chamber (PTW-Freiburg) to detect the radiation and a UNIDOS E T10008 universal dosimeter (PWT-Freiburg), which had been calibrated beforehand.

Three different doses of radiation were used during the individual RT, alongside an untreated control group. The 3 different doses can be seen in table 3.1. During irradiation the spheroids were kept in the 96-well plate and only the appropriate spheroids were irradiated, the other spheroids being covered with lead plating. Additionally, the 96-well plate was sealed using a strip of Parafilm to avoid contamination of the spheroids during treatment.

3.2.2. Hyperthermia

The second individual treatment used was HT. This type of treatment was performed by first transferring the spheroids to individual U-shaped 8-well microplate strips (Greiner Bio-One GmbH). These strips

Table 3.1: The different radiation doses and their respective irradiation times used during individual RT.

Dose	Irradiation time
2 Gy	4 min
6 Gy	12 min
10 Gy	20 min

were then covered with a piece of Parafilm, again to avoid contamination of the spheroids and finally the strips were placed in a water bath. This water bath was kept at a specific temperature, depending on the thermal dose necessary, and the strips were kept in the water bath for a specific amount of time, also depending on the thermal dose necessary. The water bath used was a temperature-controlled precision immersion bath (Optima TX150, Grant), alongside an in-house made tray to keep the opening of the spheroid strips above the water. Before each treatment the water level was checked to ensure full encapsulation of the spheroids by water. After the necessary time had elapsed the strips were removed from the water bath and the spheroids were placed back in the original 96 well plate.

During the individual HT 5 different thermal doses and an untreated control group were used. These individual doses and their respective time and temperature settings can be seen in table 3.2. The thermal dose is given in cumulative effective minutes at 43°C (CEM_{43}) as described above.

Table 3.2: The different thermal doses and their respective exposure times and temperatures used during individual HT.

Thermal dose	Temperature	Exposure time
1 CEM_{43}	41°C	15 min
5 CEM_{43}	43°C	5 min
30 CEM_{43}	43°C	30 min
120 CEM_{43}	45°C	30 min
480 CEM_{43}	46°C	60 min

3.2.3. Combined treatment

The last type of treatment used was combined RT and HT, also known as CT. During this type of treatment identical procedures were followed compared to the individual treatments. However, during this treatment RT and HT would be applied to the same spheroids following each other. Between the RT and HT the spheroids were incubated for approximately 30 minutes at 37°C and 5% CO_2. Only certain doses of the individual treatments were chosen to be used. This followed from the results of the individual treatments, as doses were chosen which did show an effect on the spheroids, but were not excessively damaging the spheroids on their own. The different orders of the treatments were distinguished between by using the terms RTHT, meaning RT followed by HT, and HTRT, meaning HT followed by RT. The CT doses used in the research can be seen in table 3.3. Furthermore, an untreated control group was also used as a reference point for CT.

Table 3.3: The different combined doses used during CT.

HTRT	RTHT
30 CEM_{43}, 2 Gy	2 Gy, 30 CEM_{43}
30 CEM_{43}, 6 Gy	2 Gy, 120 CEM_{43}
120 CEM_{43}, 2 Gy	6 Gy, 30 CEM_{43}
120 CEM_{43}, 6 Gy	6 Gy, 120 CEM_{43}

3.2.4. Viability assay

Moving on to the method used to complete the viability assays. The working principle of this assay was described in chapter 2.5.1. For this research, a different method was used compared to the method that accompanies the assay kit on purchase [91]. This was done following earlier research done using these spheroids, finding this new method better equipped to handle the spheroids formed using Matrigel®.

The actual method used on day 3 and 7 after treatment started with all spheroids being imaged, like mentioned above. From these images, the spheroids that should be used for the viability assay were selected. After this selection process the assay could start. The first step was to remove as much medium from the spheroid wells as possible. Afterwards, 200 µL of PBS were added, to wash away the remaining cell medium and dead cells. The PBS was then removed as well, after which 200 µL of a 1:1 mixture of cell medium and 3D CellTiter-Glo® was added to the wells. The spheroids were then incubated for 15 minutes, before they were washed in the mixture. Washing was done by pipetting the spheroids up and down around 10 times in the mixture. Subsequently, the spheroids were incubated again. Washing of the spheroids was repeated thrice, resulting in the spheroids being incubated in the mixture for a total length of 60 minutes. Between each step the spheroids were also inspected with a microscope to check if the spheroids were starting to dissociate. If this was not the case a fourth wash and fifth incubate period was added to the method. Once the spheroids were falling apart and the method was completed the spheroids were transferred to a 96 well white bottom plate (ThermoFischer Scientific ®) and the remaining spheroids (which were not used in the viability assay) were placed back in the incubator. The white plate was then transferred to a Cary Eclipse Fluorescence Spectrophotometer (Agilent Technologies) with a microplate reader accessory. Using this accessory, the spectrophotometer was able to measure the bioluminescence of individual wells of the white plate accurately. The bioluminescence was measured using a specific method in Agilent Advanced Reads software, the settings of which can be seen in table 3.4. Only the gate time (measurement time) was varied between measurements, to make sure the detected bioluminescence remained within a detectable range. Furthermore, the measurement was repeated thrice to ensure the measured values were accurate. Afterwards, the data was exported to be analyzed and the spheroids were discarded. The measured viability data was normalized by comparing the results to the mean of the control group of that experiment. The resulting viability was expressed as a percentage of the control.

Table 3.4: Setup used to measure bioluminescence.

Setting	Value
Gate time (ms)	Variable
Emission wavelength (nm)	600
Emission slit (nm)	20
Emission filter	open
PMT voltage (V)	ON

3.2.5. Confocal microscopy

To perform experiments using confocal microscopy a LSM 710 system for fluorescence imaging (Zeiss) was used. This system consisted of an Observer Z.1 inverted microscope stand (Zeiss) with transmitted light (HAL 100), UV (HBO 50) and laser illumination sources. Additionally, the stage of the microscope is completely motorized, as well as the z-drive for focusing and the objective turret. The laser illumination consisted of an Argon Laser (LASOS), which was able to use 4 different lasers, namely a 405 nm Diode laser, an Argon laser (which could produce laser light at 458, 488 and 514 nm) and two different Helium Neon lasers, which could produce laser light at 543 nm and 633 nm. The objective turret supported 5 objectives, these being a 2.5x (air), 10x (air), 20x (air) and two 40x (oil) objectives. For this research mainly the 2.5x and the 10x objective were used. Furthermore, the system was equipped with an AxioCam MRm camera (Zeiss). Lastly, images were captured and the system was controlled using ZEN (black edition, Zeiss) software. Whilst images were being captured the room was kept as dark as possible to minimize background noise.

3.2.6. Fluorescence imaging

The 2 different methods for immunostaining mentioned in chapter 2.5.2 were used. A LIVE/DEAD® Viability/Cytotoxicity kit (L3224, Invitrogen, Therma Fischer Scientific) was used. A solution of 4:1 ethidium homodimer-1 and calcein-AM was made to be used for immunostaining. The staining itself was done by first transferring the spheroids including medium to 8-well μ-slides (Ibidi GmbH). Then, the medium was removed and the spheroids were washed up to 3 times with PBS, by adding 200 μL of PBS and removing it again each time. This was done to make sure any loose dead cells were removed.

After the final wash 200 μL of the LIVE/DEAD$_{®}$ was added. These slides were then incubated for at least 30 minutes, before the spheroids were imaged using the confocal microscope. The spheroids were observed using the 2.5x objective. During imaging the spheroids were illuminated by the 488 nm argon laser at a laser line attenuator transmission of 5, a gain of 750 and a pinhole opening of 18.8 μm. Fluorescence was detected at around 515 nm for the calcein and 635 nm for the ethidium homodimer-1. Afterwards the spheroids were removed from the staining kit and placed back in a 96-well plate with normal culture medium. This type of staining was done 7 days after treatment.

The second method involved the aforementioned PI (25535-16-4, Sigma-Aldrich). Staining with PI was done by adding PI straight to the used culture medium. This was done as it was found that PI does not influence growth of spheroids when added to the culture medium [92]. PI was added at a concentration of 5 μg/mL. As there was difficulty with accurately weighing such low amounts, the culture medium with PI was made in large batches of up to 50 mL. Again spheroids were incubated for at least 30 minutes after staining [93]. Imaging was done using the 10x objective to focus on individual spheroids. During imaging, the spheroids were illuminated by the 543 nm helium neon laser at a laser line attenuator transmission of 5, a gain of 650 and a pinhole opening of 95 μm. The resulting fluorescence were observed in a spectrum around 617 nm. After imaging the spheroids were transferred back to their original 96-well plate and the PI filled medium was replaced by normal fresh culture medium, to ensure the spheroids grow like normal. PI staining was done to follow the behaviour of spheroids over a longer period of time. To that end, the spheroids were first stained and imaged the day before treatment and the day after treatment. After that the spheroids were imaged every 2 to 3 days for up to 2 weeks.

3.3. Data analysis

As mentioned above, every spheroid was imaged multiple times over the course of an experiment. All these images were analyzed using either ImageJ or ZEN 3.5 (Blue edition, Zeiss) freeware depending on the microscope the image was taken with. The use of both software types will be shortly discussed in the following section.

Starting with ImageJ. ImageJ was used to estimate the size of the spheroids for the images captured with the normal microscope. First, the system was calibrated using glass beads of a known size. With this calibration, the images could be scaled in ImageJ. Following that, the images were turned into 16-bit images to increase the contrast between the spheroid and the surrounding medium, after which the area of the spheroid was selected and measured using ImageJ. After using different techniques to measure (or calculate) the diameter of the spheroids, it was chosen to use the Feret's diameter function of ImageJ. Feret's diameter is defined as the longest distance between any two points along the selection boundary [94]. This method was chosen as the spheroids are assumed to be spherical, meaning the longest distance between two points would only result in a small error. The measured diameter of the spheroids was then transferred to Excel to be processed. Spheroids that were not predominantly spherical, like spheroids affected by fibers in the medium used, were disused before measurement as their size and shape would disturb the results gotten from the actual spherical spheroids.

Table 3.5: The different signs used in result graphs to indicate the significance of results. Herein ns indicates no significance present and an increase in stars indicates an increase in significance.

Sign	P-value
ns	0.1234
*	0.0332
**	0.0021
***	0.0002
****	<0.0001

The resulting measured data was then copied to GraphPad Prism (version 8.0.2, GraphPad Software, Dotmatics) to create different graphs. In these graphs all results were presented by the mean $\pm$ the standard deviation. The number of spheroids used to calculate the mean (n) differs between

experiments and will be mentioned for each experiment individually in the next chapter. Statistical analysis was also performed using GraphPad. P-values, the significance level at which the comparison between results would barely be considered significant, were determined for comparable sets of viability results using the two-way ANOVA function of GraphPad followed by the Bonferroni's multiple comparisons correction. Results with a P-value of $p < 0.05$ were found to be in the selected 95% confidence interval and thus these results were assumed to be significantly different. The level of significance is also indicated in the graphs following the guidelines shown in table 3.5.

The images taken using the confocal microscope were evaluated using ZEN 3.5 freeware. This software was used to adjust the images to limit background noise. Afterwards, the adjusted images could be exported to be used elsewhere.

4

Results

In the following chapter the results of the experiments performed during the research will be displayed, along with a description of those results. This is done with the goal in mind to show the differences between different single treatments and to show the change in effect when combining those treatments. To this end, first the single treatments will be discussed, followed by the combined treatments and lastly the results of the confocal microscopy will be discussed.

4.1. Growth experiments

In the beginning of the research a simple experiment was done to get accustomed with working with cells, in addition to getting a baseline as to how large the spheroids would grow and how quickly they would reach that size. The results of these experiment are discussed in the following section.

The spheroids were cultivated in a 96-well plate, 26 wells of the plate were seeded with 2000 cancer cells, half of which were cultured with Matrigel® and the other half without Matrigel®. These spheroids were then observed for 28 days after initial seeding, with images being taken of the spheroids every 3 days. As it was one of the first experiments done, some errors were still present in the method. As a result, during this experiment the culture medium was not refreshed every 3 days, which could well have limited growth. Initially, there were 13 spheroids for both groups, however after 4 days 4 spheroids of both groups were used in different experiments, leaving only 9 spheroids for the remaining days. The results of this experiment can be seen in figure 4.1.

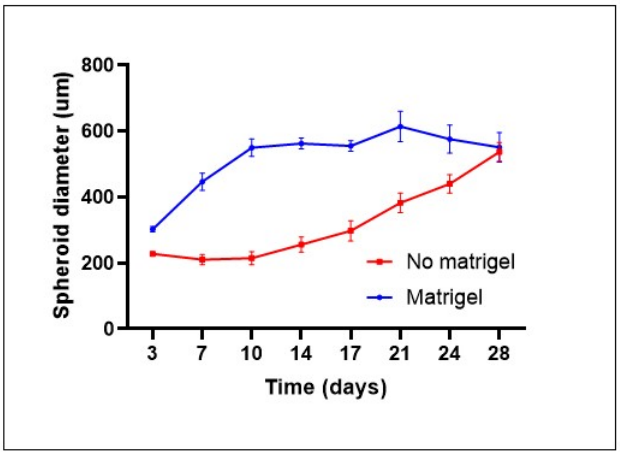

Figure 4.1: Spheroid diameter growth for spheroids cultured with Matrigel® and without as a function of time. The spheroids were untreated and observed for 28 days after initial seeding.

Looking at the figure, it is quickly seen that the growth of the spheroids cultured with Matrigel® is significantly faster compared to the spheroids cultured without it. Additionally, the spheroids started at a size of about 303 μm and reached a final size of around 550 μm after 10 days, after which the growth stopped. The group cultured without Matrigel® on the other hand shows no growth at all until day 10, after day 10 the growth rate increases over the final 18 days of the experiment. Both groups reach a similar size at the final measurement on day 28 and the error for both groups remains well within a 10% margin of the total size of the spheroids over the entire experiment. Therefore, the results are assumed to depict an accurate representation of spheroid growth for FaDu cells.

A similar experiment was performed to confirm the results found earlier. This time, however, the cell viability was also measured after 3, 7 and 14 days to visualize the difference in growth between both groups in terms of cell viability. Furthermore, during this experiment the culture medium was refreshed every 3 days. At the start of this experiment there were 24 spheroids per group and during every viability assay 6 spheroids of each group were used. The results of this experiment can be seen in figure 4.2. As can been seen in 4.2.a, the growth of the Matrigel® cultured spheroids is similar to the experiment before. Starting at a larger size of around 423 μm and reaching a size of around 588 μm this time on day 11. Afterwards the growth stopped and some spheroids even started to shrink, whilst the difference in size between spheroids started to increase. The error, however, stayed within the aforementioned 10% of the total size of the spheroids. The growth of the non-Matrigel® cultured spheroids is significantly different, as no growth was seen over the duration of the entire experiment. Seemingly indicating that changing medium every 3 days for this group only had a negative influence on the growth. Moving on to the second graph shown in figure 4.2.b. This graph shows the cell viability of both groups on day 3, 7 and 14 during the experiment. These results were obtained by performing a viability assay 3 times as mentioned in chapter 3.2.4 with 6 spheroids for each group. In this graph the viability of the Matrigel® cultured spheroids was taken as a control group compared to the non-Matrigel® cultured spheroids. Therefore, the cell viability of the Matrigel® cultured spheroids was set at 100%. The graph itself shows that the viability of the second group is significantly lower compared to the control, which explains the lower (or absent) growth of those spheroids. Overall the growth of the spheroids cultivated using Matrigel® was thought to be quite reliable and therefore it was decided to move on to the experiments in which different treatments will be compared. Additionally, as the growth of spheroids stopped after about 10 days, it was decided that future experiments should only investigate the time period between treatment, which is seen as day 0 of the experiment, and day 11, as afterwards the growth would stop even without any form of treatment. It was therefore chosen to look at treated spheroids for 7 days after treatment, with two viability assays being done on day 3 and 7.

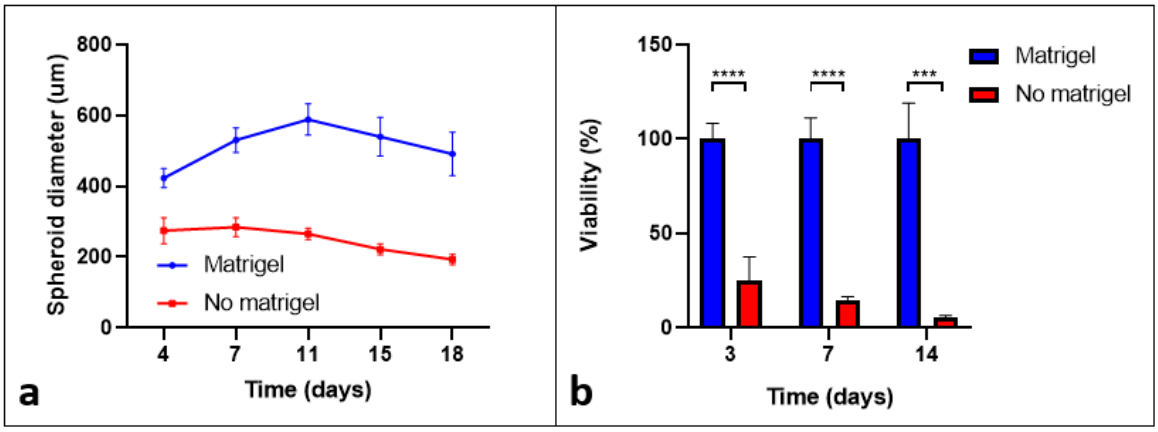

Figure 4.2: Comparison of results for spheroids cultured with Matrigel® and without. **a)** The spheroid size as a function of time for the two different culturing conditions. **b)** The viability of the cells as a function time for the non-Matrigel® cultured spheroids compared to the Matrigel® cultured spheroids. Significance of these results is indicated with n=6 per group. * = p=0.0332, ** = p=0.0021, *** = p=0.0002 and **** = p<0.0001

4.1.1. Spheroid malformations

Whilst the method for creating spheroids is fairly straightforward and in an ideal world every spheroid seeded comes out perfectly spherical, problems still occur when forming the spheroids. Three examples of these malformations are shown in figure 4.3. During all experiments three main forms of malformations occurred, of which two are different parts of the same problem. These are shown in 4.3.a and 4.3.b, where a) shows a spheroid that consists of multiple sections connected in the middle and b) shows two separate spheroids being formed after seeding. Due to the spheroids still being quite soft during seeding and treatment, they are easily deformed during this period. This can result in sections of the spheroid disconnecting either partly or completely and thus it can result in spheroids that are not spherical or in significantly smaller "twin" spheroids. The second type of problem occurs when fibers, that are present in the medium, disturb the spheroid formation. An example can be seen in figure 4.3.c, the fiber is indicated by the dark stripe straight through the spheroid. Whilst the medium used is filtered, these fibers do still exist in the medium and the cells used in the experiments like to grow around these fibers (or any surface in general). This results in "spheroids" that are misshapen compared to normal spheroids and most often they tend to grow notably faster than normal spheroids. Therefore, the size of these spheroids would not compare to normally formed spheroids. Generally, all these problems lead to spheroids that are either significantly smaller or significantly larger compared to other correctly formed spheroids in the experiments. Therefore, when it was detected on day 0 that a problem occurred, all the results of these spheroids were not used for further analysis.

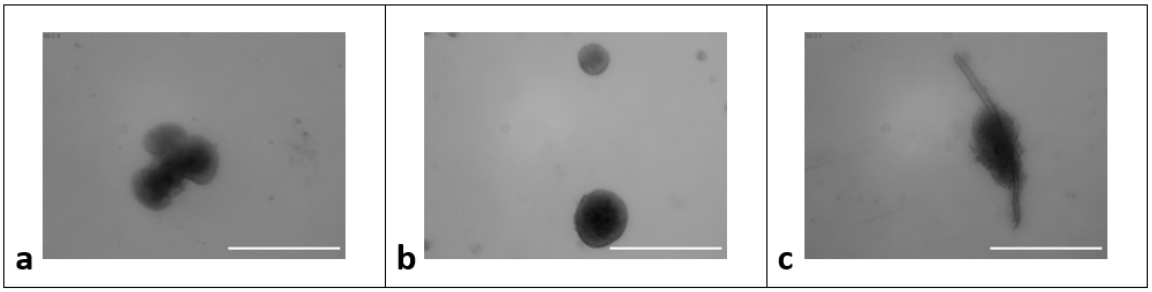

Figure 4.3: Images of the three different spheroid malformations that occurred during spheroid formation. The scale bar in each picture is equal to 600 μm. **a)** A spheroid that consist of multiple sections connected in the middle. **b)** Two separate spheroids formed during seeding. **c)** A fiber from the medium interfering with normal spheroid formation.

4.2. Results of the single treatment experiments

For the single treatments, four different data sets will be shown. First, the growth of the spheroids will be displayed as a graph showing the spheroid size over time. Following that, the function of growth will be shown again, this time compared to the initial size of the spheroids upon treatment. Thirdly, the viability assessments will be shown and lastly, some general images of the spheroids will be shown, to show the spheroid characteristics at different stages in the experiment. All this data is used to look at the overall state of the spheroids near the end of the treatment.

4.2.1. Radiotherapy

During these first experiments, the spheroids were treated once using RT. The radiation doses used for this treatment can be seen in table 3.1 in the previous chapter. A control group was added, which received no radiation dose during treatment, to show the difference in growth due to the treatment. The control group consisted of 6 spheroids, of which 3 were used for each viability assay. The treated groups consisted of 12 spheroids each, of which 6 were used for each viability assay.

The results of this experiment in terms of spheroid diameter can be seen in figure 4.4. Spheroids were treated on day 0 at a similar size compared to the earlier growth experiment of around 403 μm. Additionally, the control group grew to a comparable size of 601 μm, albeit after only 7 days. Furthermore, the growth of the treated groups followed an expected pattern with a higher dose resulting in less growth over time. Due to different initial sizes between spheroids it was decided from this point on

to also show the net growth of spheroids, as a function of the size of the spheroids on day 7 compared to the initial size on day 0. It was deemed that this would give a more accurate indication of the actual growth of the spheroids.

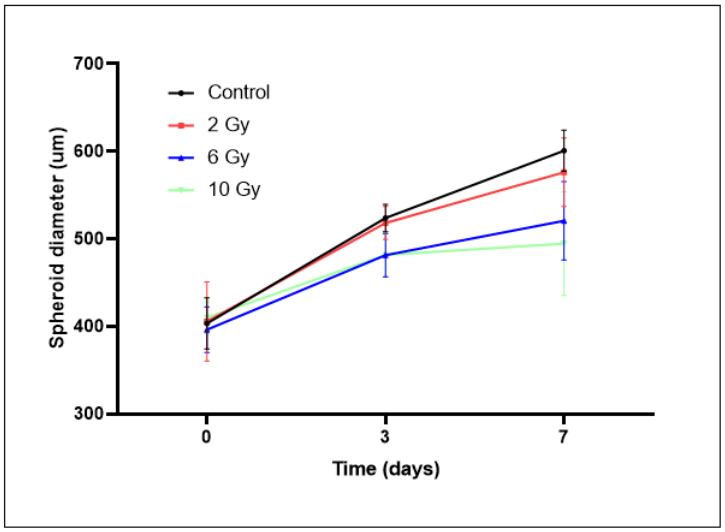

Figure 4.4: The spheroid diameter as a function of time for spheroids exposed to a dose of 0 (control), 2, 6 and 10 Gy of radiation using x-rays.

The net growth of the spheroids, as well as the viability, can be seen in figure 4.5 a and b respectively. Figure 4.5.a shows a similar trend as seen above, only now the growth over time can be directly read. The image therefore confirms the trend seen in figure 4.4 with the lowest dose resulting in the most growth. The difference between the control and 2 Gy group is rather negligible, growing about 115 μm in the first 3 days and showing a growth of around 180 μm in total after 7 days. The 6 Gy group grows around 81 μm in the first 3 days and up to a total of 122 μm after 7 days. The 10 Gy group shows a growth of around 61 μm after 3 days, which increases slightly up to 64 μm after 7 days. In total the growth of the 6 Gy group is about two thirds of the growth of the control group after 7 days and the growth of the 10 Gy group is about one third of the control group after 7 days. It is also important to note the standard deviation for the 6 and 10 Gy groups. This standard deviation occurred due to the fact that it was difficult for some spheroids of those groups to determine their size accurately. The spheroids started to lose solidity after 7 days and this resulted in loose cells and groups of cells being present around the edges of the spheroids, making the determination of the spheroid edge difficult to do and increasing the uncertainty in the spheroid size. Moving on, figure 4.5.b shows the result of the viability assays performed on day 3 and 7 of the experiment. The viability is normalized to the control group, with the viability of that group seen as 100%. The results confirm the trend shown in the growth of the spheroids. After 3 days only the 6 and 10 Gy groups show a difference in viability, with their value dropping to 87±10% and 85±4% respectively. On day 7 larger differences are visible. A viability difference between the control and 2 Gy groups is again not present with the 2 Gy group showing a cell viability of around 104±9%. However, the viability of the 6 Gy group is halved compared to the control group with a value of 47±8%. The difference for the 10 Gy group is also increased, with a cell viability that is only 25±0% of the viability of the control group. From these results it was chosen to use the 2 Gy and 6 Gy treatment doses for the further combined treatment. This was chosen because an improvement in the efficacy of the 2 Gy treatment should be easier to see as there seems to be no effect when treated only by radiation and the 6 Gy treatment could possibly be improved to match the effectiveness of the 10 Gy treatment.

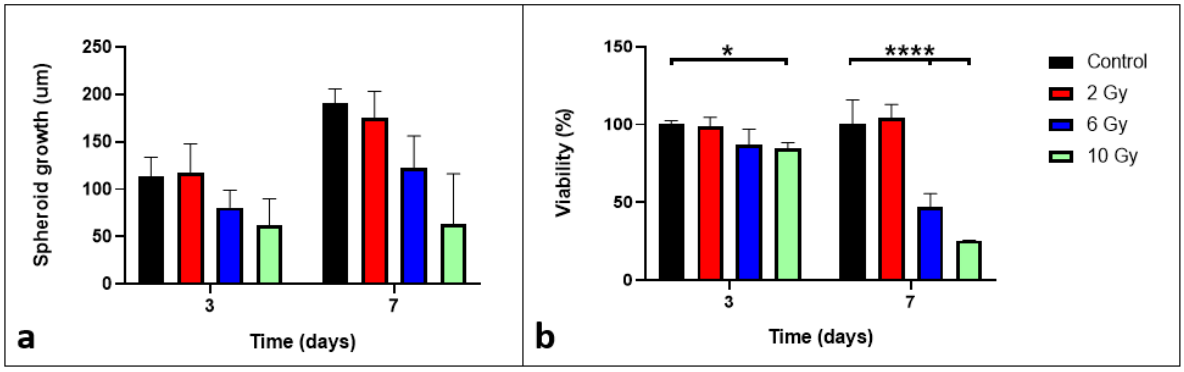

Figure 4.5: Two sets of results of a single RT experiment for spheroids exposed to 0 (control), 2, 6 and 10 Gy of radiation dose using x-rays. **a.** The net growth of the spheroids diameter on day 3 and 7 compared to the size of the spheroid diameter on day 0. **b.** The cell viability on day 3 and 7. The cell viability of the control group was used as a reference point on day 3 and 7. The cell viability of this control group was therefore seen as 100%. Significance of these results is indicated with n=6 for the 2, 6 and 10 Gy groups, whilst n=3 for the control group. * = p=0.0332, ** = p=0.0021, *** = p=0.0002 and **** = p<0.0001

Moving on to the bright-field light microscope images of one selected spheroid of each of the 4 used groups taken on day 0, 3 and 7. These images are shown in figure 4.6. The images on day 0 were taken right before treatment, whilst the images on day 3 and 7 were taken before performing the viability assay of that day. The scale bar on the bottom right of each picture represents 600 μm in the picture. Looking at the images, there is no difference between the 4 groups on day 0, which indicates that all spheroids have grown similarly up to this point. On day 3 the 6 and 10 Gy groups show a slight decrease in size compared to the control and 2 Gy groups. On day 7 the control and 2 Gy group are still similar in size, which corresponds to the results found in figure 4.5. The 6 Gy and 10 Gy groups are of more interest. The spheroids for these groups show a loss of some solidity, indicated by the presence of light and dark spots within the spheroid. Furthermore, both groups also show slightly smaller spheroids compared to the control group, which was expected. Lastly, the spheroid of the 10 Gy group also shows some flakiness around the edge of the spheroids. This is due to clumps of cells being loosened from the spheroids. Overall, visually an effect can be seen on the 6 and 10 Gy groups after 7 days, which was also shown by the results in figure 4.5. Meanwhile, the control and 2 Gy group show similar growth and the 2 Gy group shows no reaction to the treatment.

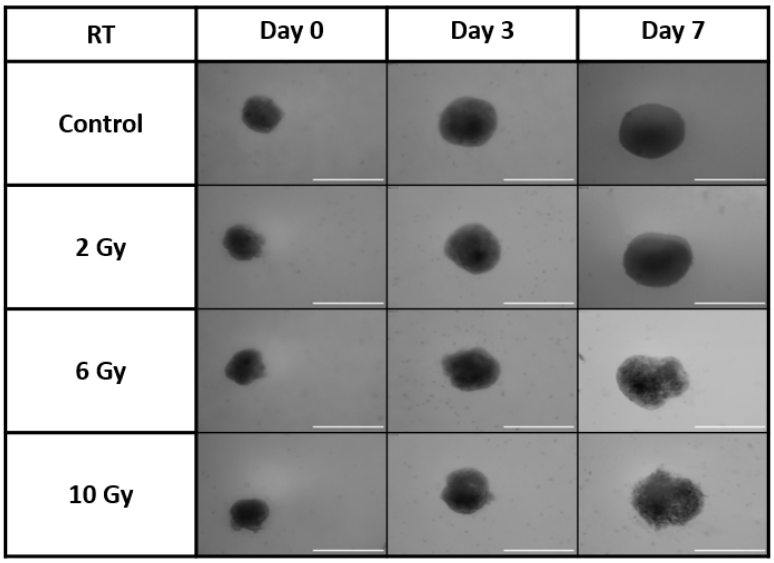

Figure 4.6: Bright-field light microscope images of a selected spheroid exposed to 0 (control), 2, 6 and 10 Gy dose of radiation using x-rays on day 0, 3 and 7. Spheroids were treated on day 0. The scale bar in the bottom right of each image is equal to 600 μm.

This single RT experiment was carried out three times in total. The results of the second and third experiment can be seen in Appendix A. These repeats roughly confirmed the results shown in the graphs displaying the spheroid growth. Net growth showed a similar trend for the second single RT experiment compared to the one seen in figure 4.5. The third single RT experiment showed less growth for the control group compared to the earlier experiments. No additional information was found that allowed to compare the viability of the different groups, as both viability assays failed to provide a usable control group measurement on day 7. The viability assays, therefore, lacked a baseline to normalize the results to. Nevertheless, the viability results shown in figure 4.5 are assumed to be quite accurate as they follow a logical decrease of size and viability with increasing radiation dose.

4.2.2. Hyperthermia

The second type of single treatment experiment performed involved treating spheroids with HT. The treatment doses used in these experiments are shown in the previous chapter in table 3.2. Here a control group was added as well, which received no treatment during the experiment. 10 spheroids were seeded for the control group and every treated group, of which 5 were used for each viability assay.

The results for the single HT experiment are shown in figure 4.7. The results are shown in three different data sets, similar to the single RT results. First looking at the spheroid diameter growth over time in figure 4.7.a. All spheroids start at a size of around 400 μm and grow up to a size of around 570 μm, apart from the 120 and 480 CEM_{43} groups. With the 120 CEM_{43} group showing a slightly smaller growth up to only 495 μm and the 480 CEM $_{43}$ group shrinking to a size of 278 μm after the initial measurement on day 0. Differentiating between the control group and the 1, 5 and 30 CEM_{43} in this graph is difficult. The difference between those groups is more easily seen in figure 4.7.b. Here it can be seen that the control groups show the largest net spheroid diameter growth with 146 μm and 213 μm after 3 and 7 days respectively. The 1 CEM_{43} group is next with a growth of 139 μm and 195 μm. Followed by the 5 CEM_{43} group with 130 μm and 182 μm and the 30 CEM_{43} group with 112 μm and 149 μm. The 120 CEM_{43} group then shows a growth of 92 μm and 95 μm and lastly, the 480 CEM_{43} group shows a decrease in size with a growth of -105 μm and -119 μm after 3 and 7 days. A trend can be seen with each additional bit of thermal dose resulting in less growth over the 7 days compared to the control. Surprisingly even the 1 and 5 CM_{43} groups show a decrease in net growth compared to the control group. Comparable results are shown in the results of the viability assays shown in figure 4.7.c. Here the measured cell viability of the control group is seen as a value of 100%. Compared to that value, the 1 and 5 CEM_{43} groups show a similar response with a cell viability of 100±6% and 105±1% respectively on day 3 and 83±8% and 82±7% respectively on day 7. The decrease in cell viability is more significant for the 30 and 120 CEM_{43} groups, with a cell viability of 106±6% and 62±10% on day 3 respectively and 104±6% and 39±7% on day 7 respectively. Finally, the 480 CEM_{43} group shows little viability on both day 3 and day 7 with values of 16±3% and 3±1% respectively.

Moving on to bright-field light microscope images of a selected spheroid of each group taken on day 0, 3 and 7. These images are shown in figure 4.8. On day 0, the spheroids of all groups show a similar shape and size, indicating successful seeding of the spheroids. However, on day 3 a difference can be seen. Whilst, the spheroids of the control group and the 1, 5 and 30 CEM_{43} groups are still similar in shape and size. A decrease can be seen for the spheroids of the 120 and 480 CEM_{43} groups, with the 120 CEM_{43} spheroid showing a decrease in growth compared to the control spheroid and the 480 CEM_{43} spheroid showing a decrease in size compared to the day 0 image as well. On day 7, the size of the control and 1 CEM_{43} spheroids is still similar, whilst the size of the 5 and 30 CEM_{43} spheroids is decreased compared to the control spheroid. This effect is even more apparent for the 120 CEM_{43} spheroid. Finally, the 480 CEM_{43} spheroid showed to have lost its spherical shape, with parts of the spheroid detaching from each other. Furthermore, flakiness can be seen around the edges of the spheroid. The image of day 7 for the 480 CEM_{43} spheroid, which showed an increase in size, might seem contradictory to the results shown in figure 4.7, which stated that the spheroids shrank further between day 3 and 7. This is only seemingly the case, as the protuberances at the side are not considered to be part of the spheroid anymore as these mostly consist of lose clumps of cells, alike the 10 Gy group for the RT experiments. Therefore, the part of the actual spheroid that should be considered is still smaller. It should be noted that this difficulty in defining what the actual spheroid is, does increase the error in measuring the size of this group.

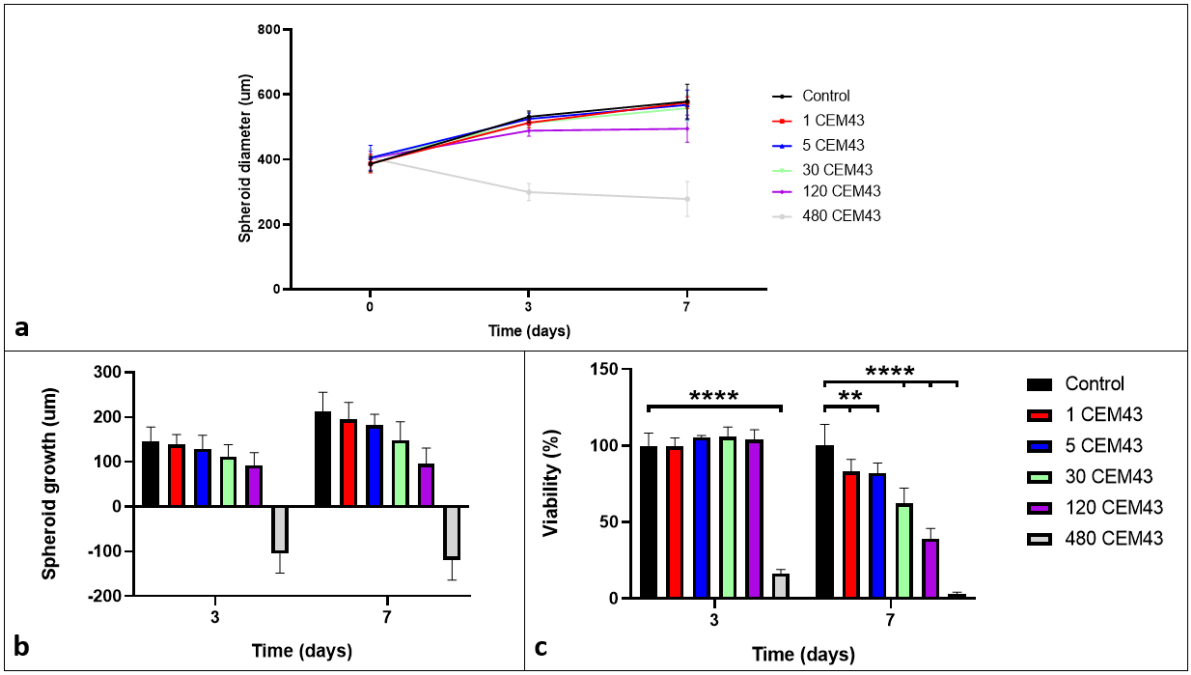

Figure 4.7: Three data sets showing the results of a single HT experiment for spheroids exposed to 0 (control), 1, 5, 30, 120 and 480 CEM_{43} of thermal dose using hyperthermia. **a.** The growth in spheroid diameter as a function of time after treatment. **b.** The net growth of the spheroid diameter on day 3 and 7 compared to the size of the spheroid diameter on day 0. **c.** The cell viability on day 3 and 7. The cell viability of the control group was used as a reference point on day 3 and 7. The cell viability of this control group was therefore seen as 100%. Significance of these results is indicated with n=5 per group. * = p=0.0332, ** = p=0.0021, *** = p=0.0002 and **** = p<0.0001

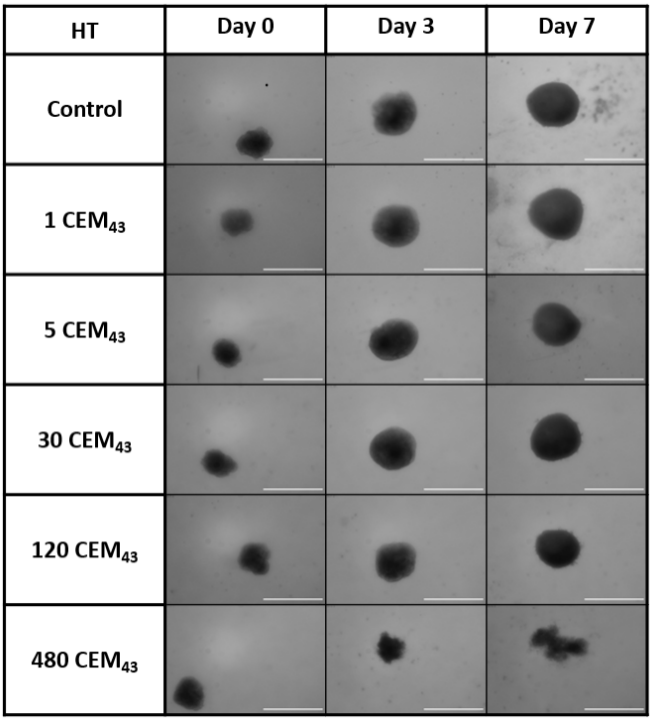

Figure 4.8: Bright-field light microscope images of a selected spheroid exposed to a thermal dose of 0 (control), 1, 5, 30, 120 and 480 CEM_{43} using hyperthermia on day 0, 3 and 7. Spheroids were treated on day 0. The scale bar in the bottom right of each image is equal to 600 μm.

Considering all results shown above for the HT experiments, it was decided to move on with the two treatment doses below the highest 480 CEM_{43} dose. The 30 CEM_{43} was chosen as it does show an effect on the spheroid growth and viability, this effect nonetheless is not as significant that no effect of the combined treatment could possibly be detected. On the other hand, the 120 CEM_{43} does already show a significant effect on growth and cell viability, however the bright-field light microscope images showed no morphological effect yet. Combining this treatment with radiation might clearly show a visible increase in effect as well, which could hopefully lead to a dose of 120 CEM_{43} combined with radiation having the same effect as a dose of 480 CEM_{43}. To this end, the 30 and 120 CEM_{43} HT doses were used during the combined experiments.

The single HT experiments were carried out in triplicate, with the results of the other two experiments shown in Appendix A. Whilst, the results of the second single HT experiment were difficult to interpret due to a longer waiting time before treatment, thus resulting in the spheroids already reaching their final size before treatment. The results of the third single HT experiments were useful. The results mainly confirmed the results found in the experiment shown above, whilst also helping justifying the choice of HT doses to work with during the combined experiments. Therefore, the results shown in figure 4.7 are assumed to be reliable, as they follow a logical trend of a decrease in size and viability at higher heating dose.

4.3. Results of the combined treatment experiments

The next presented results are those of the CT experiments performed. First, the results for the experiments with HT preceding RT are displayed (HTRT), followed by the results for the experiments that treat the spheroids the other way around (RTHT). The results will be displayed in three figures per experiment. The first figure will show the spheroid diameter growth over time, as well as the net spheroid diameter growth over time. The second figure will show the cell viability of the treated groups compared to the cell viability of the single treatment experiments over time. Lastly, some bright-field light microscope images of the different used groups are shown over time.

4.3.1. HTRT

The results shown below belong to a combined HTRT experiment. Four different treatment groups and a control group were used during this experiment, the treatment dose of each can be seen in table 4.1. The table also shows that the different treatment groups will be given a name to make reading of the following section easier. For this experiment, 6 spheroids were seeded for the control group and 9 spheroids were seeded per treatment group. Consequently, there were 3 control spheroids and 4 treated spheroids available per viability assay, with one spheroid being left as a reserve if spheroids formation failed or spheroids were lost during the experiment.

Table 4.1: The names of the different treatment groups used in the HTRT experiments, as well as the combined thermal dose the groups were exposed to using hyperthermia and subsequently the radiation dose applied using x-rays.

Group name	Treatment dose
Control group	No treatment
Group A	30 CEM_{43}, 2 Gy
Group B	30 CEM_{43}, 6 Gy
Group C	120 CEM_{43}, 2 Gy
Group D	120 CEM_{43}, 6 Gy

The measured growth of the spheroids for each group is shown in figure 4.9.a. It can be seen that the spheroids of the control group grow from a size of 233 μm on day 0 to 437μm on day 7. The spheroids started at a smaller size compared to earlier experiments and end on a smaller size as well. It should be noted that a similar trend is seen in this figure, where a higher treatment dose leads to a decrease in spheroid growth. Nevertheless, it is more interesting to look at the net growth of the spheroid diameter for the different groups in figure 4.9.b. Starting with the control group, the spheroids

show a growth of 121 μm on day 3 and 179 μm on day 7, which is in a similar range compared to earlier experiments. The trend shown in the spheroid diameter growth is seen in this figure as well. The net growth of the treated groups on day 7 equals 125 μm, 88 μm, 78 μm and 39 μm for group A, B, C and D respectively. Group B and C showed limited growth between day 3 and 7 and group D even showed a decrease in size from day 3 to day 7. Overall the response of group B and C being similar seems logical, as both groups contain the lower treatment dose of one type of treatment and the higher dose of the other, the overall treatment dose for both groups being comparable as a result. Furthermore, it is interesting to note that in contrary to single treatments, even after three days effects are already seen in the growth of the spheroids.

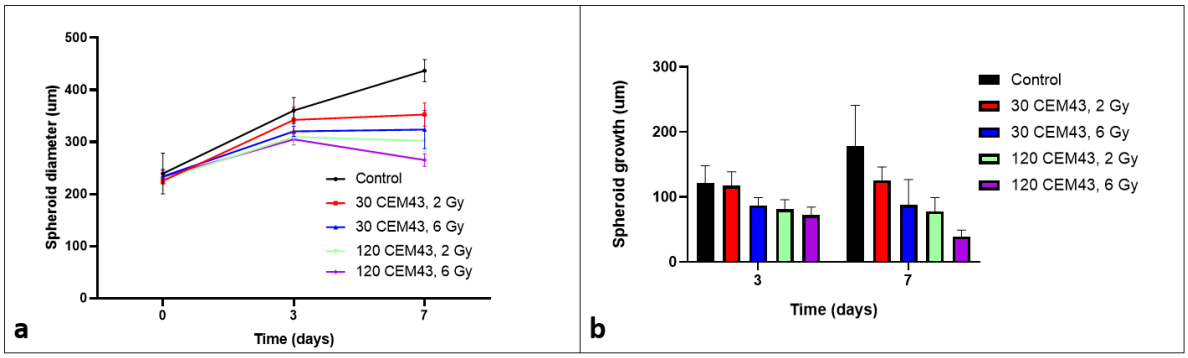

Figure 4.9: Two data sets showing the results in terms of growth for a HTRT experiment. The results are given for a control group and 4 groups that were treated with a combination of a thermal dose of 30 and 120 CEM_{43} applied using hyperthermia and a radiation dose of 2 and 6 Gy applied using x-rays. **a.** The size of the spheroid diameter for each group on 0, 3 and 7 days after treatment. **b.** The net growth of the spheroid diameter for same groups on day 3 and 7 compared to the diameter size on day 0.

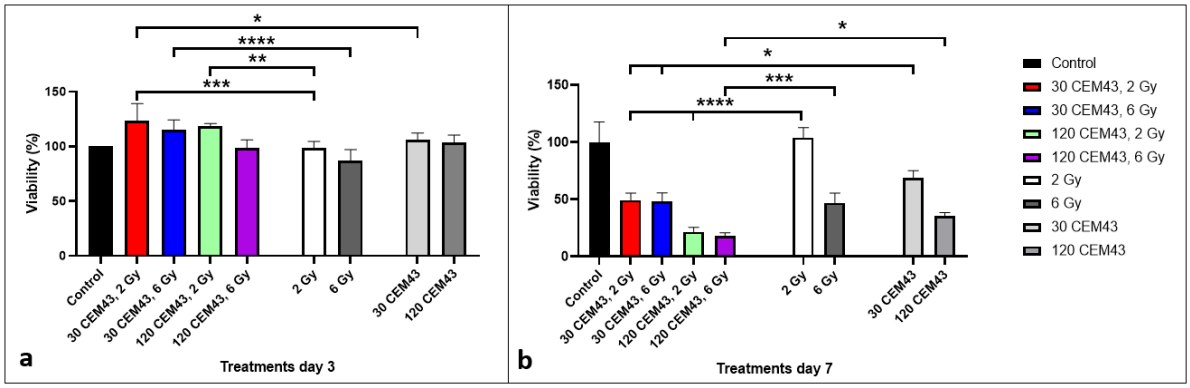

Figure 4.10: Two data sets showing the results in terms of cell viability of a HTRT experiment. The results are given for a control group and 4 groups that were treated with a combination of a thermal dose of 30 and 120 CEM_{43} applied using hyperthermia and a radiation dose of 2 and 6 Gy applied using x-rays. Significance of these results is indicated compared to the results of the single treatment experiment. * = p=0.0332, ** = p=0.0021, *** = p=0.0002 and **** = p<0.0001 **a.** The cell viability of the different groups on day 3 after treatment. **b.** The cell viability of the different groups on day 7 after treatment.

Table 4.2: The cell viability values after 3 and 7 days for the chosen single treatments applied using HT and RT used in the CT experiments.

Treatment dose	Viability (day 3)	Viability (day 7)
2 Gy	99±6 %	104±9%
6 Gy	87±10 %	47±8%
30 CEM_{43}	106±6 %	62±10%
120 CEM_{43}	104±6 %	39±7%

Continuing with the cell viability, as seen in figure 4.10. The results on day 3 and 7 are normalized to the control group, which is assumed to show 100% cell viability. After three days an increase in cell viability is seen for all treated groups compared to the control group. It should be said that the viability assessment for the control group was flawed, as only one of the three control group spheroids produced a usable result. After seven days a different trend is seen, where groups A and B, both treated with the 30 CEM_{43} dose, showed a similar cell viability on day 7 of 50±6% and 48±8% respectively. Groups C and D, both treated with the 120 CEM_{43} dose, also showed a similar cell viability on day 7 with a value of 22±4% and 18±3% respectively. To compare these results to the single treatments, the viability of the single treatments after seven days are summarized in table 4.2. Comparing the values on day 3 does show significantly different results, however only a significant increase in viability is seen for the treated groups compared to the single treatments. It is more interesting to compare the results on day 7. Here it is seen that the cell viability for groups treated with 2 Gy is significantly lower, whilst less of a difference can be seen between the groups treated with 30 CEM_{43}, with group A showing the most significant decrease in cell viability compared to the single treatments. Group B is the only group that shows an increase in effect compared to the single treatments with a cell viability of 48±8% on day 7. Lastly, the cell viability of group C and D is also lower compared to both single treatments, albeit less significant compared to group A. This indicates that an improved effect was seen for the treated groups A, C and D. This effect was most significant for group A.

Lastly, the bright-field microscope images of the experiment, shown in figure 4.11, are considered. Starting on day 0, all groups show a spheroid of similar size and shape. On day 3 the spheroids of every treated group are slightly smaller compared to the control group. The final images on day 7, show an increased difference from day 3 between the size of the control group and the four treated groups. Furthermore, group A, B, C and D all show some form of flakiness around the edge of the spheroid, with clumps of dead cells releasing from the spheroid. This is effect is the least apparent for group A, whilst it is most clear for group C and D, with group C showing a less solid spheroid overall on day 7 and group D mainly showing a solid core as all that is left of the spheroid. Overall, these effects are in agreement with the single results, where such effects would also happen on day 7 after a treatment dose of 6 Gy and 120 CEM_{43}. The day 3 picture of group C is vaguer due to condensation on the lid of the 96-well plate, therefore blocking proper imaging.

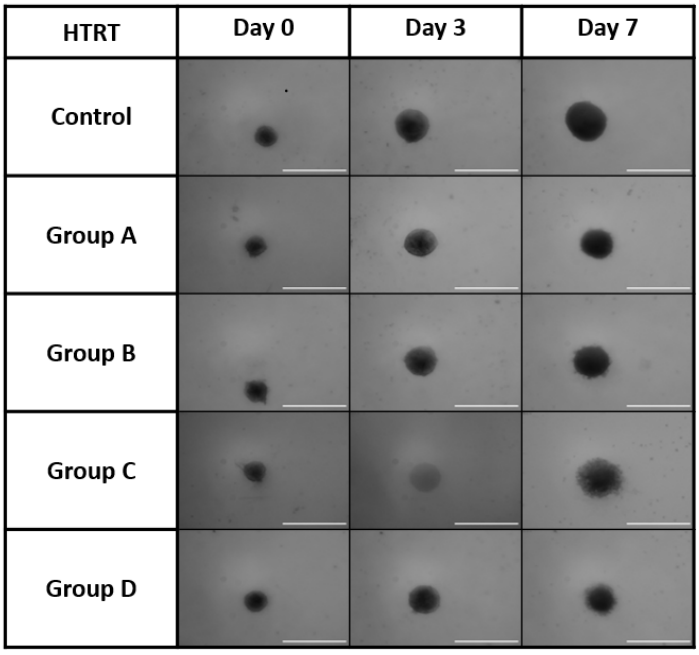

Figure 4.11: Bright-field light microscope images of a selected spheroid for a control group and 4 groups that were treated with a combination of a thermal dose of 30 and 120 CEM_{43} applied using hyperthermia and a radiation dose of 2 and 6 Gy applied using x-rays, wherein the thermal dose was first applied before the radiation dose. Spheroids were treated on day 0 and imaged on day 0, 3 and 7. The scale bar in the bottom right of each image is equal to 600 μm.

To confirm these results, the HTRT experiment was carried out four times in total. The results of the other three HTRT experiments can be seen in appendix B. The growth results of these experiments confirmed the trend seen where a higher treatment leads to a decrease in spheroid growth over the 7 days of an experiment. Furthermore, cell viability results of one of the experiments showed a significant increase in effect for all treated groups even on day 3 after treatment, whilst another experiment only showed an increased effect for spheroids of group A. This effect is also visible when inspecting the spheroids with a bright-field light microscope, with all spheroids showing a significant decrease in growth on day 3 and 7. Furthermore, flakiness around the edges of the spheroids of each group on day 7 also suggest an increased effect is seen.

4.3.2. RTHT

The results of a RTHT experiment are shown below. Here again reading will be made easier by giving each treatment group a name. The names and the subsequent treatment doses associated with that group can be seen in table 4.3. For these experiments, the same number of spheroids were seeded as for the HTRT experiment above. There were 6 control spheroids seeded and 9 spheroids per treatment group, with 3 control spheroids and 4 treated spheroids available per viability assay, with one spheroid being left as a reserve if spheroids formation failed or spheroids were lost during the experiment.

Table 4.3: The names of the different treatment groups used in the RTHT experiments, as well as the combined radiation dose the groups were exposed to using x-rays and subsequently the thermal dose applied using hyperthermia.

Group name	Treatment dose
Control group	No treatment
Group A	2 Gy, 30 CEM_{43}
Group B	2 Gy, 120 CEM_{43}
Group C	6 Gy, 30 CEM_{43}
Group D	6 Gy, 120 CEM_{43}

The results for the RTHT experiment can be seen in figures 4.12 and 4.13. Starting with the spheroid diameter at different time points in figure 4.12.a. All spheroids start at a size of around 270 μm and the control grows up to a size of 569 μm. The size of the control group on day 7 is similar to earlier experiments, whilst the starting size of 270 μm is slightly lower. Looking at the treated groups a similar trend to the HTRT experiments can be seen, with increasing dose leading to a decrease in growth. Similarly to the HTRT experiments as well, groups B and C, of which both consist of a higher dose of HT or RT and a lower dose of the other treatment type, show a comparable size on day 7 of the experiment after shrinking slightly from day 3 onward. Contrasting to the HTRT experiments, group A, the group with the lowest treatment dose, does still grow after day 3 and follows the trajectory of the control group quite closely. Additionally, group D also grows up to day 3, after which the spheroids start shrinking in size to a similar size as on day 0. The net growth shows these same trends in figure 4.12.b, with group D barely growing, group B and C growing similarly and group A growing slightly less than the control group. The control group has a net growth of 290 μm after 7 days, which is significantly more than the net growth in earlier experiments.

The viability results in figure 4.13 do show some differences compared to the HTRT experiments. First, on day 3 the viability of all treated groups is already slightly lower than the control group, with group B and C on a similar viability of 87±3% and 87±5% respectively. The cell viability of group D was only a slight step below that at 80±5%. A decrease in cell viability is seen on day 7, where the viability of group B, C and D all decreased significantly, their viability being 13±2%, 18±3% and 9±2% respectively. Group A retains a higher viability of 55±8%. Comparing these values to the viability values of the single treatments, shows that each treated group showed a significant increase in effect compared to the single treatments. This effect is most significant for group B, showing the largest drop in viability after 7 days.

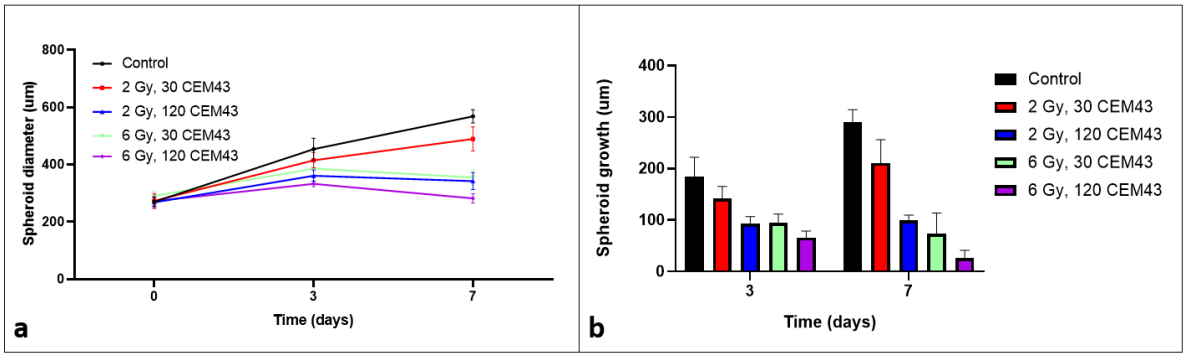

Figure 4.12: Two data sets showing the results in terms of growth for a RTHT experiment. The results are given for a control group and 4 groups that were treated with a combination of a radiation dose of 2 and 6 Gy applied using x-rays and a thermal dose of 30 and 120 CEM_{43} applied using hyperthermia. **a.** The size of spheroid diameter for each group on 0, 3 and 7 days after treatment. **b.** The net growth of the spheroid diameter for same groups on day 3 and 7 compared to the diameter size on day 0.

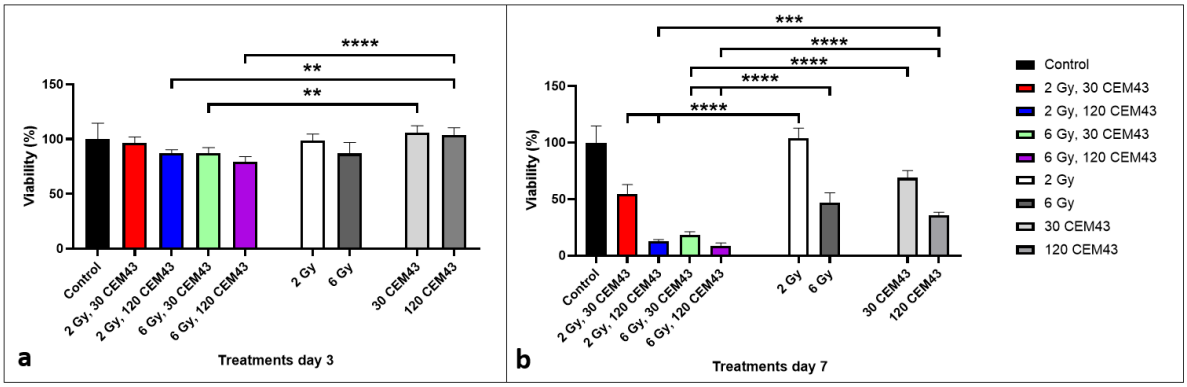

Figure 4.13: Two data sets showing the results in terms of cell viability of a RTHT experiment. The results are given for a control group and 4 groups that were treated with a combination of a radiation dose of 2 and 6 Gy applied using x-rays and a thermal dose of 30 and 120 CEM_{43} applied using hyperthermia. Significance of these results is indicated compared to the results of the single treatment experiment. * = p=0.0332, ** = p=0.0021, *** = p=0.0002 and **** = p<0.0001 **a.** The cell viability of the different groups on day 3 after treatment. **b.** The cell viability of the different groups on day 7 after treatment.

Bright-field light microscope images of a selected spheroid of each treatment group used during the RTHT experiment are also shown in figure 4.14. Again on day 0, all the spheroids for each group start at a similar size and shape. On day 3, all treated groups show a decrease in size compared to the control group. Lastly, on day 7 it can be seen that the spheroid of group A has grown and is only slightly smaller compared to the control group spheroid. As expected, following the viability results, group B, C and D all show significantly smaller spheroid on day 7, with all spheroids experience flaking around the edge of the spheroid. This effect is most clearly seen in group D, with a darker core remaining present in the spheroid on day 7. This clearly represents the cell viability effect shown on day 7.

An attempt was also made to confirm these results by carrying out this experiment three more times. The results of these experiments can be seen in appendix B. From the results of these experiments it can be seen that a decrease in effect is shown in each of the treated groups compared to the single treatments. However, as every experiment lacked in spheroid growth, no clear conclusion can be drawn from these results. It was interesting to note that group B and D often showed a similar cell viability on day 7, sparking the idea that for RTHT experiments the thermal dose is mostly responsible for the response seen in the spheroids, with the radiation dose mattering little. No further significant conclusions could be drawn from the results of these three RTHT experiments.

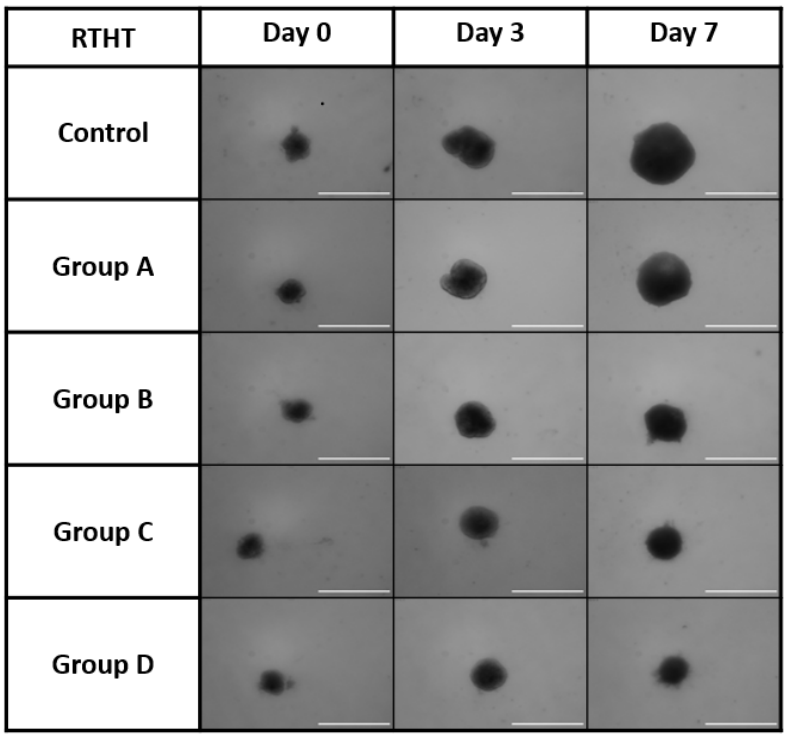

Figure 4.14: Bright-field light microscope images of a selected spheroid for a control group and 4 groups that were treated with a combination of a thermal dose of 30 and 120 CEM_{43} applied using hyperthermia and a radiation dose of 2 and 6 Gy applied using x-rays, wherein the radiation dose was first applied before the thermal dose. Spheroids were treated on day 0 and imaged on day 0, 3 and 7. The scale bar in the bottom right of each image is equal to 600 μm.

4.4. Confocal imaging

This final section of the results will show the results obtained using confocal imaging. Due to time constraints, only two experiments were done in which spheroids were stained and imaged. One experiment included staining the spheroids with a mixture of calcein-AM and ethidium homodimer-1 and the other experiment used PI, of which both methods are explained in chapter 3.2.6. Only qualitative results in the form of images will be presented in this chapter.

4.4.1. Live and dead imaging

The first experiment was only a trial to see if live and dead cells in spheroids could be easily imaged without sectioning the spheroids first. The images from this experiment can be seen in figure 4.15, with the spheroids visible under normal light in a, the same spheroids visible under illumination by a 488 nm argon laser in image b and c. Image b shows the detected light spectrum around 515 nm and image c does the same for 635 nm. The final image, d, shows all spectra overlapping. The spheroids used in this experiment did not undergo any treatment. It can be quickly seen that the resulting fluorescence due to the laser can only be seen at the height of the spheroid that is in focus, meaning the center of the spheroid remains dark. Furthermore, both calcein and ethidium homodimer-1 images are similar in shape and brightness. As both images should be recorded using different parts of the light spectrum, it was checked during the experiment to see if this was not an error made by the user and it turned out that this was not the case as all settings were correct. No further experiments using this type of cell staining kit were done, as spheroids were discarded after confocal imaging, therefore resulting in difficulty in following the effects of different treatments on the spheroids over time.

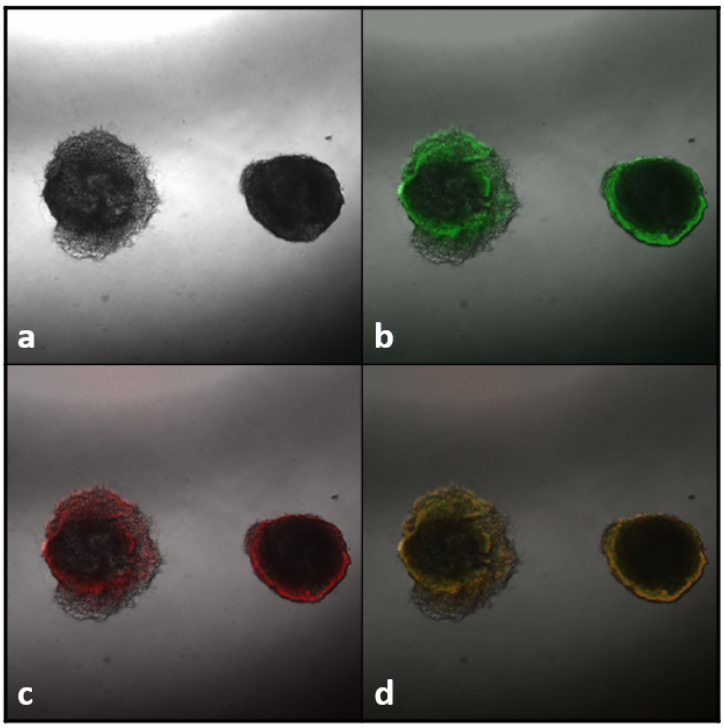

Figure 4.15: 4 images of calcein-AM and ethidium homodimer-1 stained untreated spheroids captured using a confocal imaging microscope with a 2.5x objective. **a)** Bright-field light image of the two spheroids. **b)** Overlapping image of both the bright-field light image and the calcein imaging spectrum. **c)** Overlapping image of both the bright-field light image and the ethidium homodimer-1 imaging spectrum. **d)** Overlapping image of all three images combined.

4.4.2. Propidium iodide

The last experiment performed during this research involved staining spheroids with PI. The spheroids used in this experiment were imaged both using the bright-field light microscope, as well as the confocal microscope under light conditions and under illumination by a 543 nm helium neon laser. A control group, as well as 8 differently treated groups of spheroids were used, with 6 spheroids seeded per treatment group and the same 3 spheroids used during each confocal imaging session, to visualize the change over time in these spheroids. The treatment groups chosen for this experiment can be seen in table 4.4. These groups are also given a name to make reading of the following section easier. The treatment dose named first is the treatment modality used first, with the second treatment modality following after a period of 30 minutes. The spheroids were treated on day 1 of the experiment, leaving the measurement on day 0 as a baseline for the rest of the experiment.

Table 4.4: The different treatment groups used during the PI experiment, with the treatment doses the spheroids of the group experienced. The treatment dose named first was the treatment dose administered to the spheroid first. The second treatment dose followed after a period of 30 minutes.

Group name	Treatment dose
Control	No treatment
Group 1	30 CEM_{43}
Group 2	120 CEM_{43}
Group 3	2 Gy
Group 4	6 Gy
Group 5	30 CEM_{43}, 6 Gy
Group 6	2 Gy, 120 CEM_{43}
Group7	6 Gy, 120 CEM_{43}
Group 8	120 CEM_{43}, 6 Gy

The results of the experiment can be seen in figure 4.16, with a selected spheroid of each group presented over time in a row in the figure. Looking at the results, starting with the control group, a similar response is seen for each day, apart from day 14, which is also in agreement with the day 0 image of groups 1 to 8. On day 2, the day after treatment, an immediate response can be seen in groups 2 and 7, whilst no significant response is seen for groups 1, 3, 4, 5, 6 and 8. This is changed on day 6, where group 4 and 5 show a severe increase in dead cells. Whilst it was expected that the largest response would be seen in the groups containing either (or both) the 6 Gy or the 120 CEM_{43} treatment dose, it is surprising to see group 5 have a significant response on day 6. The increase in response for group 1 on day 6 is due to a fiber being present in the spheroid. On day 8, the response of all spheroids is decreased. Whilst on day 10, an increase in dead cells is seen for groups 3, 4, 5, 6, 7 and 8. On day 14, a significant increase in dead cells is seen in both the control group and group 1.

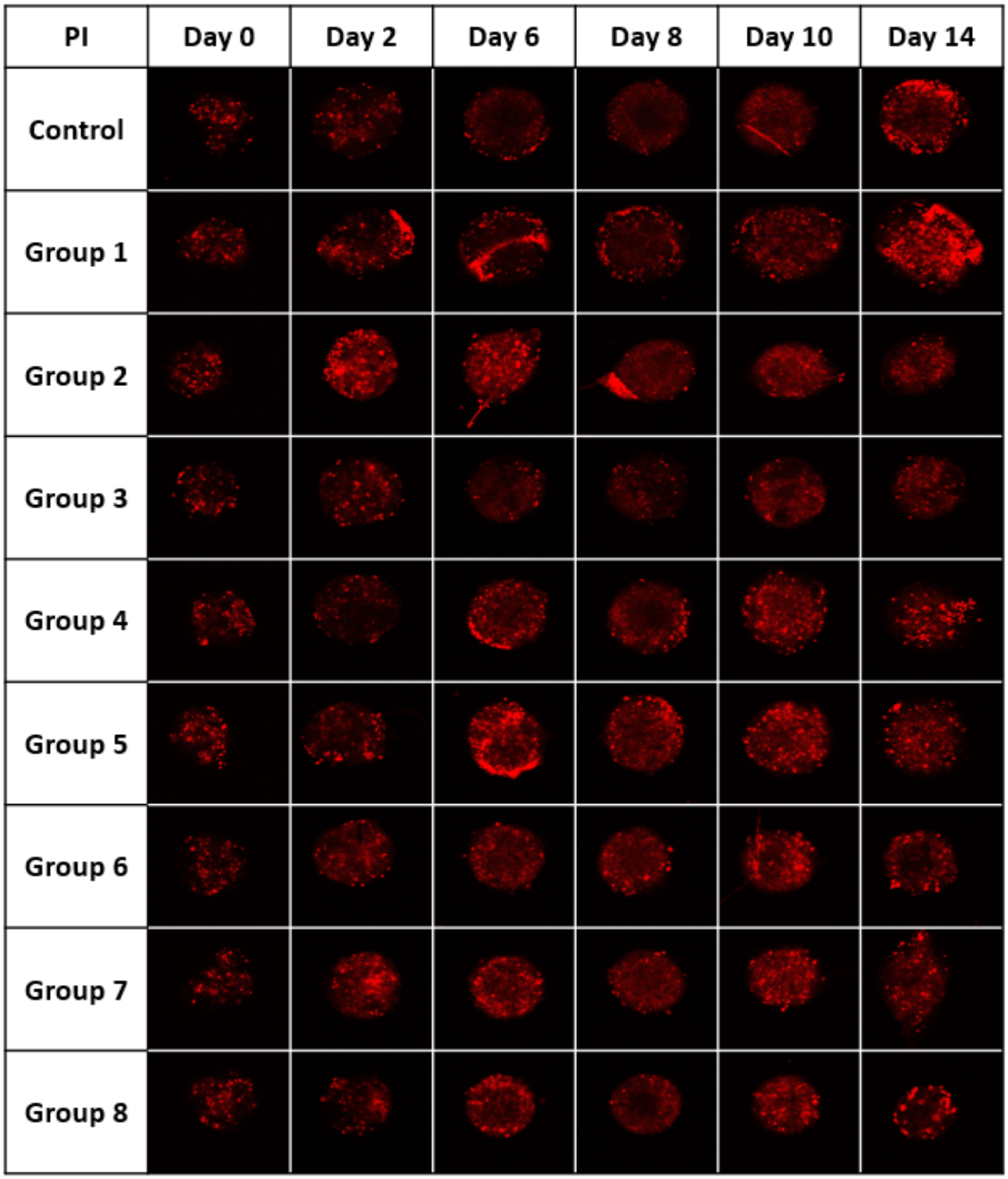

Figure 4.16: Confocal images of a spheroid of each of the 9 different groups exposed to none, either or both thermal and radiation dose after being stained with PI and illuminated by a 543 helium neon laser. Images were taken on day 0, 2, 6, 8, 10 and 14 with a 10x objective. The same selected spheroid of each group is shown over time. Treatment was done on day 1, leaving the day 0 images as a baseline measurement.

5

Discussion

In the following chapter the results presented in chapter 4 will be discussed and some improvements will be suggested. To this end, possible limitations in the experimental methods will be proposed in an effort to explain the outcome of certain experiments. Furthermore, some results will also be compared to results found in literature. This discussion is divided in 4 sections, each covering one of the experimental sets shown in chapter 4.

5.1. Spheroid growth

The growth experiments performed in this research were the simplest experiments. They were mainly done as a baseline to check the size up to which the spheroids would grow if left untreated. A size of 550 μm to 600 μm was generally reached after 7 to 10 days for spheroids seeded with Matrigel®, which was significantly more compared to spheroids formed without Matrigel®. This is in agreement with other research done into the effect of Matrigel® on the growth of spheroids [95], which is expected to improve both cell proliferation and the overall morphology of the cells [96]. The only real limitation found during these experiments was the limit in size a spheroid could adopt after a time period, which has also shown to be a problem in other research reports [97]. This was most probably caused by both the initial cell seeding density and the size of the microwells used [98]. During these experiments it was decided to only compare the results of viability assays to a control group used during that specific viability assay. As spheroids grow over time, this will automatically influence the viability, as larger spheroids mean more cells and therefore more ATP present. Using a control group in this manner would present a baseline of viability over time, which would make comparisons easier.

Different options for measuring the spheroid diameter were also considered. This was done as a way to minimize the error in measuring the spheroid diameter. Two methods were mainly considered, the first of which was using the Feret's function in ImageJ. This function most likely overestimates the diameter of the spheroids, as it shows the distance between two points of a measured area that are apart the furthest. This method most often overestimates the spheroid diameter, as spheroids are never perfectly symmetrical. The second method considered was calculating the diameter from the area of the measured spheroid. Here both underestimates and overestimates would happen as selecting the boundary of the spheroid precisely in ImageJ is impossible. For simplicity it was chosen to use the Feret function, as it was the easiest method to implement to measure the spheroid diameter. This method would still produce an error whilst measuring the spheroid diameter, yet it was deemed that this error would be most significant for spheroids that deviate the most from the spherical shape. As these non-spherical spheroids were often disregarded during experiments the resulting error due to the Feret function would also be minimized. Additionally, FaDu cells tend to take up a spherical shape, when cultured in U-shaped wells, minimizing the error even further [99][100].

5.2. Single treatments

At the start of these experiments the results were thought to be straightforward, both in terms of spheroid growth and cell viability, with increasing treatment dose resulting in a decrease in spheroid

growth and cell viability. The initial results seemed to confirm this, however problems occurred when repeating both single HT and RT experiments. For single RT experiments the main problem was the lack of a useful control group. As the treated groups could not be related to this control group, it became difficult to say anything meaningful about these results. For the single HT experiments the problem was found in the growth over time, with one experiment showing no growth from treatment until the end of the experiment and the other experiment showing an increase in growth between day 3 and 7. As the proliferative state of spheroids is severely influenced by the presence of ATP [101][102], it can be imagined that increased growth or an absence of growth can significantly influence the results of a cell viability assay based on measuring the presence of ATP. Nevertheless, as research showed a similar effect of increased radiation dose on the viability of FaDu cells [103][104], it was assumed that the results shown in figure 4.5 are a reliable representation of the therapeutic response. A similar conclusion was drawn for the single HT results, with the effect of hyperthermia on FaDu cells already being shown in research [105].

Even so, some of the problems that occurred during the single treatment experiments could easily be solved. A first simple improvement would be to seed more control spheroids for each experiment. As said during the RT repeat experiments the number of control spheroids usable for the viability assay were often limited, leading to results that were meaningless. As the control group is the most important group of all, with a lack of a control group leading to all other results being meaningless, increasing the number of seeded control spheroids would easily solve this problem. Additionally, the third single RT experiment shows quite significant errors in spheroid diameter and net growth, this is due to the fact that the spheroids were seeded using a 12-channel pipette. This specific pipette had an offset, which made half of the channels not tuned correctly. This resulted in certain pipette tips collecting more medium and thus cells and resulted in those wells containing more cells compared to the others. Upon measuring half of all spheroids seeded were significantly larger than the other half. By checking if a pipette is properly tuned beforehand, this problem could be negated in future experiments. Another possible issue occurred in the first single HT experiment. As seen in figure 4.7, both the 1 and 5 CEM_{43} groups show a response in both growth and viability, whilst for these treatments doses a visible effect was not expected. A possible reason for this could be that those spheroids are transferred from a 96-well plate to an 8-well strip and back to a 96-well plate during treatment. During this transfer cells in the spheroid could be damaged by the pipette tips used. As the control spheroids are left untouched, this could be a reason for the difference. A solution for this could be to transfer the control spheroids to a strip and back to the original plate, limiting errors in this part of the experiment.

5.3. Combined treatments

More interesting are the results of the combined treatments. 2 significant errors were made during the time period in which these experiments took place. First, whilst the FaDu cells were in a sub-culturing flask, they were exposed to normal culture medium without the F10 addition. This was not supposed to be the case. The medium in which cells grow severely impacts both the growth rate and the viability [106]. Therefore these cells probably needed to adjust themselves when exposed to the F10 medium used to seed the spheroids, resulting in a difference in spheroid growth and thus viability. The second problem is visible in both RTHT and HTRT experiments, with the overall growth reducing from the first combined treatment experiment to the fourth experiment. Over the course of performing all these experiments the same original batch of F10 medium was used and whilst the medium was preserved in a fridge when not in use, this medium would still age. As time went by it is now assumed that the aging of this medium affected the growth of the spheroids. This can be seen in the overall growth decreasing with later experiments.

Moving on to a discussion about the results of these experiments. The HTRT experiments showed an increased effect for the 30 CEM_{43}, 2Gy, the 120 CEM_{43}, 2 Gy and the 120 CEM_{43}, 6 Gy groups. Carrying out the HTRT experiment a second time confirmed these results, with an effect even visible on day 3 after treatment, whilst two further HTRT experiments showed no significant response. The RTHT experiments initially did show an increased effect for each of the treated groups, most significantly for the groups involving the 120 CEM_{43} HT dose and the 6 Gy, 30 CEM_{43} group. An effect was even seen on day 3 after treatment. However, confirming these results proved difficult, as a reduced overall

growth negatively influenced the results. Nevertheless, these additional experiments did all seem to show that the 120 CEM_{43} thermal dose was most influential in the overall growth and cell viability of the spheroids. Comparing both experiment types, it therefore seems to be the case that the HT dose is most significant in determining the overall effect of combined treatment, with the 120 CEM_{43} group showing the highest cell killing potential in combination with both radiation doses in both HTRT and RTHT experiments. When comparing cell viability results of both the HTRT and RTHT experiments only a significant difference is seen between the cell viability of the 2 Gy, 120 CEM_{43} and the 120 CEM_{43}, 2 Gy groups, with RT preceding HT showing a lower cell viability of 13±3% after 7 days compared to 48±8% for HT preceding RT. This would suggest that irradiating spheroids before treating them with hyperthermia could be more beneficial in combined treatment. The lack of reproducibility, however, makes it difficult to say this with certainty. Whilst performing both treatment modalities at the same time maximizes the cell killing potential [69], it has also been shown by Overgaard (1980) that RT preceding HT with a period of at least 4 hours in between does improve the thermal enhancement ratio of these treatments [107]. Overgaard (1980) ascribed this effect to "the direct heat killing of radioresistant tumor cells". This would mean that the increased effect in the RTHT experiment could be correct. This could be explained as hyperthermia is able to inhibit the BRCA2 protein, a protein that is vital in nonhomologous end joining [108]. Inhibiting these repair mechanisms after RT could well enhance cell killing, even in the short term. The results of the HTRT experiments could also be decently compared to values found in literature, in which the groups containing the 30 CEM_{43} dose could be directly compared. In supplemental table 1 in chapter 3 of the book by Van den Tempel (2017) [109], the surviving fraction of cells treated by 30 CEM_{43} followed by 4 Gy of radiation is shown. This value is found to be equal to 41% for a combination of 4 cell lines (BLM, HeLa, FaDu and VH10-SV40). This value is quite close to the values of 50±6% and 48±8% for 30 CEM_{43} followed by 2 and 6 Gy respectively found in this research. An additional paper by Hu et al. (2020) also showed that combining a radiation dose of 5 Gy and a thermal dose of 120 CEM_{43} resulted in a survival fraction for FaDu cells of less than 10% post-treatment [110]. This coincides well with the cell viability of 9±2% for the 6 Gy, 120 CEM_{43} group on day 7 in the RTHT experiment.

5.4. Confocal imaging

Lastly, the confocal imaging experiments will be discussed. Starting with the measurement visualizing the live and dead cells. Only one data set was collected using this method and this data set showed a similar response for both types of staining. This led to the belief that the Matrigel® was influencing the outcome by both the staining molecules being taken up by the Matrigel® inside the spheroids, resulting in a similar image for both spectra. The method used was therefore deemed unable to differentiate between live and dead cells effectively in these spheroids formed with Matrigel®. A possible means to check this would be to image spheroids seeded without Matrigel® and to check if these spheroids do present two different spectra. Furthermore, another useful improvement to this method could be to use a staining mixture of calcein-AM and PI. As both compounds are activated by a different wavelength, the resulting spectra should definitely be different if the Matrigel® was not the problem. Additionally, the combination of calcein-AM and PI has shown to work in earlier research investigating the effect of HT on tumour cells [111].

To see if it was possible to accurately image dead cells and to possibly see if the Matrigel® was causing a problem, the simpler PI method was used afterwards. Furthermore, an additional goal of this experiment was to show results similar to what was seen in the paper by Brüningk et al. (2020) [92], where the PI intensity of spheroids treated with HT could be clearly seen over time. This would include a clear view at the necrotic core of the spheroids. The first problem during this experiment occurred, due to the confocal microscope being located in a different lab in a different building. This microscope was used by multiple users, resulting in some problems with the set up as it was difficult to use the exact same settings for each experiment. Furthermore, due to these multiple users, time-lapse imaging methods were not possible. This resulted in the spheroids being moved between labs and cell plates, possible affecting the results, as these actions could possibly damage the outer cells of the spheroids, thereby increasing the relative PI intensity. Moving the spheroids furthermore meant that a different surface of the same spheroid could be imaged each time, reducing comparability. Additionally, despite playing around with multiple different settings, it was found that the setup used was only able to detect the fluorescence of the outer layer of the spheroids. As this surface damage could also be due to

moving the spheroids, the PI intensity would tell little about the actual effectiveness of the treatments performed on the spheroids. Not to mention the fact that only a small slice of the spheroid could be imaged sharply at a time, resulting in an incomplete total picture of the spheroid. Another problem seen in the images is the influence of fibers. These fibers show up bright in images, disrupting the PI intensity being shown by dead cells. Lastly, the growth experiments performed early in the research showed that the spheroids tend to decrease in size after about 10-14 days. It is therefore unknown if the increase in PI intensity from day 10 onward is due to the treatment performed on the spheroids or just due to the spheroids losing viability naturally. The effect seen in the control group on day 14 would suggest the latter.

6

Conclusion and recommendations

Due to the widespread nature of cancer, it is important to look at different treatment modalities to improve the efficacy of cancer treatment. To this end combining hyperthermia with different treatment modalities showed great potential in increasing both cell killing directly and sensitizing cancer cells to the different treatment modalities. Furthermore, using 3D tumour cell aggregates to mimic *in vivo* conditions *in vitro* would also bring cancer research one step closer to real-life tumours. This project focused on the combined effect of radiotherapy and hyperthermia on both growth and cell viability in multicellular tumour spheroids formed from FaDu tumour cells.

In this project, spheroids were formed of FaDu tumour cells using Matrigel® as a scaffolding agent. The spheroids formed were found to grow fast and up to a size of 550-600 μm reliably. These spheroids could then be used in different treatment settings, using both single and combined hyperthermia and radiotherapy to treat the spheroids and the effect on the spheroids was measured using both bioluminescence and fluorescence methods, as well as by visibly measuring the growth of the spheroids over time.

The single treatments showed results that were deemed logical, as a higher treatment dose resulted in a decrease in both cell viability and spheroid growth for both radiotherapy and hyperthermia. These results, however, proved to be difficult to replicate, as factors like older medium used and errors in the spheroid seeding method hindered the collection of comparable results. Furthermore, the lack of useful control group spheroids proved to be an obstacle in comparing the cell viability of experiments to other similar experiments. The thermal doses of 30 and 120 CEM_{43} and radiation doses of 2 and 6 Gy were chosen to be used in the combined treatment experiments. Due to the fact that these doses still showed room for an improved effect on cell viability, whilst ensuring that an effect would always be present in the experiments.

Combined treatment showed an improved effect on the retardation of cell growth and the decrease of cell viability for most treatment groups, both for hyperthermia followed by radiotherapy and the other way around, with the determining factor seemingly being the thermal dose. The highest thermal and radiation dose of 120 CEM_{43} combined with 6 Gy showed the highest cell killing potential, with 9±2% of the cells remaining viable when using radiotherapy before hyperthermia and 18±3% when starting with hyperthermia before using radiotherapy. The most significant difference in effect due to the order in which radiotherapy and hyperthermia were administered was seen in the 2 Gy, 120 CEM_{43} group. With radiotherapy preceding hyperthermia resulting in a cell viability of 13±2% on day 7 after treatment, whilst hyperthermia preceding radiotherapy resulted in a cell viability of 48±8%. The improved effect for most groups was seen in terms of viability, but could also be seen in cell growth and also by visual inspection of the spheroids. The treated groups that showed an increased effect showed less growth, as well as flaking around the edges of the spheroids upon visual inspection. This flaking was the result of cell clumps releasing from the spheroids, indicating an increase in cell death.

Visualizing the effect the treatment had on spheroids using confocal microscopy had some difficulties. Both using a live and dead cell staining kit, as well as PI staining proved ineffective in accurately

visualizing the dead cells in spheroids with the setup used during the research. Furthermore, the multiple steps transferring spheroids from plate to plate and to a different lab, where the confocal microscope used was positioned, did not improve the overall result of these methods. Some differences between the treatment groups could be seen, but it was uncertain if these differences were due to the treatment or due to other external factors. Additionally, only the signal of the outer layer of the spheroids could be detected, these results thus lacking in information about the entire spheroid.

Concluding, an improved effect was seen in terms of viability and cell growth when combining both radiotherapy and hyperthermia as treatment modalities for spheroids made of FaDu tumour cells. This effect was also visible when examining the spheroids under a bright-field light microscope. Experiments attempting to show this effect using confocal imaging, however, proved unsuccessful.

Lastly, some recommendations are provided for future research on this topic. Starting with the reproducibility of experiments, which proved difficult during this project. Often a lack of a proper control group made results meaningless. This lack of control spheroids can be easily fixed by seeding more of these spheroids, whilst simple errors, like using the wrong medium, can be ironed out quickly and effectively. Furthermore, the emphasis of the data collected during the research should lie on means of measuring the cell viability. Whilst spheroid size and growth are easy to measure, these results are often not an accurate indication of the liveliness of spheroids, which is the most important factor when considering the effectiveness of treatments. Viability assays often offer a quantitative method to measure this, giving a better indication of the overall viability of spheroids. The difference between a live and a dead cell in a spheroid is difficult to notice using a microscope and impossible to measure using images, whilst this difference is clearer for viability assays, as a live cell produces ATP, whilst a dead cell will not. Moving on, research has shown that the dose rate in which radiation is applied to tumour cells also influences the cell viability [112]. It is possible that the low dose rate used in this project has influenced the results. Investigating the effect of the dose rate on cell viability of spheroids might be useful. Thirdly, research by Oseroff et al. (1988) showed an improved effect when combining hyperthermia and photo-chemotherapy to treat FaDu tumour cells [113]. This effect was even shown at low temperatures. It might therefore be of interest to see if the addition of photo-chemotherapy could improve overall efficacy. Lastly, if confocal imaging is of interest, it is important to take a deep look at literature and evaluate the possibilities with the equipment at hand. Multiple ideas were proposed during this research of which not many were achievable. Plans that were achievable often did not provide desired result. Researching these topics sufficiently beforehand could significantly reduce the risk of coming up empty handed after performing an experiment for multiple days. For instance, when staining spheroids with PI it could be beneficial to leave the spheroids in medium with dissolved PI for the duration of the entire experiment, as PI showed no influence on spheroid growth [92].

A

Appendix A: Single treatment results

This appendix shows the results of all the repeated experiments using only single treatments over the time of this research project. The results will be presented in the same way as in the main text, only without the bright-field light microscope images. The results will be accompanied by a short description of the noteworthy elements visible in the results.

A.1. Results of the single RT experiments

As mentioned in the main text the single RT experiments were repeated twice more, the last 2 sets of results shown below. During these experiments the same amount of spheroids were used, so in total 6 control spheroids were used, of which were used 3 per viability assay, whilst 12 spheroids were used per treated group, of which 6 were used per viability assay.

The results of the second single RT experiment are shown in figure A.1. The growth of the spheroid diameters is similar to the earlier shown results, with the exception being that the spheroids started and ended at a slightly lower size, 307 μm and 496 μm respectively for the control group. However, the net growth of the spheroid diameter shows the growth to be similar to the earlier mentioned results. This time the control group grew 118 μm after 3 days and 185 μm in total after 7 days. The 2 Gy group spheroid diameters grew 123 μm and 170 μm after 3 and 7 days. The growth of spheroid diameter of the 6 Gy group was slightly lower with a value of 101 μm and 150 μm after 3 and 7 days. Lastly, the growth of spheroid diameter of the 10 Gy group was smallest with a value of 97 μm and 101 μm after 3 and 7 days. The standard deviation for the control, 2 and 10 Gy group is increased on day 7 compared to the earlier shown results. The cell viability on day 3 was 95±12%, 94±8% and 90±7% for the 2, 6 and 10 Gy groups respectively, which is slightly higher for the 6 and 10 Gy groups compared to the results in the main text. The viability assay on day 7, however, lacked a usable control group measurement. Due to this the viability results could not be normalized properly. These results therefore show a meaningless viability percentage. Furthermore, the cell viability of the 2 Gy and 10 Gy group was similar, with the 6 Gy cell viability being slightly higher, which is also interesting.

The results of the third single RT experiment are shown in figure A.2. Looking at the spheroid diameter growth in a) it can be seen that the control group grew less compared to the earlier experiments, growing from a size of 318 μm to 426 μm after 7 days. The control group spheroids also started at a smaller diameter size compared to the 2, 6 and 10 Gy groups. This growth trend for the control group is also seen in the net growth in the spheroid diameter in b), with the growth of the control group being 98 μm after 3 days and 118 μm after 7 days. The 2 Gy group grew the most with 84 μm after 3 days and 147 μm after 7 days. The 6 and 10 Gy groups grew 98 μm and 80 μm and 108 μm and 49 μm after 3 and 7 days respectively. The growth of every group was lower than that of the other two experiments. A similar result is seen in the viability assays of this experiment. The cell viability on day 3 of the 2, 6 and 10 Gy groups was 80±34%, 97±25% and 97±9% respectively and on day 7 this was 161±74%, 110±43% and 44±28% respectively. Both the net spheroid diameter growth and the cell viability show similar results for the control and 6 Gy groups. Therefore it was assumed that the smaller start size of the control group negatively influenced the results of the experiment.

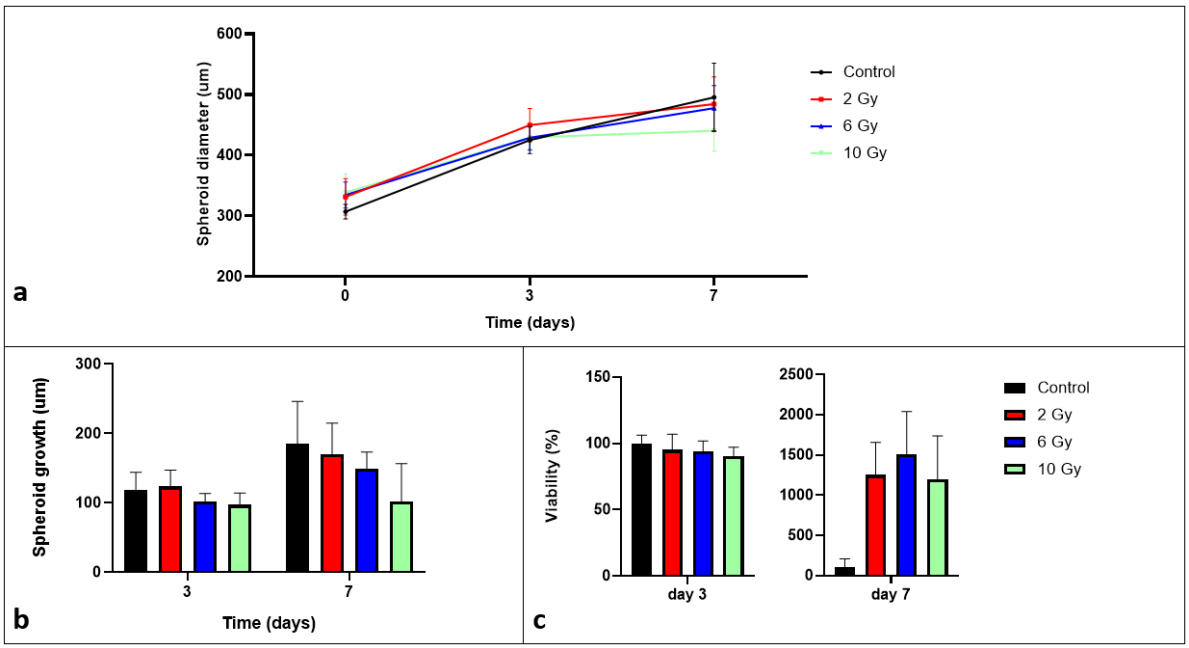

Figure A.1: Three data sets showing the results of the second single RT experiment for spheroids exposed to 0 (control), 2, 6 and 10 Gy of radiation dose using X-rays. **a.** The growth in spheroid diameter as a function of time after treatment. **b.** The net growth of the spheroid diameter on day 3 and 7 compared to the size of the spheroid diameter on day 0. **c.** The cell viability on day 3 and 7. The cell viability of the control group was used as a reference point on day 3 and 7. The cell viability of this control group was therefore seen as 100%. No meaningful significance was found.

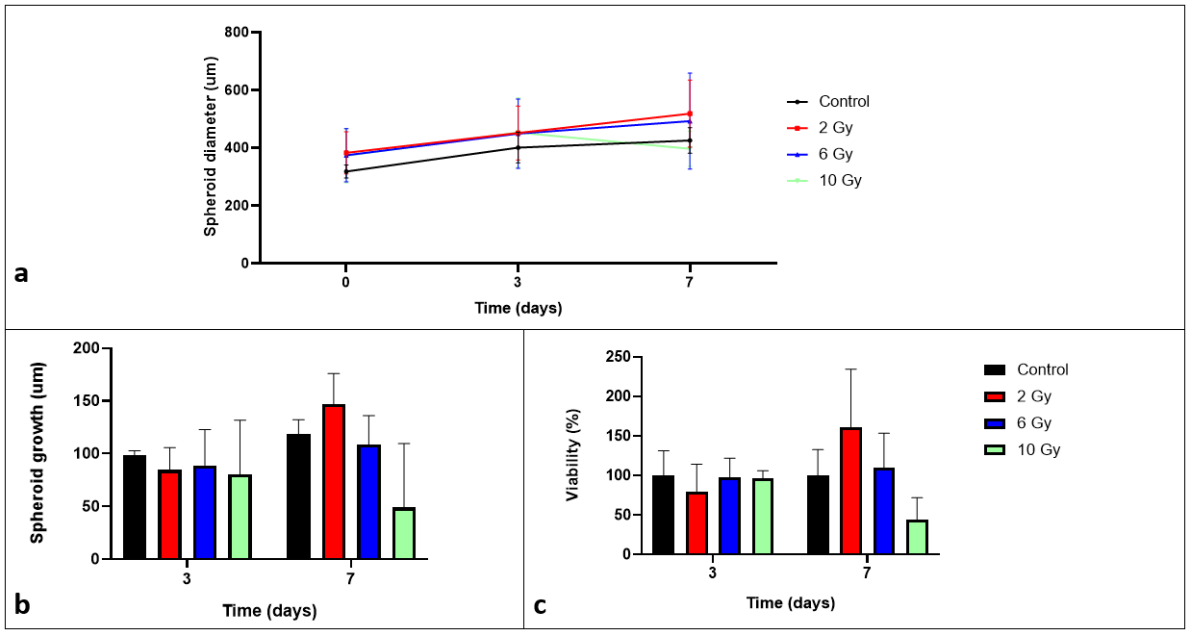

Figure A.2: Three data sets showing the results of the third single RT experiment for spheroids exposed to 0 (control), 2, 6 and 10 Gy of radiation dose using X-rays. **a.** The growth in spheroid diameter as a function of time after treatment. **b.** The net growth of the spheroid diameter on day 3 and 7 compared to the size of the spheroid diameter on day 0. **c.** The cell viability on day 3 and 7. The cell viability of the control group was used as a reference point on day 3 and 7. The cell viability of this control group was therefore seen as 100%. No meaningful significance was found.

Overall, the second and third single RT experiments lack information in terms of viability. As the growth still roughly follows an inversely proportional trend for the second experiment, with a higher dose leading to a lower growth over time, it was expected that the viability would also show this trend

like in the earlier data. However, lacking a proper control group to relate the treated groups to, hinders the viability results for both the repeats.

A.2. Results of the single HT experiments

The HT experiments were carried out 3 times in total as well, with the final 2 data sets shown below. During both experiments 10 spheroids per group were used, with 5 being used during each viability assay, similar to the experiment mentioned in the main text.

The results of the second single HT experiment are shown in figure A.3. Together with the general spheroid growth experiments, this was one of the first experiments performed during the entire project. Due to this, the entire experiment was compromised slightly, with the spheroids not being treated on day 0, but after an additional 4 days of waiting. During this time most spheroids already reached a size similar to their size at the end of the experiment. The net spheroid growth of the control group was 183 μm and 193 μm on day 7 and 11 respectively. The growth of the 1 and 5 CEM_{43} group was slightly lower with values of 151 μm and 173 μm on day 7 and 176 μm and 182 μm on day 11 respectively. Whilst, the growth of the 30 and 120 CEM_{43} group was slightly higher with values of 222 μm and 201 μm on day 7 and 221 μm and 220 μm on day 11 respectively. The size growth therefore did not change much between day 7 and 11, with only the 480 CEM_{43} group showing a decrease in net spheroid growth from 189 μm on day 7 to 112 μm on day 11. Furthermore, the net growth contains a number of large error margins due to the differences in spheroid sizes. Subsequently, not much can be said about the net growth for most groups. A similar effect can be seen in the viability assay results. With the cell viability of the 1 and 5 CEM_{43} groups being slightly lower compared to the control group on day 3 and 7. The cell viability of the 30 and 120 CEM_{43} groups was slightly higher compared to the control group on day 3 and 7. Lastly, only a significant effect on the cell viability was visible for the 480 CEM_{43}, which as expected is significantly lower than the control group. It is assumed that delaying the treatment and thus the larger spheroid size in treatment effected the results.

The results of the third single HT experiment are shown in figure A.4. These results show more similarities compared to the results shown in the main text. The spheroid diameter of the control group grows from 293 μm on day 0 to 541 μm on day 7 and a decrease in spheroid diameter is seen for the 480 CEM_{43} group. The net growth shows a similar inversely proportional trend, with a higher dose leading to less spheroid growth. An outlier can be seen in the form of the 1 CEM_{43} group, which shows slightly lower net spheroid growth compared to the control group. Furthermore, the net spheroid growth of the 120 CEM_{43} group is higher compared to the results shown in the main text on day 7. Lastly, the 480 CEM_{43} group shows a net spheroid growth of only 4 μm after 7 days. Although the net spheroid growth in general is slightly higher compared to the earlier mentioned results, the overall trend is still comparable. The same can be said about the cell viability, although it should be mentioned that this time an effect is already seen after 3 days for every treated group apart from the 1 CEM_{43} group. The effect on the cell viability of the 5, 30 and 120 CEM_{43} is reduced after 7 days, with viability increasing for these groups, whilst the cell viability of the 1 CEM_{43} group is decreased on day 7 compared to the control group. Lastly, as expected the 480 CEM_{43} group shows little cell viability on both day 3 and day 7.

Concluding, whilst the second single HT experiment did not provide information on most treated groups apart from the 480 CEM_{43} group, the third single HT experiment does largely confirm the results shown earlier in the report. Strengthening the already seen trend that a higher dose leads to a reduce in growth over time, with the 480 CEM_{43} group showing a drastic response and the 1 and 5 CEM_{43} groups showing little to no effect. Both the 30 and 120 CEM_{43} groups do still show an effect on both net spheroid growth and cell viability, which is not as drastic as the response of the 480 CEM_{43} group. The choice to continue to the combined treatments with the 30 and 120 CEM_{43} groups is therefore confirmed.

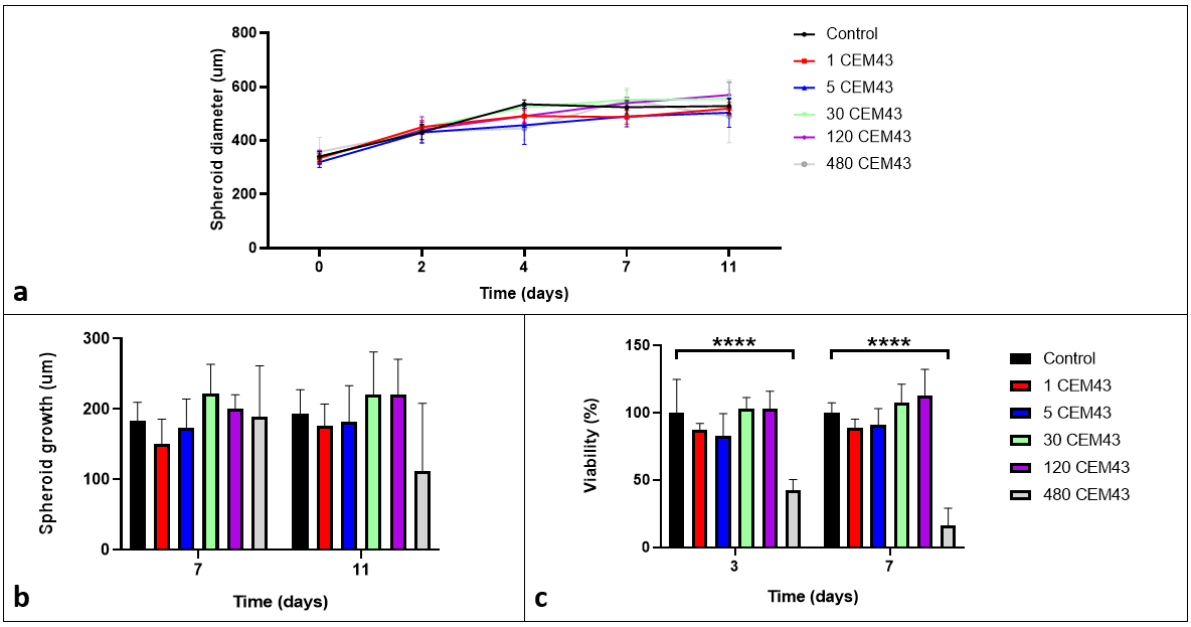

Figure A.3: Three data sets showing the results of the second HT experiment for spheroids exposed to 0 (control), 1, 5, 30, 120 and 480 CEM_{43} of thermal dose using hyperthermia. **a.** The growth in spheroid diameter as a function of time after treatment. **b.** The net growth of the spheroid diameter on day 3 and 7 compared to the size of the spheroid diameter on day 0. **c.** The cell viability on day 3 and 7. The cell viability of the control group was used as a reference point on day 3 and 7. The cell viability of this control group was therefore seen as 100%. Significance of these results is indicated with n=5 per group. * = p=0.0332, ** = p=0.0021, *** = p=0.0002 and **** = p<0.0001

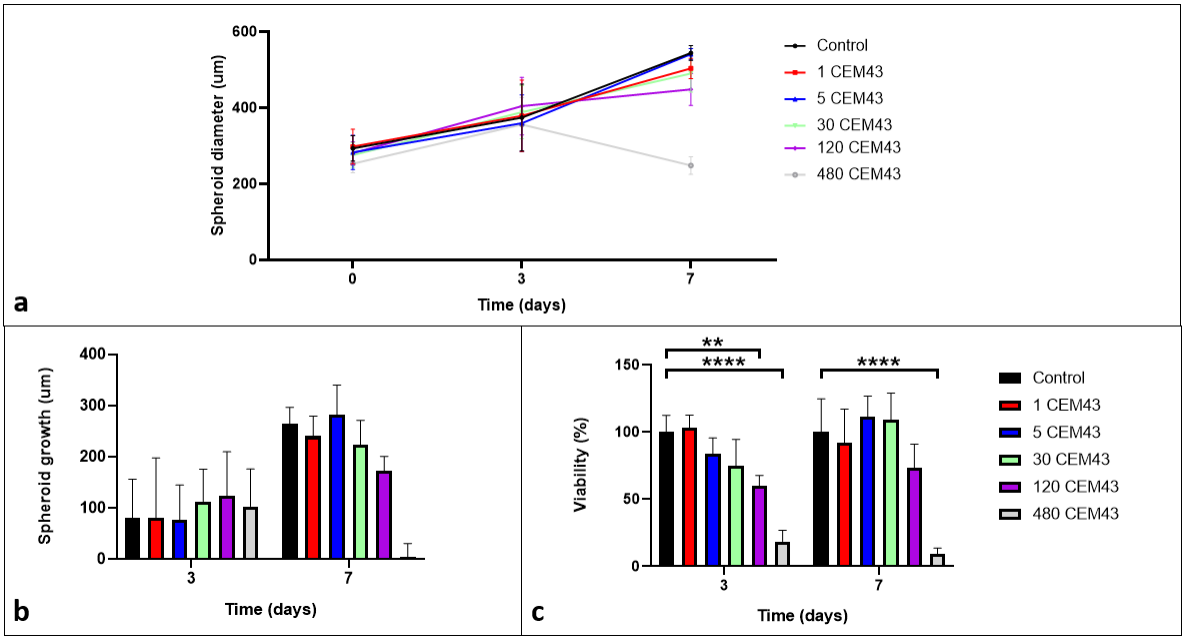

Figure A.4: Three data sets showing the results of the third HT experiment for spheroids exposed to 0 (control), 1, 5, 30, 120 and 480 CEM_{43} of thermal dose using hyperthermia. **a.** The growth in spheroid diameter as a function of time after treatment. **b.** The net growth of the spheroid diameter on day 3 and 7 compared to the size of the spheroid diameter on day 0. **c.** The cell viability on day 3 and 7. The cell viability of the control group was used as a reference point on day 3 and 7. The cell viability of this control group was therefore seen as 100%. Significance of these results is indicated with n=5 per group. * = p=0.0332, ** = p=0.0021, *** = p=0.0002 and **** = p<0.0001

B

Appendix B: Combined treatment results

Appendix B provides the results of the other combined treatment experiments. The results of both the other HTRT and RTHT experiments will be displayed after each other. The results are shown in the same form as in the main text without the bright-field light microscope images. All results will be supported by a brief description of the graphs.

B.1. Results of the combined HTRT experiments

First the results of the three HTRT experiments are discussed. In contrast to the results mentioned in the main text, the spheroid allocation per group is a bit different. To achieve the following results 6 control spheroids were used and 8 spheroids per treated group, with 3 control spheroids and 4 treated spheroids per group being used for each viability assay. The treatment dose and methods remained the same and can be seen as a reminder in table B.1.

Table B.1: The names of the different treatment groups used in the HTRT experiments, as well as the combined thermal dose the groups were exposed to using hyperthermia and subsequently the radiation dose applied using X-rays.

Group name	**Treatment dose**
Control group	No treatment
Group A	30 CEM_{43}, 2 Gy
Group B	30 CEM_{43}, 6 Gy
Group C	120 CEM_{43}, 2 Gy
Group D	120 CEM_{43}, 6 Gy

Starting off with the results of the second HTRT experiment. The growth results are shown in figure B.1. As can be seen in figure B.1.a, the control group spheroids grew from a size of 328 μm on day 0 to 521 μm on day 7. This is similar to earlier experiments. Again the treated groups followed the trend where a higher treatment dose resulted in less diameter growth over time. It is interesting to note that the spheroid diameter for all treated groups decreased between day 3 and 7. Looking at the net growth, the results followed the results in figure 4.9, apart from the total growth for the treated groups being almost halved on day 3. This negative impact on net growth was only increased on day 7. With group B and C showing the same response, whilst group A showed a larger growth and group D showed a decrease in growth compared to the middle groups, reaching a size below the spheroid diameter that the group had on day 0. In general, whilst the control group showed normal growth over the 7 days, the growth of each treated group was significantly reduced compared to the results shown in the main text. Moving on to the cell viability results shown in figure B.2. On day 3 a significant effect was already seen for each treated group. With the most significant effect shown by group B and

C. The seen effect only increased up to day 7, with all treated groups showing little viability on day 7. The most significant effect was seen for group A. The cell viability shown by this group was similar to that of the groups with higher treatment doses. Overall, the cell viability followed a similar trend as the earlier results.

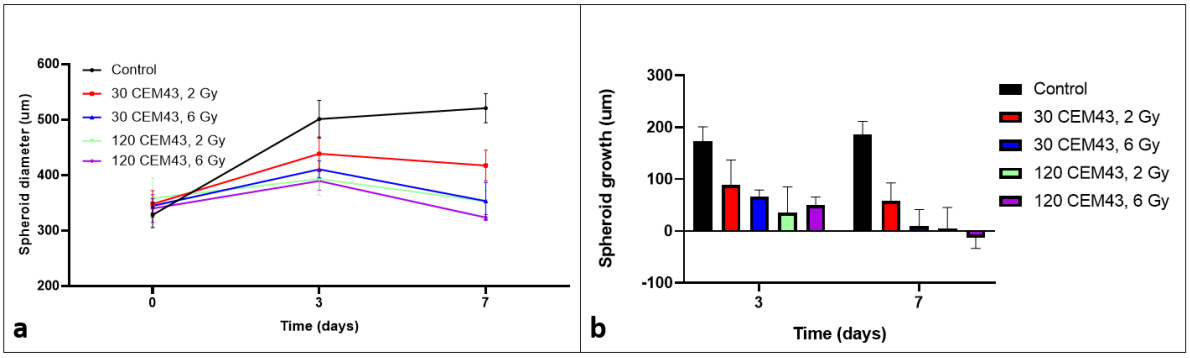

Figure B.1: Two data sets showing the results in terms of growth for the second HTRT experiment. The results are given for a control group and 4 groups that were treated with a combination of a thermal dose of 30 and 120 CEM_{43} applied using hyperthermia and a radiation dose of 2 and 6 Gy applied using X-rays. **a.** The size of spheroid diameter for each group on 0, 3 and 7 days after treatment. **b.** The net growth of the spheroid diameter for same groups on day 3 and 7 compared to the diameter size on day 0.

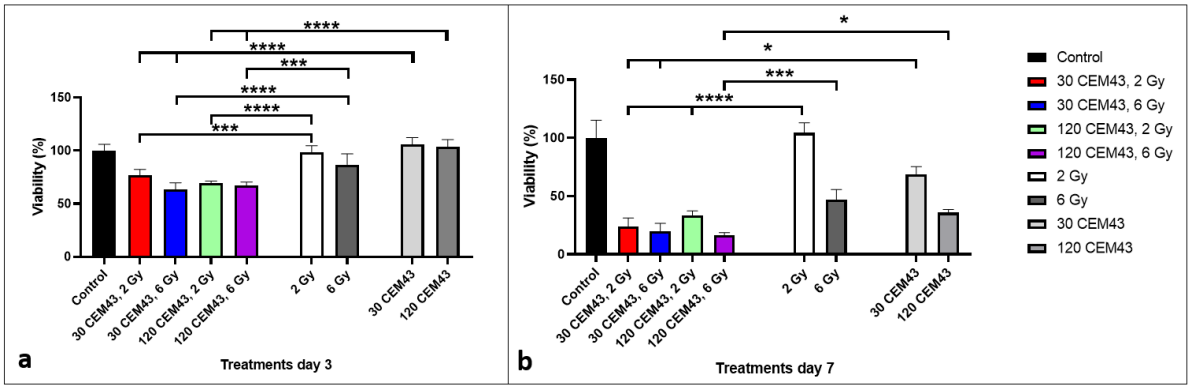

Figure B.2: Two data sets showing the results in terms of cell viability of the second HTRT experiment. The results are given for a control group and 4 groups that were treated with a combination of a thermal dose of 30 and 120 CEM_{43} applied using hyperthermia and a radiation dose of 2 and 6 Gy applied using X-rays. Significance of these results is indicated compared to the results of the single treatment experiment. * = p=0.0332, ** = p=0.0021, *** = p=0.0002 and **** = p<0.0001 **a.** The cell viability of the different groups on day 3 after treatment. **b.** The cell viability of the different groups on day 7 after treatment.

The results of the third HTRT experiment are shown in figures B.3 and B.4. The results of the growth are quite similar compared to the results shown in figure B.1. The only difference is the overall growth was lower, even for the control group, which barely grew after day 3. The net growth can be summarized by saying the group A grew the most of the treated groups after day 7, followed by group B and C, which showed a slight decrease in size after 7 days. Lastly, group D showed a significant decrease in spheroid size over the 7 days. Not much information can be learned from the cell viability assessment, as each treated group showed a similar response after 3 and 7 days. With only group A and C showing a significant increase in effect compared to single 2 Gy treatment on day 7.

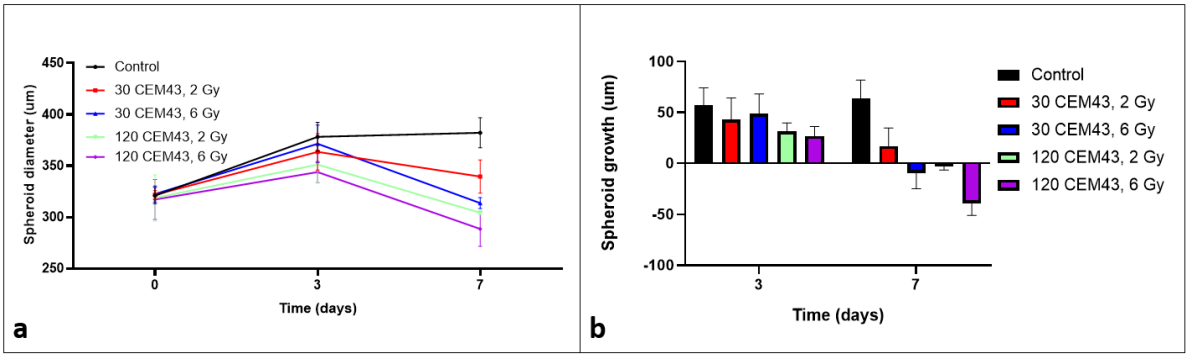

Figure B.3: Two data sets showing the results in terms of growth for the third HTRT experiment. The results are given for a control group and 4 groups that were treated with a combination of a thermal dose of 30 and 120 CEM_{43} applied using hyperthermia and a radiation dose of 2 and 6 Gy applied using X-rays. **a.** The size of spheroid diameter for each group on 0, 3 and 7 days after treatment. **b.** The net growth of the spheroid diameter for same groups on day 3 and 7 compared to the diameter size on day 0.

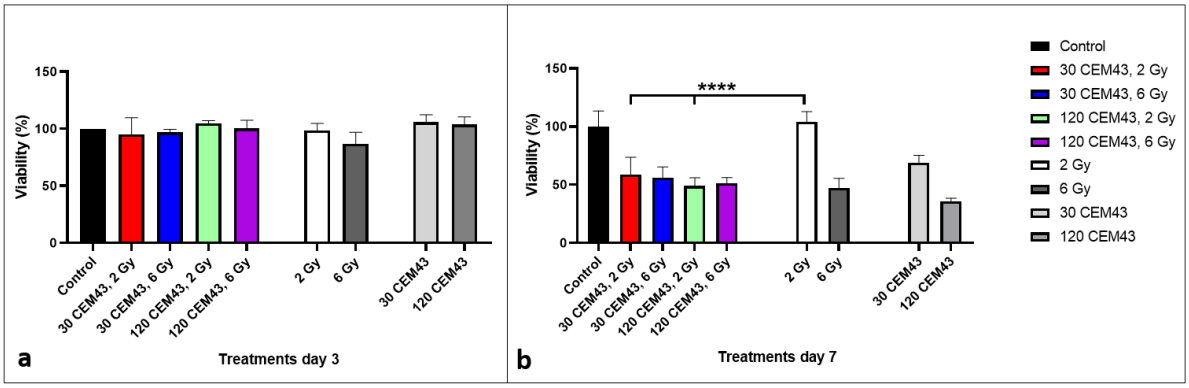

Figure B.4: Two data sets showing the results in terms of cell viability of the third HTRT experiment. The results are given for a control group and 4 groups that were treated with a combination of a thermal dose of 30 and 120 CEM_{43} applied using hyperthermia and a radiation dose of 2 and 6 Gy applied using X-rays. Significance of these results is indicated compared to the results of the single treatment experiment. * = p=0.0332, ** = p=0.0021, *** = p=0.0002 and **** = p<0.0001 **a.** The cell viability of the different groups on day 3 after treatment. **b.** The cell viability of the different groups on day 7 after treatment.

The fourth combined HTRT experiment showed some interesting results, which can be seen in figures B.5 and B.6. All spheroids shrink between days 3 to 7, even the control group. The trend shown by the net growth, however, stayed similar compared to the net growth of the first three experiments. The only exception being that group B showed a larger decrease in spheroid diameter compared to group C. Furthermore, this time a reduce in spheroid diameter was seen for each group after 7 days. The cell viability results showed no valuable information as the response of each group was similar on day 3, with an increase in viability for all treated groups compared to the control group. On day 7 the viability of group A and D was similar, whilst the other 2 groups had a slightly increased viability. Only group A showed a significant increase in effect compared to single 2 Gy treatment, whilst the other groups all showed a significant decrease in effect.

From the results of the three HTRT experiments shown in this appendix, it can be concluded that the growth follows a trend, where the 30 CEM_{43}, 2 Gy group grows the most, followed by the 120 CEM_{43}, 2 Gy and 30 CEM_{43}, 6 Gy groups, which grow similarly, and the 120 CEM_{43}, 6 Gy group which grows the least. The problems lies with interpreting the viability assessment results, as little variance is seen between the groups in most experiments. Still, in figure B.2 it could be seen that each treated group showed an increased effect compared to the single treatments.

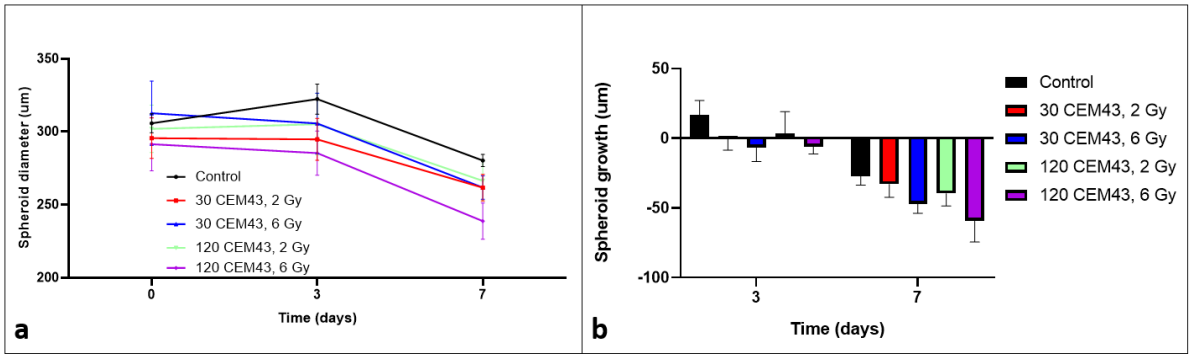

Figure B.5: Two data sets showing the results in terms of growth for the fourth HTRT experiment. The results are given for a control group and 4 groups that were treated with a combination of a thermal dose of 30 and 120 CEM_{43} applied using hyperthermia and a radiation dose of 2 and 6 Gy applied using X-rays. **a.** The size of spheroid diameter for each group on 0, 3 and 7 days after treatment. **b.** The net growth of the spheroid diameter for same groups on day 3 and 7 compared to the diameter size on day 0.

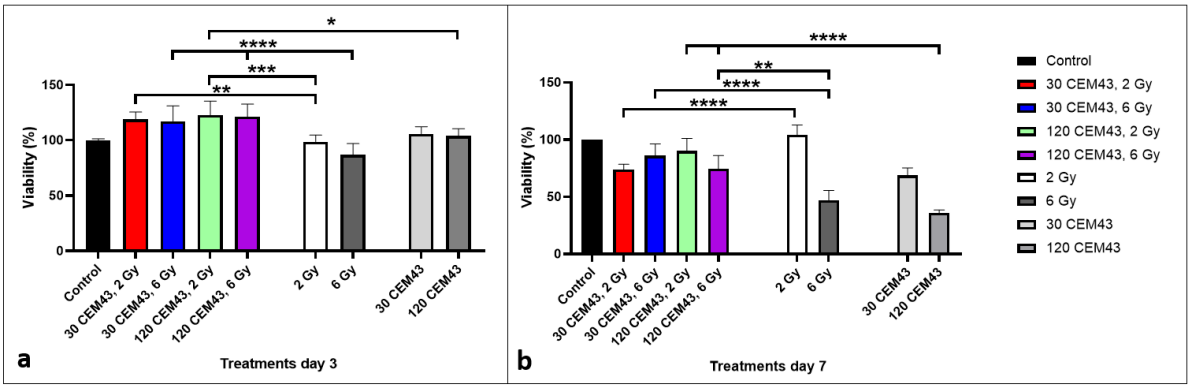

Figure B.6: Two data sets showing the results in terms of cell viability of the fourth HTRT experiment. The results are given for a control group and 4 groups that were treated with a combination of a thermal dose of 30 and 120 CEM_{43} applied using hyperthermia and a radiation dose of 2 and 6 Gy applied using X-rays. Significance of these results is indicated compared to the results of the single treatment experiment. * = p=0.0332, ** = p=0.0021, *** = p=0.0002 and **** = p<0.0001 **a.** The cell viability of the different groups on day 3 after treatment. **b.** The cell viability of the different groups on day 7 after treatment.

B.2. Results of the combined RTHT experiments

Lastly, the results of the three other RTHT experiment are discussed. Again the spheroid allocation changed a bit from the experiment in the main text. 6 control spheroids and 8 spheroids per treated group were seeded at the beginning of each experiment, resulting in 3 control spheroids and 4 treated spheroids per group being used in each viability assay. The different groups and their associated treatment doses are shown in table B.2.

Looking at figure B.7, it should be immediately noted that treatment during this experiment occurred on day 3 instead of day 0. Due to this error in the experimental method, every group barely grew between day 3 and day 10, with group C even shrinking significantly between day 6 and 10. On day 10 all treated groups end on a similar size, with only the control group spheroids being larger. Net growth for the control group was also lower compared to the RTHT experiment shown in the main text. Overall, no useful information could be retrieved from the growth results of this experiment. Moving on to the cell viability assessment, the results of which are shown in figure B.8. On day 3, only a slight decrease in cell viability is seen for each treated group, with only a slightly significant difference being shown by group C compared to the single treatments. On day 7 the cell viability does differ between the groups. Here group B shows the highest viability, followed by group A and C, that have a similar lower viability. As expected, the group treated with the highest doses, group D, shows the lowest viability after 7 days. Only a significant increase in effect is shown on day 7 by group A, whilst group B and C show a significant decrease in effect.

Table B.2: The names of the different treatment groups used in the RTHT experiments, as well as the combined radiation dose the groups were exposed to using x-rays and subsequently the thermal dose applied using hyperthermia.

Group name	Treatment dose
Control group	No treatment
Group A	2 Gy, 30 CEM_{43}
Group B	2 Gy, 120 CEM_{43}
Group C	6 Gy, 30 CEM_{43}
Group D	6 Gy, 120 CEM_{43}

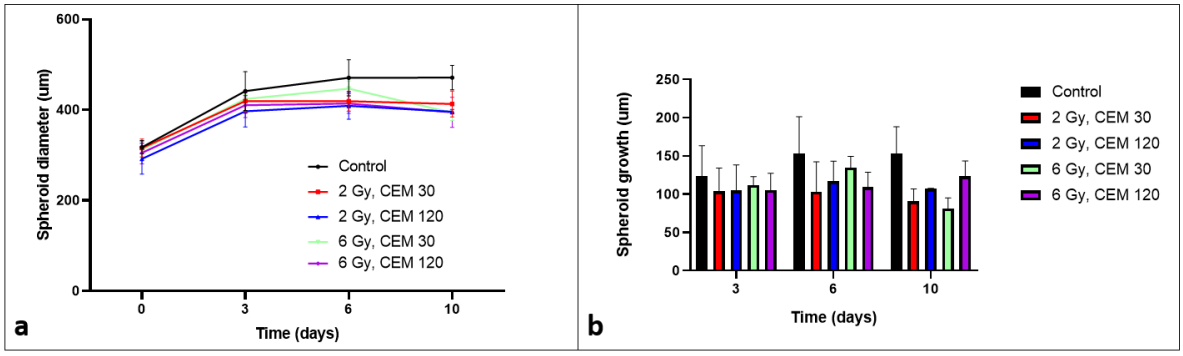

Figure B.7: Two data sets showing the results in terms of growth for the second RTHT experiment. The results are given for a control group and 4 groups that were treated with a combination of a radiation dose of 2 and 6 Gy applied using x-rays and a thermal dose of 30 and 120 CEM_{43} applied using hyperthermia. **a.** The size of spheroid diameter for each group on 0, 3 and 7 days after treatment. **b.** The net growth of the spheroid diameter for same groups on day 3 and 7 compared to the diameter size on day 0.

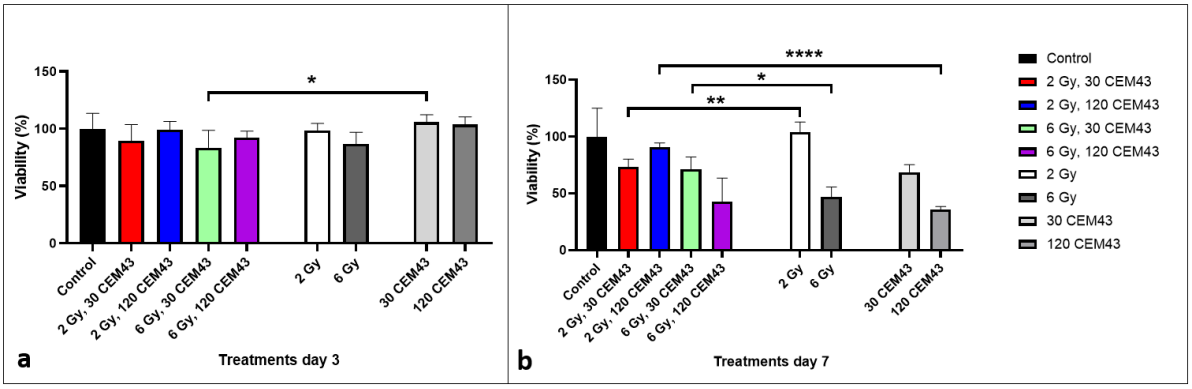

Figure B.8: Two data sets showing the results in terms of cell viability of the second RTHT experiment. The results are given for a control group and 4 groups that were treated with a combination of a radiation dose of 2 and 6 Gy applied using x-rays and a thermal dose of 30 and 120 CEM_{43} applied using hyperthermia. Significance of these results is indicated compared to the results of the single treatment experiment. * = p=0.0332, ** = p=0.0021, *** = p=0.0002 and **** = p<0.0001 **a.** The cell viability of the different groups on day 3 after treatment. **b.** The cell viability of the different groups on day 7 after treatment.

Proceeding to the results of the third RTHT experiment, shown in figures B.9 and B.10. Similarly to the results of the HTRT experiments, the overall growth decreases. During this experiment the spheroids of all groups shrank between day 3 and 7, except for group A, which slightly increased in size. A large decrease in size is seen for both group B and D. At the same time the size of group C remains quite stable at its starting size on day 0. This effect is also seen in a less obvious manner for the viability. On day 3, the cell viability of groups A, B and D is similar to the control group, whilst the viability of group C is slightly lower. After 7 days, group A shows the highest percentage of cell viability of each treated group. After that group C follows with a slightly higher viability compared to groups B and D, which show a similar viability. The net growth and cell viability both show the most effect for groups B and D. Furthermore, this distribution is also shown in the results in the main text, the main difference being that the overall cell viability is higher and the net growth is lower for this experiment.

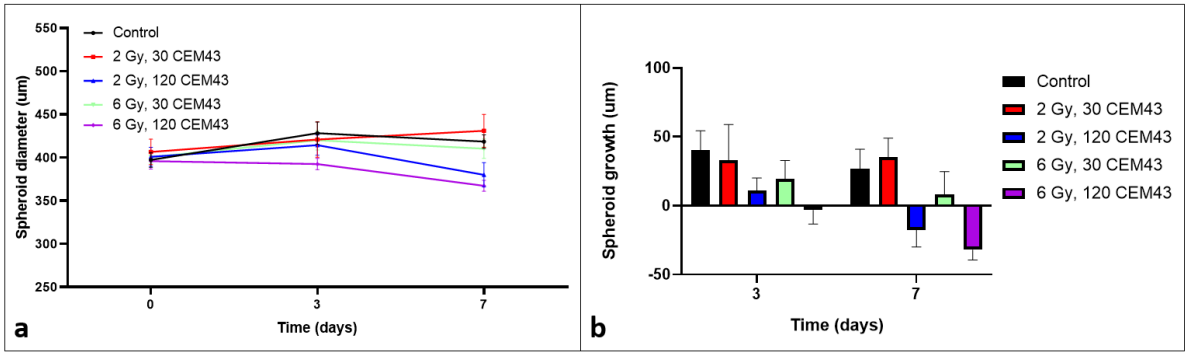

Figure B.9: Two data sets showing the results in terms of growth for the third RTHT experiment. The results are given for a control group and 4 groups that were treated with a combination of a radiation dose of 2 and 6 Gy applied using x-rays and a thermal dose of 30 and 120 CEM_{43} applied using hyperthermia. **a.** The size of spheroid diameter for each group on 0, 3 and 7 days after treatment. **b.** The net growth of the spheroid diameter for same groups on day 3 and 7 compared to the diameter size on day 0.

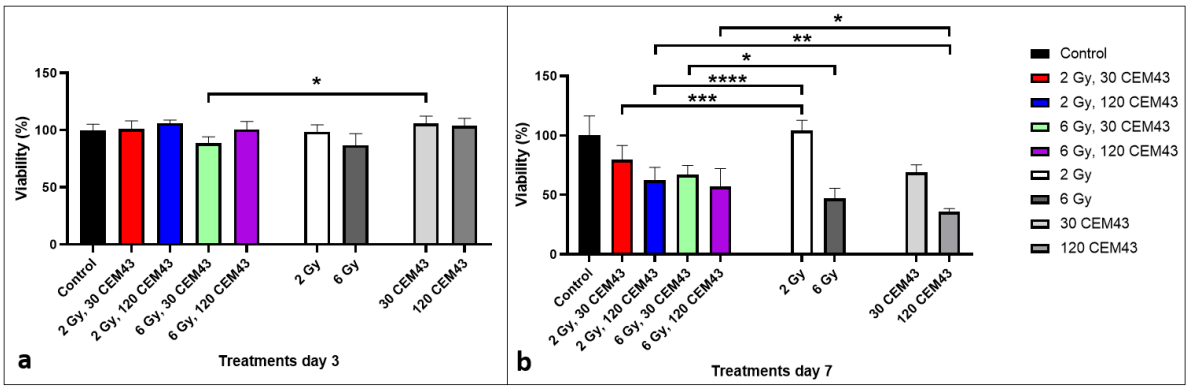

Figure B.10: Two data sets showing the results in terms of cell viability of the third RTHT experiment. The results are given for a control group and 4 groups that were treated with a combination of a radiation dose of 2 and 6 Gy applied using x-rays and a thermal dose of 30 and 120 CEM_{43} applied using hyperthermia. Significance of these results is indicated compared to the results of the single treatment experiment. * = p=0.0332, ** = p=0.0021, *** = p=0.0002 and **** = p<0.0001 **a.** The cell viability of the different groups on day 3 after treatment. **b.** The cell viability of the different groups on day 7 after treatment.

The results of the fourth RTHT experiment are shown in figures B.11 and B.12. Following the earlier shown HTRT results, here the overall growth is once again decreased, with even the control group shrinking significantly between day 3 and day 7. The results for the net growth also show this, with the control group growing similarly to the group B and groups A, C and D all showing a comparable significant decrease in size. Nevertheless, the viability results are similar to those shown in figure B.10. On day 3, the cell viability of group B, C and D is slightly increased compared to the control group, whilst group A shows a significant decrease in cell viability. On day 7, the viability of group A is subsequently increased, whilst that of group B, C and D is decreased. These three group show a similar pattern as the previous experiment, with group B and D showing a similar cell viability and that of group C being slightly higher. All treated groups show a decrease in effect compared to the single treatments.

To conclude, the three RTHT experiments in this appendix confirm none of the results shown in the main text. No clear conclusion can be drawn of the growth of the spheroids and the cell viability. In general, the largest effect on viability is seen in both groups B and D, treated with the HT dose of 120 CEM_{43}, with the radiation dose for these groups mattering little. However, every treated group only showed a decrease in effect compared to using the single treatments and therefore these results are non-conclusive.

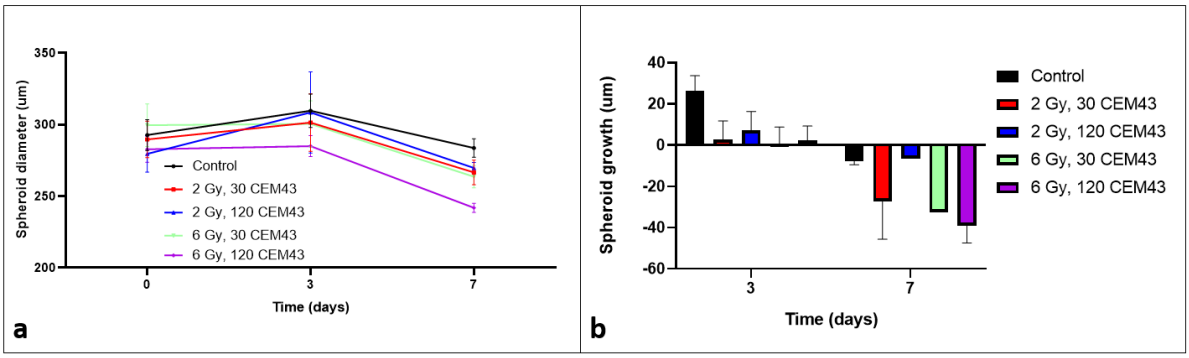

Figure B.11: Two data sets showing the results in terms of growth for the fourth RTHT experiment. The results are given for a control group and 4 groups that were treated with a combination of a radiation dose of 2 and 6 Gy applied using x-rays and a thermal dose of 30 and 120 CEM_{43} applied using hyperthermia. **a.** The size of spheroid diameter for each group on 0, 3 and 7 days after treatment. **b.** The net growth of the spheroid diameter for same groups on day 3 and 7 compared to the diameter size on day 0.

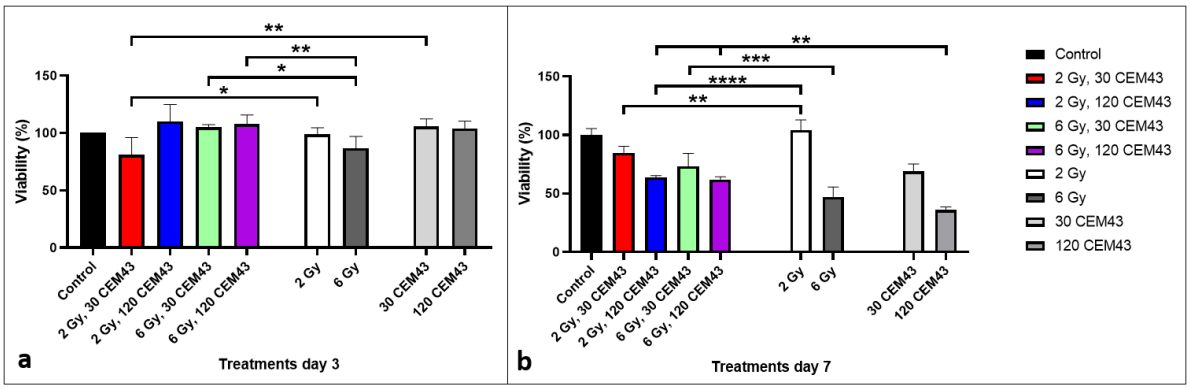

Figure B.12: Two data sets showing the results in terms of cell viability of the fourth RTHT experiment. The results are given for a control group and 4 groups that were treated with a combination of a radiation dose of 2 and 6 Gy applied using x-rays and a thermal dose of 30 and 120 CEM_{43} applied using hyperthermia. Significance of these results is indicated compared to the results of the single treatment experiment. * = p=0.0332, ** = p=0.0021, *** = p=0.0002 and **** = p<0.0001 **a.** The cell viability of the different groups on day 3 after treatment. **b.** The cell viability of the different groups on day 7 after treatment.

Bibliography

[1] National Cancer Institute, *What is cancer?* https://www.cancer.gov/about-cancer/understanding/what-is-cancer (2021).

[2] National Cancer Institute, *Cancer statistics,* https://www.cancer.gov/about-cancer/understanding/statistics (2021).

[3] European Commission, *Ecis - european cancer information system,* https://ecis.jrc.ec.europa.eu/ (2021).

[4] S. Chakraborty and T. Rahman, *The difficulties in cancer treatment,* ecancermedicalscience **6** (2012).

[5] National Cancer Institute, *Metastasis,* https://www.cancer.gov/publications/dictionaries/cancer-terms/def/metastasis (2021).

[6] W. C. Dewey, *Arrhenius relationships from the molecule and cell to the clinic,* International journal of hyperthermia **10**, 457 (1994).

[7] Z. Behrouzkia, Z. Joveini, B. Keshavarzi, N. Eyvazzadeh, and R. Z. Aghdam, *Hyperthermia: how can it be used?* Oman medical journal **31**, 89 (2016).

[8] M. Sethi and S. Chakarvarti, *Hyperthermia techniques for cancer treatment: A review,* Int. J. PharmTech Res **8**, 292 (2015).

[9] L. Sharif-Khatibi, A. Kariminia, S. Khoei, and B. Goliaei, *Hyperthermia induces differentiation without apoptosis in permissive temperatures in human erythroleukaemia cells,* International journal of hyperthermia **23**, 645 (2007).

[10] P. Wust, B. Hildebrandt, G. Sreenivasa, B. Rau, J. Gellermann, H. Riess, R. Felix, and P. Schlag, *Hyperthermia in combined treatment of cancer,* The lancet oncology **3**, 487 (2002).

[11] O. Dahl, *Interaction of hyperthermia and chemotherapy,* Application of Hyperthermia in the Treatment of Cancer , 157 (1988).

[12] J. M. Bull, *An update on the anticancer effects of a combination of chemotherapy and hyperthermia,* Cancer research **44**, 4853s (1984).

[13] N. R. Datta, S. Rogers, S. G. Ordóñez, E. Puric, and S. Bodis, *Hyperthermia and radiotherapy in the management of head and neck cancers: A systematic review and meta-analysis,* International Journal of Hyperthermia **32**, 31 (2016).

[14] M. Falk and R. Issels, *Hyperthermia in oncology,* International Journal of Hyperthermia **17**, 1 (2001).

[15] ATCC, *Fadu cell line,* https://www.atcc.org/products/htb-43 (2021).

[16] Skin Cancer Foundation, *Squamous cell carcinoma overview,* https://www.skincancer.org/skin-cancer-information/squamous-cell-carcinoma/ (2022).

[17] S. Jain, F. R. Khuri, and D. M. Shin, *Prevention of head and neck cancer: current status and future prospects,* Current problems in cancer **28**, 265 (2004).

[18] C. Liu, K. Liao, N. Gross, Z. Wang, G. Li, W. Zuo, S. Zhong, Z. Zhang, H. Zhang, J. Yang, *et al.*, *Homologous recombination enhances radioresistance in hypopharyngeal cancer cell line by targeting dna damage response,* Oral Oncology **100**, 104469 (2020).

[19] C. Liu, N. Gross, Y. Li, G. Li, Z. Wang, S. Zhong, Y. Li, and G. Hu, *Parp inhibitor olaparib increases the sensitization to radiotherapy in fadu cells,* Journal of Cellular and Molecular Medicine **24**, 2444 (2020).

[20] L. Schaaf, M. Schwab, C. Ulmer, S. Heine, T. E. Mürdter, J. O. Schmid, G. Sauer, W. E. Aulitzky, and H. van der Kuip, *Hyperthermia synergizes with chemotherapy by inhibiting parp1-dependent dna replication arrest,* Cancer research **76**, 2868 (2016).

[21] A. L. Oei, V. R. Ahire, C. Van Leeuwen, R. Ten Cate, L. J. Stalpers, J. Crezee, H. P. Kok, and N. A. Franken, *Enhancing radiosensitisation of brca2-proficient and brca2-deficient cell lines with hyperthermia and parp1-i,* International Journal of Hyperthermia **34**, 39 (2018).

[22] J. Barretina, G. Caponigro, N. Stransky, K. Venkatesan, A. A. Margolin, S. Kim, C. J. Wilson, J. Lehár, G. V. Kryukov, D. Sonkin, *et al.*, *The cancer cell line encyclopedia enables predictive modelling of anticancer drug sensitivity,* Nature **483**, 603 (2012).

[23] S. Domcke, R. Sinha, D. A. Levine, C. Sander, and N. Schultz, *Evaluating cell lines as tumour models by comparison of genomic profiles,* Nature communications **4**, 1 (2013).

[24] News-Medical, *What is squamous cell carcinoma?* https://www.news-medical.net/health/What-is-Squamous-Cell-Carcinoma.aspx (2022).

[25] K.-J. Cho, E.-J. Park, M.-S. Kim, and Y.-H. Joo, *Characterization of fadu-r, a radioresistant head and neck cancer cell line, and cancer stem cells,* Auris Nasus Larynx **45**, 566 (2018).

[26] D. Zips, A. Dörfler, K. Richter, S. Vettermann, C. Petersen, B. Beuthien-Baumann, D. Thümmler, M. Baumann, *et al.*, *Effect of the hypoxic cell sensitizer isometronidazole on local control of two human squamous cell carcinomas after fractionated irradiation,* Strahlentherapie und Onkologie **180**, 375 (2004).

[27] L. Rossow, I. Eke, E. Dickreuter, and N. Cordes, *Targeting of the egfr/β1 integrin connecting proteins pinch1 and nck2 radiosensitizes three-dimensional scc cell cultures,* Oncology Reports **34**, 469 (2015).

[28] N. T. Elliott and F. Yuan, *A review of three-dimensional in vitro tissue models for drug discovery and transport studies,* Journal of pharmaceutical sciences **100**, 59 (2011).

[29] J. Hoarau-Véchot, A. Rafii, C. Touboul, and J. Pasquier, *Halfway between 2d and animal models: are 3d cultures the ideal tool to study cancer-microenvironment interactions?* International journal of molecular sciences **19**, 181 (2018).

[30] M. Kapałczyńska, T. Kolenda, W. Przybyła, M. Zajączkowska, A. Teresiak, V. Filas, M. Ibbs, R. Bliźniak, Ł. Łuczewski, and K. Lamperska, *2d and 3d cell cultures–a comparison of different types of cancer cell cultures,* Archives of medical science: AMS **14**, 910 (2018).

[31] E. C. Costa, A. F. Moreira, D. de Melo-Diogo, V. M. Gaspar, M. P. Carvalho, and I. J. Correia, *3d tumor spheroids: an overview on the tools and techniques used for their analysis,* Biotechnology advances **34**, 1427 (2016).

[32] J. C. Fontoura, C. Viezzer, F. G. Dos Santos, R. A. Ligabue, R. Weinlich, R. D. Puga, D. Antonow, P. Severino, and C. Bonorino, *Comparison of 2d and 3d cell culture models for cell growth, gene expression and drug resistance,* Materials Science and Engineering: C **107**, 110264 (2020).

[33] S. Breslin and L. O'Driscoll, *The relevance of using 3d cell cultures, in addition to 2d monolayer cultures, when evaluating breast cancer drug sensitivity and resistance,* Oncotarget **7**, 45745 (2016).

[34] A. A. Seyhan, *Lost in translation: the valley of death across preclinical and clinical divide–identification of problems and overcoming obstacles,* Translational Medicine Communications **4**, 1 (2019).

[35] C. Jensen and Y. Teng, *Is it time to start transitioning from 2d to 3d cell culture?* Frontiers in molecular biosciences **7**, 33 (2020).

[36] R. M. Sutherland, W. R. Inch, J. A. McCredie, and J. Kruuv, *A multi-component radiation survival curve using an in vitro tumour model,* International Journal of Radiation Biology and Related Studies in Physics, Chemistry and Medicine **18**, 491 (1970).

[37] M. T. Santini and G. Rainaldi, *Three-dimensional spheroid model in tumor biology,* Pathobiology **67**, 148 (1999).

[38] R. M. Sutherland, J. A. McCredie, and W. R. Inch, *Growth of multicell spheroids in tissue culture as a model of nodular carcinomas,* Journal of the National Cancer Institute **46**, 113 (1971).

[39] M. Zanoni, S. Pignatta, C. Arienti, M. Bonafè, and A. Tesei, *Anticancer drug discovery using multicellular tumor spheroid models,* Expert opinion on drug discovery **14**, 289 (2019).

[40] J. Friedrich, R. Ebner, and L. A. Kunz-Schughart, *Experimental anti-tumor therapy in 3-d: spheroids–old hat or new challenge?* International journal of radiation biology **83**, 849 (2007).

[41] M. Millard, I. Yakavets, V. Zorin, A. Kulmukhamedova, S. Marchal, and L. Bezdetnaya, *Drug delivery to solid tumors: The predictive value of the multicellular tumor spheroid model for nanomedicine screening,* International journal of nanomedicine **12**, 7993 (2017).

[42] S. Riffle, R. N. Pandey, M. Albert, and R. S. Hegde, *Linking hypoxia, dna damage and proliferation in multicellular tumor spheroids,* Bmc Cancer **17**, 1 (2017).

[43] G. Mehta, A. Y. Hsiao, M. Ingram, G. D. Luker, and S. Takayama, *Opportunities and challenges for use of tumor spheroids as models to test drug delivery and efficacy,* Journal of controlled release **164**, 192 (2012).

[44] K. Duval, H. Grover, L.-H. Han, Y. Mou, A. F. Pegoraro, J. Fredberg, and Z. Chen, *Modeling physiological events in 2d vs. 3d cell culture,* Physiology **32**, 266 (2017).

[45] N. Sohrabi, A. Valizadeh, S. M. Farkhani, and A. Akbarzadeh, *Basics of dna biosensors and cancer diagnosis,* Artificial cells, nanomedicine, and biotechnology **44**, 654 (2016).

[46] D. C. van Gent, J. H. Hoeijmakers, and R. Kanaar, *Chromosomal stability and the dna double-stranded break connection,* Nature Reviews Genetics **2**, 196 (2001).

[47] E. M. Zeman, E. C. Schreiber, and J. E. Tepper, *Basics of radiation therapy,* in *Abeloff's Clinical Oncology* (Elsevier, 2020) pp. 431–460.

[48] M. Mognato and L. Celotti, *Micrornas used in combination with anti-cancer treatments can enhance therapy efficacy,* Mini reviews in medicinal chemistry **15**, 1052 (2015).

[49] B. van Oorschot, G. Granata, S. Di Franco, R. Ten Cate, H. M. Rodermond, M. Todaro, J. P. Medema, and N. A. Franken, *Targeting dna double strand break repair with hyperthermia and dna-pkcs inhibition to enhance the effect of radiation treatment,* Oncotarget **7**, 65504 (2016).

[50] J. M. Ford and M. B. Kastan, *Dna damage response pathways and cancer,* in *Abeloff's Clinical Oncology* (Elsevier, 2020) pp. 154–164.

[51] C. Featherstone and S. P. Jackson, *Dna double-strand break repair,* Current Biology **9**, R759 (1999).

[52] A. Sancar, L. A. Lindsey-Boltz, K. Unsal-Kaçmaz, S. Linn, *et al.*, *Molecular mechanisms of mammalian dna repair and the dna damage checkpoints,* Annual review of biochemistry **73**, 39 (2004).

[53] A. Oei, H. Kok, S. Oei, M. Horsman, L. Stalpers, N. Franken, and J. Crezee, *Molecular and biological rationale of hyperthermia as radio-and chemosensitizer,* Advanced drug delivery reviews **163**, 84 (2020).

[54] P. Kaur, M. D. Hurwitz, S. Krishnan, and A. Asea, *Combined hyperthermia and radiotherapy for the treatment of cancer,* Cancers **3**, 3799 (2011).

[55] C. W. Song, H. Park, and R. J. Griffin, *Improvement of tumor oxygenation by mild hyperthermia,* Radiation research **155**, 515 (2001).

[56] R. J. Griffin, R. P. Dings, A. Jamshidi-Parsian, and C. W. Song, *Mild temperature hyperthermia and radiation therapy: role of tumour vascular thermotolerance and relevant physiological factors,* International Journal of Hyperthermia **26**, 256 (2010).

[57] M. Ihara, S. Takeshita, K. Okaichi, Y. Okumura, and T. Ohnishi, *Heat exposure enhances radiosensitivity by depressing dna-pk kinase activity during double strand break repair,* International Journal of Hyperthermia **30**, 102 (2014).

[58] P. M. Krawczyk, B. Eppink, J. Essers, J. Stap, H. Rodermond, H. Odijk, A. Zelensky, C. van Bree, L. J. Stalpers, M. R. Buist, *et al.*, *Mild hyperthermia inhibits homologous recombination, induces brca2 degradation, and sensitizes cancer cells to poly (adp-ribose) polymerase-1 inhibition,* Proceedings of the National Academy of Sciences **108**, 9851 (2011).

[59] P. Vaupel and A. Mayer, *Hypoxia in cancer: significance and impact on clinical outcome,* Cancer and Metastasis Reviews **26**, 225 (2007).

[60] J. Overgaard, *Hypoxic modification of radiotherapy in squamous cell carcinoma of the head and neck–a systematic review and meta-analysis,* Radiotherapy and Oncology **100**, 22 (2011).

[61] M. Horsman and J. Overgaard, *Hyperthermia: a potent enhancer of radiotherapy,* Clinical oncology **19**, 418 (2007).

[62] J. Overgaard, *The current and potential role of hyperthermia in radiotherapy,* International Journal of Radiation Oncology* Biology* Physics **16**, 535 (1989).

[63] J. M. Boone, *X-ray production, interaction, and detection in diagnostic imaging,* Handbook of medical imaging **1**, 1 (2000).

[64] A. Chicheł, J. Skowronek, M. Kubaszewska, and M. Kanikowski, *Hyperthermia–description of a method and a review of clinical applications,* Reports of Practical Oncology & Radiotherapy **12**, 267 (2007).

[65] J. Beik, Z. Abed, F. S. Ghoreishi, S. Hosseini-Nami, S. Mehrzadi, A. Shakeri-Zadeh, and S. K. Kamrava, *Nanotechnology in hyperthermia cancer therapy: From fundamental principles to advanced applications,* Journal of Controlled Release **235**, 205 (2016).

[66] S. A. Sapareto and W. C. Dewey, *Thermal dose determination in cancer therapy,* International Journal of Radiation Oncology* Biology* Physics **10**, 787 (1984).

[67] G. C. van Rhoon, *Is cem43 still a relevant thermal dose parameter for hyperthermia treatment monitoring?* International Journal of Hyperthermia **32**, 50 (2016).

[68] J. A. Pearce, *Comparative analysis of mathematical models of cell death and thermal damage processes,* International Journal of Hyperthermia **29**, 262 (2013).

[69] S. A. Sapareto, G. P. Raaphorst, and W. C. Dewey, *Cell killing and the sequencing of hyperthermia and radiation,* International Journal of Radiation Oncology* Biology* Physics **5**, 343 (1979).

[70] J. Overgaard, *Formula to estimate the thermal enhancement ratio of a single simultaneous hyperthermia and radiation treatment,* Acta Radiologica: Oncology **23**, 135 (1984).

[71] T. Wilson and J. W. Hastings, *Bioluminescence,* Annual review of cell and developmental biology **14**, 197 (1998).

[72] M. Kijanska and J. Kelm, *In vitro 3d spheroids and microtissues: Atp-based cell viability and toxicity assays,* Assay guidance manual [Internet] (2016).

[73] G-Biosciences, *Luciferase reporter assays: An overview,* https://info.gbiosciences.com/blog/luciferase-reporter-assays (2019).

[74] M. Zanoni, F. Piccinini, C. Arienti, A. Zamagni, S. Santi, R. Polico, A. Bevilacqua, and A. Tesei, *3d tumor spheroid models for in vitro therapeutic screening: a systematic approach to enhance the biological relevance of data obtained,* Scientific reports **6**, 1 (2016).

[75] R. Hannah, M. Beck, R. Moravec, and T. Riss, *Celltiter-glo™ luminescent cell viability assay: a sensitive and rapid method for determining cell viability,* Promega Cell Notes **2**, 11 (2001).

[76] F. Fan and K. V. Wood, *Bioluminescent assays for high-throughput screening,* Assay and drug development technologies **5**, 127 (2007).

[77] I. D. Odell and D. Cook, *Immunofluorescence techniques,* The Journal of investigative dermatology **133**, e4 (2013).

[78] J. W. Lichtman and J.-A. Conchello, *Fluorescence microscopy,* Nature methods **2**, 910 (2005).

[79] D. Semwogerere and E. R. Weeks, *Confocal microscopy,* Encyclopedia of biomaterials and biomedical engineering **23**, 1 (2005).

[80] K. Mohan, S. Pai, R. Rao, H. Sripathi, and S. Prabhu, *Techniques of immunofluorescence and their significance,* Indian journal of dermatology, venereology and leprology **74**, 415 (2008).

[81] abcam, *Direct vs indirect immunofluorescence,* https://www.abcam.com/secondary-antibodies/direct-vs-indirect-immunofluorescence (2022).

[82] M. J. Sanderson, I. Smith, I. Parker, and M. D. Bootman, *Fluorescence microscopy,* Cold Spring Harbor Protocols **2014**, pdb (2014).

[83] Ibidi, *Confocal microscopy,* https://ibidi.com/content/216-confocal-microscopy (2021).

[84] A. Nwaneshiudu, C. Kuschal, F. H. Sakamoto, R. R. Anderson, K. Schwarzenberger, and R. C. Young, *Introduction to confocal microscopy,* Journal of Investigative Dermatology **132**, 1 (2012).

[85] G. Lazzari, P. Couvreur, and S. Mura, *Multicellular tumor spheroids: a relevant 3d model for the in vitro preclinical investigation of polymer nanomedicines,* Polymer Chemistry **8**, 4947 (2017).

[86] B. Martinez-Madrid, M.-M. Dolmans, A. Van Langendonckt, S. Defrère, A.-S. Van Eyck, and J. Donnez, *Ficoll density gradient method for recovery of isolated human ovarian primordial follicles,* Fertility and sterility **82**, 1648 (2004).

[87] S. Sanfilippo, M. Canis, L. Ouchchane, R. Botchorishvili, C. Artonne, L. Janny, and F. Brugnon, *Viability assessment of fresh and frozen/thawed isolated human follicles: reliability of two methods (trypan blue and calcein am/ethidium homodimer-1),* Journal of assisted reproduction and genetics **28**, 1151 (2011).

[88] AAT Bioquest, *Calcein,* https://www.aatbio.com/resources/application-notes/calcein (2021).

[89] C. Riccardi and I. Nicoletti, *Analysis of apoptosis by propidium iodide staining and flow cytometry,* Nature protocols **1**, 1458 (2006).

[90] ThermoFisher, *Propidium iodide,* https://www.thermofisher.com/nl/en/home/life-science/cell-analysis/fluorophores/propidium-iodide.html (2022).

[91] Promega, *Technical manual celltiter-glo® 3d cell viability assay,* https://www.promega.com/-/media/files/resources/protocols/technical-manuals/101/celltiter-glo-3d-cell-viability-assay-protocol.pdf?rev=88083aa3f7284e898ff0f218aa3c6b59&sc_lang=en (2015).

[92] S. C. Brüningk, I. Rivens, C. Box, U. Oelfke, and G. Ter Haar, *3d tumour spheroids for the prediction of the effects of radiation and hyperthermia treatments,* Scientific reports **10**, 1 (2020).

[93] J. Ma, S. Lu, L. Yu, J. Tian, J. Li, H. Wang, and W. Xu, *Fadu cell characteristics induced by multidrug resistance,* Oncology reports **26**, 1189 (2011).

[94] ImageJ, *Analyze menu,* https://imagej.nih.gov/ij/docs/menus/analyze.html (2018).

[95] M. A. Badea, M. Balas, A. Hermenean, A. Ciceu, H. Herman, D. Ionita, and A. Dinischiotu, *Influence of matrigel on single-and multiple-spheroid cultures in breast cancer research,* Slas Discovery: Advancing Life Sciences R&D **24**, 563 (2019).

[96] G. Benton, I. Arnaoutova, J. George, H. K. Kleinman, and J. Koblinski, *Matrigel: from discovery and ecm mimicry to assays and models for cancer research,* Advanced drug delivery reviews **79**, 3 (2014).

[97] C. J. Kelly, K. Hussien, and R. J. Muschel, *3d tumour spheroids as a model to assess the suitability of [18f] fdg-pet as an early indicator of response to pi3k inhibition,* Nuclear medicine and biology **39**, 986 (2012).

[98] F. Mirab, Y. J. Kang, and S. Majd, *Preparation and characterization of size-controlled glioma spheroids using agarose hydrogel microwells,* PLoS One **14**, e0211078 (2019).

[99] M. Schmidt, C.-J. Scholz, C. Polednik, and J. Roller, *Spheroid-based 3-dimensional culture models: Gene expression and functionality in head and neck cancer,* Oncology reports **35**, 2431 (2016).

[100] Y. Li, H. A. Rogoff, S. Keates, Y. Gao, S. Murikipudi, K. Mikule, D. Leggett, W. Li, A. B. Pardee, and C. J. Li, *Suppression of cancer relapse and metastasis by inhibiting cancer stemness,* Proceedings of the National Academy of Sciences **112**, 1839 (2015).

[101] L. Yvan-Charvet, T. Pagler, E. L. Gautier, S. Avagyan, R. L. Siry, S. Han, C. L. Welch, N. Wang, G. J. Randolph, H. W. Snoeck, *et al.*, *Atp-binding cassette transporters and hdl suppress hematopoietic stem cell proliferation,* Science **328**, 1689 (2010).

[102] H. Wang, F. Wang, W. Ouyang, X. Jiang, and Y. Wang, *Bcat1 overexpression regulates proliferation and c-myc/glut1 signaling in head and neck squamous cell carcinoma,* Oncology Reports **45**, 1 (2021).

[103] D. W. Lee, J. E. Kim, G.-H. Lee, A. Son, H. C. Park, D. Oh, K. Jo, and C. Choi, *High-throughput 3d tumor spheroid array platform for evaluating sensitivity of proton-drug combinations,* International Journal of Molecular Sciences **23**, 587 (2022).

[104] L. Kadletz, G. Heiduschka, J. Domayer, R. Schmid, E. Enzenhofer, and D. Thurnher, *Evaluation of spheroid head and neck squamous cell carcinoma cell models in comparison to monolayer cultures,* Oncology letters **10**, 1281 (2015).

[105] W.-L. Yang, G. Yang-Biggs, Y. Wu, X. Ye, G. Gallos, R. P. Owen, and T. Ravikumar, *Development of cross-resistance between heat and cisplatin or hydroxyurea treatments in fadu squamous carcinoma cells,* Journal of Surgical Research **111**, 143 (2003).

[106] H. Acker, J. Carlsson, G. Holtermann, T. Nederman, and T. Nylen, *Influence of glucose and buffer capacity in the culture medium on growth and ph in spheroids of human thyroid carcinoma and human glioma origin,* Cancer research **47**, 3504 (1987).

[107] J. Overgaard, *Simultaneous and sequential hyperthermia and radiation treatment of an experimental tumor and its surrounding normal tissue in vivo,* International Journal of Radiation Oncology* Biology* Physics **6**, 1507 (1980).

[108] N. van den Tempel, M. R. Horsman, and R. Kanaar, *Improving efficacy of hyperthermia in oncology by exploiting biological mechanisms,* International journal of hyperthermia **32**, 446 (2016).

[109] N. van den Tempel, *Hyperthermia-induced degradation of BRCA2: from bedside to bench and back again* (Erasmus University Rotterdam, 2017).

[110] S. Hu, X. Zhang, M. Unger, I. Patties, A. Melzer, and L. Landgraf, *Focused ultrasound-induced cavitation sensitizes cancer cells to radiation therapy and hyperthermia,* Cells **9**, 2595 (2020).

[111] M. Ohtake, M. Umemura, I. Sato, T. Akimoto, K. Oda, A. Nagasako, J.-H. Kim, T. Fujita, U. Yokoyama, T. Nakayama, *et al.*, *Hyperthermia and chemotherapy using fe (salen) nanoparticles might impact glioblastoma treatment,* Scientific Reports **7**, 1 (2017).

[112] B. S. Sørensen, A. Vestergaard, J. Overgaard, and L. H. Præstegaard, *Dependence of cell survival on instantaneous dose rate of a linear accelerator,* Radiotherapy and Oncology **101**, 223 (2011).

[113] A. Oseroff, D. Ohuoha, and G. Ara, *Mild hyperthermia synergistically enhances killing of malignant cells by the cationic photosensitizer edkc: Implications for a" selective photo-hyperthermic therapy",* in *New Directions in Photodynamic Therapy*, Vol. 847 (SPIE, 1988) pp. 11–14.